LUT
Lappeenranta
University of Technology

Jussi Karttunen

CURRENT HARMONIC COMPENSATION IN DUAL THREE-PHASE PERMANENT MAGNET SYNCHRONOUS MACHINES

Thesis for the degree of Doctor of Science (Technology) to be presented with due permission for public examination and criticism in the Auditorium 3310 at Lappeenranta University of Technology, Lappeenranta, Finland on the 30th of June, 2017, at noon.

Acta Universitatis
Lappeenrantaensis 751

Supervisor Professor Pertti Silventoinen
LUT School of Energy Systems
Lappeenranta University of Technology
Finland

Reviewers Professor Iustin Radu Bojoi
Department of Electrical Engineering
Politecnico di Torino
Italy

Professor Mario J. Duran
Department of Electrical Engineering
University of Málaga
Spain

Opponent Professor Iustin Radu Bojoi
Department of Electrical Engineering
Politecnico di Torino
Italy

ISBN 978-952-335-097-7
ISBN 978-952-335-098-4 (PDF)
ISSN-L 1456-4491
ISSN 1456-4491

Lappeenrannan teknillinen yliopisto
Yliopistopaino 2017

Abstract

Jussi Karttunen
Current Harmonic Compensation in Dual Three-Phase Permanent Magnet Synchronous Machines
Lappeenranta 2017
80 pages
Acta Universitatis Lappeenrantaensis 751
Diss. Lappeenranta University of Technology
ISBN 978-952-335-097-7, ISBN 978-952-335-098-4 (PDF)
ISSN-L 1456-4491, ISSN 1456-4491

Dual three-phase electric machines can bring significant benefits over conventional three-phase machines in many applications. Although increasing the phase number of the electric machine can deliver significant advantages, it also introduces problems with stator current harmonics. In dual three-phase machines, even a small voltage excitation of certain frequency components can produce significant corresponding stator current harmonics. Current harmonics cause adverse effects such as additional losses, which degrade the efficiency of the machine. Thus, the target is usually to eliminate the harmonics.

The established solution to eliminate current harmonics is to use some current harmonic compensation method. In the literature, a variety of methods have been suggested for the purpose. The objective of this doctoral dissertation is to show that in addition to the traditional methods, an inverse-based current harmonic controller can be effectively used to eliminate stator current harmonics in dual three-phase machines. Further, it is demonstrated that, compared with the traditional methods, the inverse-based structure of the proposed controller is very advantageous in the theoretical analysis. Another novel approach for harmonic compensation is obtained by recognizing that the current harmonics can be modelled as caused by a lumped disturbance signal. Hence, it is possible to use a disturbance-observer-based control to eliminate the current harmonics. The results show that the disturbance observer provides a high-performance alternative to the conventional harmonic compensation solutions.

The well-known current harmonic compensation methods reported in the literature and the new approaches developed in this doctoral dissertation are extensively compared in terms of stability and performance. A detailed theoretical analysis of the methods is given by using a modern multi-input multi-output technique based on a structured singular value analysis. In addition, the performance of the methods is studied with experimental results. The main contribution of this dissertation is to establish the most favourable current harmonic compensation method for dual three-phase permanent magnet synchronous machines. All in all, the results show that the current harmonics can be eliminated robustly and efficiently with the right type and parameters of the harmonic compensation.

Keywords: current control, dual three-phase, disturbance observer, harmonic, multiphase, resonant controller, robust stability, robust performance, structured singular value.

Acknowledgements

There is a saying that you can do anything, but you cannot do everything. When we achieve, we usually do so because others have helped. Completing this work would have not been possible without the participation and assistance of some important people. Please accept this attempt to gratefully acknowledge your contribution and know that you have my sincerest appreciation.

Most of the research presented in this dissertation was carried out in the Department of Electrical Engineering at Lappeenranta University of Technology, Finland, between 2011 and 2015. Then after joining the R&D team at Visedo Oy in 2016, writing my dissertation continued as an evening hobby (not the most relaxing one, I must say) until finally finishing it in June 2017.

The financial support by the Finnish Foundation for Technology Promotion (TES), Ulla Tuominen Foundation, Emil Aaltonen Foundation, Research Foundation of Lappeenranta University of Technology, Walter Ahlström Foundation and Fortum Foundation is highly appreciated. I value the trust you have put into me and I hope that you will find this work to be worthy of your support.

I want to thank Professors Iustin Radu Bojoi and Mario J. Duran for taking the time to act as preliminary examiners of my dissertation. Your effort in reviewing the manuscript is greatly appreciated. It was an honor and privilege that such distinguished experts in the field evaluated my work. I could not have hoped for better reviewers. Major thanks to Professor Bojoi for also agreeing to act as my opponent at the public examination.

I would like to express my gratitude to my supervisor Professor Pertti Silventoinen for all the support and guidance he has given me. I am eternally grateful for the opportunity to work in your laboratory. Thank you for your patience and giving the freedom to pursue my goals. I know that it took longer than it should have but hopefully you are happy about the outcome. Thanks for being such a great professor.

My warmest thanks belong to the co-authors of my publications: Professor Olli Pyrhönen, Dr. Pasi Peltoniemi, Dr. Samuli Kallio, and Mr. Jari Honkanen. It was truly a pleasure to work with you. I am very grateful for all the time you used reading and commenting my work. Thank you for sharing your knowledge and experience with me and being such an important part of this process. I would like to particularly thank Samuli for volunteering his time and effort to help me. I am extremely thankful for your technical insight and deep expertise about the subject of this dissertation. You sir are one of the finest gentlemen I know. Many thanks to Jari for generously letting me to use his own computer to run the most computationally intensive calculations of this dissertation. It was very helpful and saved me a lot of time.

I will always be grateful to Dr. Hanna Niemelä for revising the language of this dissertation and my papers. Your expertise in English continues to impress me over and over again. You went above and beyond what I could have ever asked for and I will never

forget that. I am having a hard time putting my gratitude into words but I hope you know how much I appreciate all the hard work you have done to help me. Thank you so much. I want to also thank another important member of the staff Ms. Piipa Virkki. You are a lifesaver. I cannot thank you enough for helping me with the practical arrangements and cumbersome bureaucratic hurdles of the university.

My former and present colleagues and friends, it is difficult to describe how extremely thankful I am for all the laughs and great discussions along the way. Thanks for always listening to me, assisting me, and encouraging me. You have made working with you an interesting and memorable experience. I want to tell you how much I have appreciated your company. From the bottom of my heart, I thank you for being there and providing enjoyable moments inside and outside the office. Special thanks to Nina for the invaluable peer support during this journey. I feel very lucky to know you.

Above all, nobody has been more important to me in the pursuit of the degree of Doctor of Science than the members of my family. I owe an enormous debt to you. Know that you always have my deepest gratitude and love. I would not be even close to where I am today without your support and guidance. Thank you for believing in me.

Two words: endless gratitude. The rest of this dissertation is just details.

Jussi Karttunen
June 2017
Lappeenranta, Finland

The road

to wisdom?

Well, it's plain
and simple to express:
Err and err and err again,
but less and less and less.

-Piet Hein, scientist and poet

Contents

List of publications

This doctoral dissertation is based on the following publications. The rights have been granted by the publishers to include the material in the dissertation.

I. J. Karttunen, S. Kallio, P. Peltoniemi, P. Silventoinen, and O. Pyrhönen, "Dual Three-Phase Permanent Magnet Synchronous Machine Supplied by Two Independent Voltage Source Inverters," in *21st edition of the IEEE International Symposium on Power Electronics, Electrical Drives, Automation and Motion (SPEEDAM 2012)*, Sorrento, pp. 741–747, 2012.

II. J. Karttunen, S. Kallio, P. Peltoniemi, P. Silventoinen, and O. Pyrhönen, "Decoupled Vector Control Scheme for Dual Three-Phase Permanent Magnet Synchronous Machines," *IEEE Transactions on Industrial Electronics*, vol. 61, no. 5, pp. 2486–2494, May 2014.

III. J. Karttunen, S. Kallio, P. Peltoniemi, and P. Silventoinen, "Transforming Dynamic System Models Between Two-Axis Reference Frames Rotating at Different Angular Frequencies," in *16th European Conference on Power Electronics and Applications (EPE'14-ECCE Europe),* Lappeenranta, pp. 1–10, 2014.

IV. J. Karttunen, S. Kallio, P. Peltoniemi, and P. Silventoinen, "Current Harmonic Compensation in Dual Three-Phase PMSMs Using a Disturbance Observer," *IEEE Transactions on Industrial Electronics*, vol. 63, no. 1, pp. 583–594, Jan. 2016.

V. J. Karttunen, S. Kallio, P. Peltoniemi, J. Honkanen, and P. Silventoinen, "Inverse-Based Current Harmonic Controller for Multiphase PMSMs," *International Review of Electrical Engineering (I.R.E.E.)*, vol. 11, no. 4, pp. 359–396, Aug. 2016.

VI. J. Karttunen, S. Kallio, P. Peltoniemi, J. Honkanen, and P. Silventoinen, "Stability and Performance of Current Harmonic Controllers for Multiphase PMSMs," *Control Engineering Practice*, vol. 65, pp. 59–69, Aug. 2017.

VII. J. Karttunen, S. Kallio, P. Peltoniemi, J. Honkanen, and P. Silventoinen, "Partial Current Harmonic Compensation in Dual Three-Phase PMSMs Considering the Limited Available Voltage," *IEEE Transactions on Industrial Electronics*, vol. 64, no. 2, pp. 1038–1048, Feb. 2017.

Author's contribution

The author of this doctoral dissertation is the principal author and the primary contributor in all the papers. The contents of the papers are designed, analysed, and written by the author. The co-authors have participated in the preparation of the papers by discussing the results, offering comments, and suggesting revisions. In addition, Dr. Kallio's contribution to the development of the experimental setup was essential for obtaining the measurement results.

The author has also participated in the following papers closely related to the subject of this dissertation.

- S. Kallio, J. Karttunen, M. Andriollo, P. Peltoniemi, and P. Silventoinen, “Finite Element Based Phase-Variable Model in the Analysis of Double-Star Permanent Magnet Synchronous Machines,” in *21st edition of the IEEE International Symposium on Power Electronics, Electrical Drives, Automation and Motion (SPEEDAM 2012)*, Sorrento, pp. 1462–1467, 2012.

- S. Kallio, M. Andriollo, A. Tortella, and J. Karttunen, ”Decoupled d-q Model of Double-Star Interior Permanent Magnet Synchronous Machines,” *IEEE Transactions on Industrial Electronics*, vol. 60, no. 6, pp. 2486–2494, Jun. 2013.

- S. Kallio, J. Karttunen, P. Peltoniemi, P. Silventoinen, and O. Pyrhönen, “Online Estimation of Double-Star IPM Machine Parameters Using RLS Algorithm,” *IEEE Transactions on Industrial Electronics*, vol. 61, no. 9, pp. 4519–4530, Sep. 2014.

- S. Kallio, J. Karttunen, P. Peltoniemi, P. Silventoinen, and O. Pyrhönen, “Determination of the Inductance Parameters for the Decoupled d–q Model of Double-Star Permanent-Magnet Synchronous Machines,” *IET Electric Power Applications*, vol. 8, no. 2, pp. 39–49, Feb. 2014.

- S. Kallio, M. Andriollo, J. Karttunen, P. Peltoniemi, and P. Silventoinen, “Model of Double-Star IPM Machines with General Mutual Inductance Relationships Between the Two Three-Phase Winding Sets,” *International Review of Electrical Engineering (I.R.E.E.)*, vol. 8, no. 6, pp. 1717–1727, Dec. 2013.

The author is a co-inventor in the following patent, which is partly based on the results also presented in this dissertation.

- T. Knuutila, R. Pöllänen, J. Karttunen, S. Kallio, and P. Peltoniemi, ”Method and an apparatus for controlling an electrical machine with two or more multiphase stator windings,” *US Patent* US9444386 B2, Filed May 25, 2012, Published Sept. 13, 2016, Also published as CN104396139A, EP2856631A1, US20150229261, and WO2013175050A1.

Nomenclature

In the present work, all variables and constants are denoted in slanted style (*a, A*). Among the variables, vectors are denoted using bold lower-case letters (***a***), and matrices are denoted using bold upper-case letters (***A***). Abbreviations, function names, and operators are denoted in regular style.

Latin alphabet

a	first phase in the three-phase winding set	-
b	second phase in the three-phase winding set	-
c	third phase in the three-phase winding set	-
C	current controller	-
d	direct axis in the synchronous reference frame	-
d	disturbance	V
D	direct axis in the synchronous reference frame	-
E	error transfer function matrix	-
f	transfer function	-
g	transfer function	-
h	order of the frequency component	-
H	Hilbert space	-
H	closed-loop transfer function matrix	-
I	identity matrix	-
k	robustness margin	-
K	gain	V/A
L	self-inductance, Lebesgue space	H,-
M	mutual inductance, interconnection matrix	H,-
n	rotational speed, order of the frequency component	r/min,-
N	interconnection matrix	-
p	polynomial	-
P	plant model	-
q	quadrature axis in the synchronous reference frame	-
Q	quadrature axis in the synchronous reference frame	-
Q	interconnection matrix, disturbance observer filter	-
R	resistance	Ω
i	current	A
j	imaginary unit	-
s	Laplace-domain variable	-
t	time	s
T	time	s
T	transformation matrix	-
u	voltage	V
w	scalar weighting function	-
W	matrix weighting function	-
x	input signal	-

z	output signal	-

Greek alphabet

α	control design parameter, alpha-axis	rad/s,-
A	alpha axis in the stationary reference frame	-
β	beta axis in the stationary reference frame	-
B	beta axis in the stationary reference frame	-
δ	parameter uncertainty	-
θ	angle	rad
λ	partial compensation control variable, decay rate	-,1/s
μ	structured singular value	-
τ	time constant	s
ψ	flux linkage	Wb
ω	angular speed	rad/s

Subscripts

0	nominal
I	first three-phase winding set
II	second three-phase winding set
α	alpha axis
A	alpha axis
β	beta axis
B	beta axis
abc	phase variables of the three-phase winding set
d	direct axis, delay
D	direct axis
di	from disturbance to measured currents
dc	direct current
dg	diagonal
DOB	disturbance observer
INV	inverse
m	main
M	robust stability interconnection matrix
max	maximum
N	robust performance interconnection matrix
nat	natural
off	off-diagonal
out	outer loop
p	performance, proportional
pm	permanent magnet
PR	proportional resonant
q	quadrature axis

Q	quadrature axis
r	rotor
rot	rotation
RS	robust stability
s	stator, secondary, sampling
U	voltage
VPR	vector proportional resonant

Abbreviations

AC	alternating current
APF	active power filter
DC	direct current
DOB	disturbance observer
DTC	direct torque control
EMF	electromotive force
FOC	field-oriented control
IM	induction machine
INV	inverse
LTI	linear time invariant
MIMO	multi-input multi-output
MMF	magnetomotive force
MPC	model predictive control
PI	proportional integral
PR	proportional resonant
PMSM	permanent magnet synchronous machine
PWM	pulse width modulation
SISO	single-input single-output
SSV	structured singular value
VPI	vector proportional integral
VPR	vector proportional resonant
VSD	vector space decomposition
VSI	voltage source inverter

1 Introduction

Electric machine drives are the single largest consumer of electricity in the world [1]. At the present moment, they already account for nearly half of the total global electricity consumption, and their proportion is likely to even increase in the future. Considering that electric machines are also used to produce nearly all the electricity on earth, it is obvious that this technology is of great importance. Thus, achieving improvements in the field of electric machine drives has been and continues to be a topic of significant interest.

Conventional three-phase electric machines are predominantly used in the industry. However, in modern electric machine drives supplied with a frequency converter, it is possible to freely choose the number of the phases to be more than three. Electric machines with more than three phases are commonly known as multiphase machines. Over the last decades, multiphase electric machines have been increasingly recognized as a valuable area of interest. Multiphase machines can be an attractive alternative in many electric drive applications as increasing the phase number of the machine provides several important advantages. Because of these advantages, a conventional three-phase electric machine is not necessarily the best solution for all cases.

Through the history of multiphase machines, the most popular multiphase machine type has been a dual three-phase machine. Dual three-phase machines are characterized by the multiphase structure with two sets of three-phase stator windings in the same stator frame. As a disadvantage, dual three-phase machines can suffer from problems with undesired stator current harmonics. To solve this problem, current harmonic compensation in dual three-phase permanent magnet synchronous machines (PMSM) is thoroughly discussed in this doctoral dissertation.

1.1 From history to present

The history of dual three-phase machines can be traced back to the late 1920s [2]. At that time, building of larger generator units was restricted by the availability of circuit breaker interrupting capacity and large bus reactors needed to limit the fault currents. To overcome these limitations, generators with two three-phase winding sets (back then called ‘double winding generators’) were introduced. Because the separate winding sets could be connected to different sections of the power station bus, the problem with overly high fault currents was avoided. For a while, this solution was considered satisfactory. However, the fault current problem was later solved more conveniently by using step-up transformers with conventional three-phase units instead of dual three-phase generators.

The rapid growth in the generator power levels in the 1960s caused common three-phase generators to reach their present technical limits again. Consequently, the dual three-phase structure made a comeback as an attractive alternative. To further improve the performance of the dual three-phase generators, it was first proposed to displace the two three-phase stator winding sets by 30 electrical degrees [3]. This concept has then become

a standard solution with dual three-phase machines. In order to better understand the behaviour of such machines, one of the first important contributions to mathematically model a dual three-phase synchronous machine was published in 1974 [4]. At the same time, dual three-phase machines also started to attract interest in motor applications. The invention of the voltage source inverter (VSI) had removed the limits of the number of phases in electric motor drives. The problem then was that supplying a conventional three-phase induction machine (IM) with a six-step modulated VSI caused a notable undesired sixth harmonic torque pulsation. Pioneer analysis of IMs with an arbitrary displacement between the winding sets suggested that displacing the windings by 30 electrical degrees could significantly reduce the sixth harmonic torque pulsation [5]. In the 1970s, dual three-phase machines were also introduced for simultaneous generation of AC and DC power [6]. In this solution, DC power was supplied from one winding set connected to a bridge rectifier, and thus, the other winding set could be used to supply AC power.

In the 1980s, dual three-phase machines received only limited attention. However, some important contributions were still published. Synchronous machines with simultaneous AC and DC connection continued to be a topic of interest. For example, dual three-phase machines were studied for a novel AC to DC conversion system where a DC source supplied one three-phase stator winding set through a current source inverter, and the AC voltage output was obtained from the other winding set [7]. Simultaneous generation of AC and DC power was also discussed in [8]. In that paper, a detailed circuit model that includes the stator mutual leakage inductances was presented for the machine. At the time, such generators were proposed as power supplies on aircrafts and ships because they reduced cost and weight and even required less filtering.

A need to further improve the modelling of dual three-phase machines was recognized in the 1980s. A two-axis model for dual three-phase IMs taking into account the slot leakage coupling was published [9]. However, that model and all the previous models were based on the conventional Park transformation. A different approach was taken in [10] to model a six-step inverter-fed dual three-phase IM. The novel idea was to represent the asymmetrical winding structure of the dual three-phase machine equivalently as a symmetrical 12-phase machine. This manipulation enabled to apply the Fortescue transformation [11] for symmetrical multiphase systems to a dual three-phase machine. With the selected approach, those frequency components that produce torque and those that do not interact with the rotor were mapped into separate decoupled reference frames (i.e., subplanes). The presented results provided a comprehensive mathematical explanation why certain harmonics in dual three-phase machines do not produce torque pulsation. This feature was also shown to be the cause of the easily occurring large stator current harmonics. Ahead of its time, the presented approach [10] resulted in a machine model that later has become a standard in modelling of dual three-phase machines. However, such a model did not gain widespread acceptance until a transformation leading to an equivalent result with [10] was published and popularized with the name ‘vector space decomposition’ (VSD) [12] for more than ten years later.

Dual three-phase machines started to become more popular in the 1990s. The emergence of pulse width modulation (PWM) for the control of VSIs inspired new studies. One of the first investigations into the operation of a dual three-phase machine supplied with a PWM-controlled VSI was reported in [13]. The modelling took its most important steps forward when the VSD transformation was published [12]. Although it is not well known, the same transformation was presented simultaneously elsewhere with the name 'extended Park's transformation' [14]. Practically all modern control methods are based on the VSD transformation. The VSD transformation results in a machine model that is the same as published in [10] already in 1984. However, the framework in [12] made the VSD transformation more approachable and thus enabled its wide spread in the research community.

At the beginning of the 21st century, the interest of the research community shifted towards development of control methods. Several seminal papers on vector control and direct torque control (DTC) of IMs were published. The rapid pace of progress in the field continued, and by the year 2008, the growing body of literature had developed to a state where several survey papers had been published [15]–[17]. The overview of the work reported in those papers indicated that some level of maturity had been achieved in the modelling and basic control solutions for dual three-phase IMs. However, it was clear that many topics still needed attention.

Over the last decade, the level of interest has been further increasing with a rapidly growing number of publications and new industrial applications. The most recent survey papers [18]–[20] published in 2016 demonstrate a highly active area of investigation, which has now become an established part of the mainstream research in the field of electric machine drives. Dual three-phase PMSMs, in particular, have drawn more attention in recent years with a significant progress in design, modelling, and control. In addition, popular topics have been, for example, the fault tolerant control and innovative ways of using the additional degrees of freedom. The continuous desire to improve the performance further has also brought topics such as current harmonic compensation into the focus.

1.2 Background and motivation

A long history of success and the wide off-the-shelf availability of conventional three-phase machines make them a preferred solution in most industry applications. However, dual three-phase electric machines have raised the attention of the industry and the scientific community owing to the fact that increasing the phase number can provide important advantages, which can justify the higher number of phases in some specific cases. The most frequently discussed applications cover electric and hybrid vehicles, locomotive traction, ship propulsion drives, aircrafts, wind power generation, and general high-power industrial applications such as turbo-compressors [15], [19]–[30].

The benefits of dual three-phase machines compared with their conventional three-phase counterparts are well documented in the literature [15], [31], [32]. The known advantages include:

- Fundamental component of the stator current produces a magnetomotive force (MMF) waveform with a lower space-harmonic content. Because of the more sinusoidal MMF, it is possible that the noise caused by the machine decreases and the efficiency can be higher than in a three-phase machine.
- Certain time-harmonic components in the stator current are prevented from contributing to the air-gap flux and consequently, torque pulsation. For example, the sixth harmonic torque pulsation is eliminated.
- There is a potential to increase the efficiency of the machine as a result of reduced stator copper losses compared with an equivalent three-phase machine.
- The output power of the machine is divided between a larger number of phases, thereby enabling the use of semiconductor switches of lower rating.
- The machine can continue to operate after a loss of one or more phases. The much improved reliability is achieved as a result of better fault tolerance.
- The DC link current can have a lower harmonic content.
- A dual three-phase machine can be built by dividing the phase belt of a conventional three-phase machine into two parts. As a result, the DC link voltage of the inverter can be reduced to half without a change in the air-gap flux level of the machine.
- The additional degrees of freedom can be used for various innovative purposes. The proposed ideas include, for example, the DC link capacitor voltage balancing process [33], fully integrated onboard battery charging of electric vehicles [34], implementation of multimotor drive systems with independent control from a single VSI supply [35], [36], and performance enhancement of the braking process in drives with unidirectional power flow [37], [38].

In addition to the common benefits of the multiphase machines, dual three-phase machines have the advantage that the structure with multiple three-phase winding sets is simple to integrate with conventional three-phase technology. Although there are several reasons to choose a dual-three phase machine instead of a conventional three-phase machine, it appears that the high overall system reliability and reduction in the total power per phase are the features with the most practical relevance in the industry. The ability to achieve a fault tolerant operation has also been a subject of intense research in recent years [39]–[46].

Although increasing the phase number of the machine can provide significant benefits, it also introduces some disadvantages. The increased number of the required power electronics to supply the machine is undeniably a major drawback. The system cost and

complexity are negatively affected by the higher phase number. Hence, a careful consideration is needed to justify the higher complexity compared with the conventional three-phase solution.

Another major drawback of dual three-phase machines is a problem with easily occurring large stator current harmonics. Certain current harmonic components arise easily in dual three-phase machines because these harmonic components do not produce air-gap flux and are thus only limited by the stator resistance and leakage inductance of the machine. Because of the low-impedance current path, even a small voltage excitation can produce significant current harmonics. Current harmonics cause adverse effects such as additional losses, which degrade the efficiency of the machine. Therefore, the harmonics are usually desired to be eliminated.

The current harmonic problem has been well known since the early days of the dual three-phase machines. Comments about the subject can be found in papers from the 1970s [5], 1980s [10], 1990s [12], 2000s [47]–[52], and in the last decade [53]–[55]. Although the problem of stator current harmonics in dual three-phase machines is widely recognized and has been known for a long time, the solution to the issue is a much more recent topic. Satisfactory control based solutions started to appear in 2013 [56]–[58], and more discussion has then followed [59]–[66].

To understand why the current harmonic problem has not been solved until recently, it must be noted that up to recent years there has been a particularly strong focus on IMs in the field of multiphase machine research. The current harmonics caused by the VSI have been the main concern in dual three-phase IMs. The VSI can cause current harmonics if the supplied voltage contains unwanted low-frequency voltage harmonics. However, with a suitable modulation method, the low-frequency harmonic components from the supplied voltage can be minimized and the current harmonic problem can be tolerated. In dual three-phase PMSMs instead, back-EMF harmonics can act as another significant source of current harmonics. Even if the supplied voltages do not contain any harmonic components, the internal nonidealities of the machine are difficult to avoid completely. Thus, some level of problems with current harmonics is likely in dual three-phase PMSM drives. It can be stated that the stator current harmonics are a much more serious problem in PMSMs than in IMs.

In the last couple of years, there has been a significant growth in interest towards dual three-phase PMSMs [67]–[74]. This trend has emphasized the need to properly solve the current harmonic problem. It is clear that in a rapidly increasing number of dual three-phase PMSM drives the potential benefits of the machine cannot be fully achieved if the system suffers from undesirable stator current harmonics. The motivation behind this dissertation is to help to improve the performance dual three-phase PMSM drives by providing a comprehensive solution for current harmonic compensation.

1.3 Aim and scope of the work

The aim of this doctoral dissertation is to provide exhaustive treatment of the current harmonic compensation in dual three-phase PMSMs. The presented results include detailed solutions to all relevant aspects of the current harmonic compensation problem: establishing a control scheme with transformations and modulation, transforming controllers between reference frames, selecting a correct compensation method, introducing control parameter design principles, providing stability and performance analysis, and addressing the effect of the limited DC link voltage.

The scope of the dissertation is limited to methods that do not require external modifications or additional hardware to the system. The methods proposed in this dissertation aim to solve the current harmonic problem solely by improving the control system of the electric drive. In other words, only software changes are assumed to be required to exploit the presented results. All the methods have been designed to operate as part of vector control schemes and cannot be straightforwardly applied to other control strategies. In addition, if the dual three-phase machine is supplied with two separate three-phase VSIs (as is commonly the case), it is required that the control of both VSIs is centralized or the communication between the VSIs is fast enough to enable synchronized current control between the units.

Before the current harmonic compensation can be performed, the base control scheme must be established. To this end, this dissertation presents a vector control scheme for dual three-phase PMSMs. The objective of the control scheme is to make it possible to obtain high-performance current control using well-established techniques for conventional three-phase PMSMs and, at the same time, to provide the means for solving characteristic problems of dual three-phase machines. This topic has been discussed in **Publication I** and **Publication II**.

Current harmonic compensation can be successfully implemented in reference frames rotating at any angular frequencies. Different reference frames have advantages of their own, and thus, it can be desirable to transform the designed harmonic compensation system into another frame. Each rotational invariant controller has a mathematically equivalent linear time invariant (LTI) representation in every reference frame. The aim of this dissertation is to derive a general form for the transformation that gives an equivalent representation of LTI system models in different two-axis reference frames. No specific structure of the system is assumed as has been previously done in the literature. The transformation derived in the dissertation offers insight into the behaviour of nonrotational invariant controllers and plants. The results also indicate some design limitations for multiple reference frame control systems that can result from implementation of current harmonic compensation. This topic has been discussed in **Publication III**.

Current harmonic compensation in dual three-phase PMSMs is a relatively recent topic. Therefore, it is worth considering innovative alternatives for harmonic compensation that

may bring benefits in terms of performance and robustness. An interesting approach is to recognize that the current harmonics are a result of disturbances, and thus, use a disturbance-observer-based control to eliminate the harmonics. This dissertation aims to show that the disturbance observer (DOB) can be effectively used to eliminate stator current harmonics in dual three-phase PMSMs. Established principles for conventional applications of disturbance observers are extended to multiphase machines. The study provides a detailed analysis of the solution including the design principles. This topic has been discussed in **Publication IV**.

The further aim of this dissertation is to demonstrate that the inverse-based current harmonic controller is a high-performance alternative for current harmonic compensation in dual three-phase PMSMs. It is shown that the inverse-based structure of the proposed controller is very advantageous in the theoretical analysis. This aspect enables much simpler multi-input multi-output (MIMO) controller design and analysis than for other methods. This topic has been discussed in **Publication V**.

A variety of different methods have been suggested for harmonic control. All the methods have been shown to work and can be applied to harmonic control in dual three-phase machines. However, these methods are not equally good in terms of stability and performance. Comparative studies on harmonic controllers have been published for active power filters (APFs), but not for multiphase machines. This dissertation aims to compare the robust stability and robust performance of harmonic controllers for dual three-phase PMSMs. Classical single-input single-output (SISO) techniques have commonly been used to analyse the harmonic control methods for grid-connected inverters. However, modern control analysis techniques can contribute to more in-depth understanding of the robustness of the system. In this dissertation, a MIMO approach based on a structured singular value (SSV) analysis is applied to study harmonic controllers. This topic has been discussed in **Publication VI**.

Finally, it is shown that the working principle of the active harmonic compensation is to cancel current harmonics by adding correct voltage harmonic components to the output voltage of the VSI supplying the machine. As a result, current harmonic compensation can increase the magnitude of the output voltage vector of the VSI. Because the maximum possible voltage vector is limited by the DC link voltage of the VSI, complete elimination of the current harmonics may not be achievable in every operating point. The aim of this dissertation is to introduce a method, based on the principle of realizable references, to recalculate the current reference of the VSI when the maximum available voltage is reached so that the required voltage vector does not exceed the maximum value. The strategy for recalculation of the current harmonic reference is derived from the objective of the optimal disturbance rejection. This topic has been discussed in **Publication VII**.

1.4 Scientific contributions

The scientific contributions of the publications comprising this dissertation can be summarized as follows:

- **Publication I**: The main contribution of the paper is a comprehensive analysis of the expected performance level if the present off-the-shelf three-phase converter technology with a conventional three-phase vector control is used to supply a dual three-phase PMSM.
- **Publication II**: The main contribution of the paper is the novel vector control scheme for dual three-phase PMSMs that takes into account the latest developments in modelling of such machines. The presented results cover reference frame transformations, the machine model, decoupling of the current control loops, model-based selection of current control parameters, and modulation.
- **Publication III**: The main contribution of the paper is the general form for the transformation that gives equivalent representation of LTI system models in different two-axis reference frames rotating at any angular frequencies. The transformation does not assume any specific structure of the system.
- **Publication IV**: The main contribution of the paper is the current harmonic compensation method for dual three-phase PMSMs using the DOB-based control. The contribution includes the working principles and analysis of the DOB and the application-specific design rules.
- **Publication V**: The main contribution of the paper is the detailed discussion of an inverse-based current harmonic controller for dual three-phase PMSMs. The inverse structure is shown to be very advantageous in the theoretical analysis. The results verify the high performance of the proposed method.
- **Publication VI**: The main contribution of the paper is the stability and performance comparison of three distinct fundamental synchronous reference frame current harmonic controllers for dual three-phase PMSMs. The results indicate multiple problems in the stability and performance of the traditional proportional-resonant (PR) controller. Because clearly superior alternatives are available, it is recommended to avoid using the PR controller.
- **Publication VII**: The main contribution of the paper is the strategy for partial current harmonic compensation in dual three-phase PMSMs under voltage constrains. The strategy helps to minimize the adverse effects caused by the current harmonics also in those operating points where the voltage constraint has previously prevented using the active harmonic compensation.

From the combined contributions of the papers, the main outcome of this dissertation is to establish the most favourable current harmonic control method for dual three-phase PMSMs. This dissertation also contributes by providing a comprehensive set of new analytical control design principles. The additional value of the dissertation is that the

theoretical discussion provides a detailed tutorial-style presentation of the SSV robustness analysis applied to the current control of PMSMs. All the necessary expressions to perform the analysis are explicitly given so that practicing engineers and researchers can directly use the results in their applications. In addition to dual three-phase PMSMs, the proposed analysis is suitable, for example, to study current control of grid-connected inverters and conventional three-phase electric machines without any modifications.

1.5 Structure of the doctoral dissertation

This doctoral dissertation consists of an introductory part and seven original papers. The content of the publications included in this dissertation can be summarized as follows:

Publication I investigates a dual three-phase PMSM supplied by two independent three-phase VSIs. Instead of six-phase converters and special vector controls, it would be a very interesting alternative to supply dual three-phase machines by two conventional three-phase VSIs as they are readily commercially available. This paper shows that the proposed supply method can be used successfully although it suffers from a decrease in the dynamic performance and an error in the estimation of torque. On the other hand, two independent VSIs do not cause additional low-frequency current harmonics and guarantee balanced current sharing between the winding sets, thereby avoiding the two most common problems with dual three-phase machines. Experimental results are given to verify the conclusions. The results suggest that the simple supply method of two conventional VSIs could be a feasible alternative for many industrial applications.

Publication II introduces an improved vector control scheme for dual three-phase PMSMs. The study offers detailed solutions for the key parts of the control such as reference frame transformations, decoupling of the current control loops, and modulation. The performance of the control scheme is evaluated using finite-element analyses and experimental results. The results show that the scheme can produce desired dynamics for the current control and guarantee balanced current sharing between the winding sets. In addition, the solution is capable of reducing current harmonics produced by the internal structure of the machine. This problem is, however, only partly solved because complete elimination of harmonic components is not achieved. Nevertheless, the suggested control scheme overcomes many of the disadvantages found with other control solutions. The improved control performance allows the full benefits of dual three-phase drives to be utilized even in demanding applications.

Publication III describes a general method to transform dynamic system models between two-axis reference frames that are rotating at different angular frequencies. Such a transformation is needed in the analysis and implementation of a control system where the entire system is not given in the same reference frame. Detailed derivation of the transformation for transfer function matrices is presented. Contrary to the previous solutions, the proposed transformation is not limited by the structure of the transfer function matrix of the system. Application examples illustrate the theory. The theoretical

analysis indicates important design limitations especially for multiple frame control systems. Experimental results verify the analysis.

Publication IV suggests a current harmonic compensation method based on a DOB to solve the disadvantage of easily occurring large stator current harmonics. The study provides a detailed analysis and design principles for the method. The performance of the proposed approach is verified by experimental results. The results show that nearly complete elimination of harmonic components is achieved. In addition, it is shown that the method is robust against uncertainties. The DOB offers a simple yet effective alternative for solving the issue of stator current harmonics in dual three-phase drives, and the results of the paper can easily be applied also to other multiphase machine types.

Publication V presents an inverse-based current harmonic controller to eliminate the current harmonics. A detailed theoretical analysis of the proposed harmonic controller is given including a comprehensive set of analytical design principles. The robustness of the method is studied with a MIMO approach based on a SSV and $\mathcal{H}_\infty$ norm analyses. In addition to the theoretical work, the performance of the harmonic controller is investigated with experimental results from a dual three-phase PMSM. The analysis and results of this paper show that the inverse-based current harmonic controller is a robust and high-performance method to eliminate the current harmonics in multiphase PMSMs.

Publication VI compares different current harmonic controllers in terms of stability and performance under model uncertainty. The harmonics can be eliminated by various current harmonic control methods. However, there appears to be no clear agreement on the most suitable method for multiphase machines. A detailed theoretical analysis of the harmonic controllers is given by taking a modern MIMO approach based on a SSV analysis. Further, the performance of the harmonic controllers is studied with experimental results from a dual three-phase PMSM. The analysis and results of this paper show how to design robust high-performance current harmonic controllers for multiphase machines.

Publication VII proposes a strategy for a partial compensation of the current harmonics. Using the active harmonic compensation can increase the required output voltage of the inverter supplying the machine. Because the maximum voltage is limited, complete elimination of the current harmonics may not always be possible. The strategy aims to produce a maximum reduction in the magnitude of the harmonics when the available voltage is limited. The strategy is verified by experimental results.

Chapter 2 is based on **Publication I** and **Publication II**. This chapter introduces the prerequisites for a model-based current harmonic compensation. First, a brief review is given of the main control strategies available for dual three-phase machines. Then, the selection of vector control scheme is justified and details of the control are discussed. The focus of the chapter is in modelling and reference frame transformations.

Chapter 3 is based on **Publication IV**, **Publication V**, and **Publication VI**. This chapter focuses on the applied analysis techniques to evaluate the stability and performance of the current harmonic compensation methods. The presented main theoretical approach is a multivariable SSV robustness analysis.

Chapter 4 is based on all of the publications. More specifically, Section 4.1 is based on **Publication IV** and Section 4.2 on **Publication III**, **Publication V**, and **Publication VI**. Again, Section 4.3 is based on **Publication IV** and Section 4.4 on **Publication IV** and **Publication VI**. Finally, Section 4.5 is based on **Publication VII**. Chapter 4 provides an extensive study of current harmonic compensation. Alternative methods are introduced and compared. Detailed results of the stability and performance of the methods are reported. Finally, the problem with the limited DC link voltage is addressed.

Chapter 5 concludes the doctoral dissertation.

2 Control of dual three-phase PMSMs

A dual three-phase machine is the most common multiphase machine structure. Dual three-phase machines have two sets of three-phase stator windings in the same stator frame. Displacement between the winding sets can take different values. However, only 0, 30, or 60 electrical degrees are actually encountered in practice. If the winding sets are not spatially shifted, the resulting machine is essentially a conventional three-phase machine with two parallel winding sets. On the other hand, displacing the winding set by 60 electrical degrees results in a symmetrical six phase machine. Although both of these alternatives can offer some advantages, the most popular solution is that the star-connected three-phase stator windings are spatially shifted by 30 electrical degrees, and the neutral points of the sets are galvanically isolated from each other.

Fig. 2.1 shows this configuration, which is also known in the literature as an asymmetrical six-phase machine, a split-phase machine, and a double-star machine. From the perspective of control, it is important to note that such a machine has a strong magnetic coupling between the winding sets. Another characteristic feature is that there are four independent phase currents that can be controlled. Only two current components are required to produce torque, and thus, two degrees of freedom in the current control process can be used for other purposes. In this dissertation, the selected purpose is current harmonic compensation.

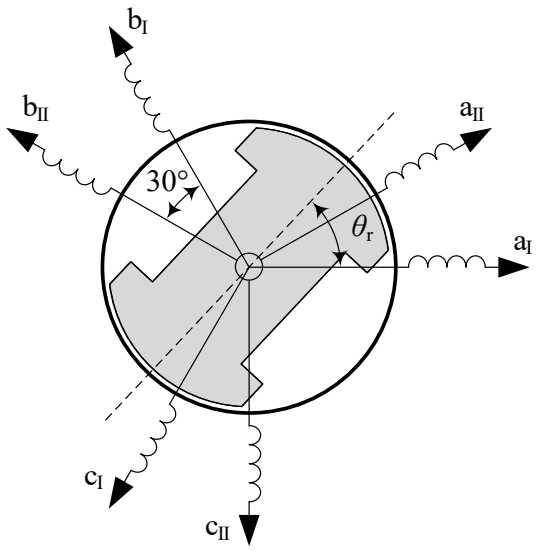

Fig. 2.1. Dual three-phase permanent magnet synchronous machine. Two sets of three-phase windings that are spatially shifted by 30 electrical degrees share the same stator frame but are galvanically isolated from each other (separate neutral points). The rotor angle θ_r refers to the angle between the direct axis of the rotor and the magnetic axis of phase a_I.

2.1 Alternative control methods

Various control schemes for dual three-phase machines have been suggested in the literature. The most feasible strategies are direct torque control (DTC), model predictive control (MPC), and vector control, which is commonly known as field-oriented control (FOC) in the case of IMs.

In conventional three-phase machines, the direct torque control (DTC) has proven itself to be a highly successful control strategy. The potential advantages of the DTC are well known. These benefits include a simple structure without a need for current control loops, fast torque response, and low sensitivity to parameter variation. Although the first DTC-based control schemes for dual three-phase machines were published already over a decade ago [75]–[77], the development of the DTC has still drawn considerable interest in recent years [70], [78]–[81]. The main problem with the DTC is that a straightforward extension of the classical three-phase DTC technique to dual three-phase machines introduces significant stator current harmonics. Because of the inherent nature of the DTC, it is difficult to achieve high-performance control of dual three-phase machines by this control strategy. It is clear that selecting a single voltage vector in each switching period solely relying on stator flux and torque requirements can easily lead to neglecting the other degrees of freedom in the current control process. Some recent papers have put a great deal of effort to reduce the current harmonics caused by the DTC [70], [78]–[81]. Although important progress has been achieved, it cannot yet be recommended to use DTC as a preferred control strategy for dual three-phase PMSM drives if current harmonics are aimed to be minimized.

Another potential way of implementing a high-performance drive control is the model predictive control (MPC) scheme. Predictive current control strategies use a model of the system to predict the future evolution of the currents. This prediction is evaluated for each possible alternative VSI switching state to determine the option that minimizes a specified cost function. Because the MPC predicts the optimal switching states for the VSI with a system model, it can avoid using separate current controllers and modulation methods. Several studies about the MPC applied for dual three-phase machines have been published [82]–[86]. Although it has been noted that the MPC can yield fast torque response, its feasibility is reduced by the fact that the prediction requires intensive computation and relies heavily on the accuracy of the system model and its parameters. Sensitivity to electrical parameter variations of the MPC in multiphase drives has been studied, and it has been shown that the accuracy of the inductance parameter values notably affects the control performance [88]. In addition, comparison with a vector control scheme has shown that the MPC can cause significantly higher average phase current ripple than the vector control [87]. From the perspective of current harmonic compensation, the problem of the MPC is that the cost function specifying the optimal VSI switching state becomes more complicated because the errors for all four independent current components must be considered. Thus, it cannot yet be recommended to use the MPC as a preferred control strategy for dual three-phase PMSM drives if current harmonics are aimed to be minimized.

Vector control, also known as field-oriented control (FOC), has been a very popular and well-proven control strategy for dual three-phase machines [12], [47], [49], [59]–[61], [89], [90]. It can also be noted that most of the challenges in the control of dual three-phase machines are related to issues with stator currents. Because the currents are directly controlled variables in vector control schemes, they can be effectively manipulated with these methods. This property offers a very effective way to solve current-related problems and strongly supports vector control as the recommended control method. There are two approaches for the vector control of dual three-phase machines. Both alternatives are discussed in the following sections.

For the purpose of the control, the machine model should adequately describe the dynamics of the machine as simply as possible. Thus, it is assumed in the following control schemes that the winding sets of the machine are geometrically and electromagnetically symmetrical, saturation and iron losses are negligible, and the PM flux and inductances contain only a fundamental component. Deviations from this ideal model such as PM flux harmonics are taken into consideration by treating them as external disturbance signals and model uncertainty.

2.2 Independent vector control of each winding set

The first approach for modelling and control of dual three-phase PMSMs is familiar from the early studies of multiphase machines. This method is nowadays called a double d–q winding representation [5], [9]. The double d–q winding approach considers both three-phase winding sets separately. Because both winding sets are modelled independently, the resulting machine model has two pairs of coupled d–q equations.

A conventional Clarke transformation is used to transform the measured phase currents into two-axis stationary reference frames of each winding set

$$\boldsymbol{T}_{\mathrm{abc}\rightarrow\alpha\beta} = \frac{2}{3}\begin{bmatrix} 1 & -\frac{1}{2} & -\frac{1}{2} \\ 0 & \frac{\sqrt{3}}{2} & -\frac{\sqrt{3}}{2} \end{bmatrix}, \tag{2.1}$$

$$\begin{aligned} \boldsymbol{i}_{\alpha\beta\mathrm{I}} &= \boldsymbol{T}_{\mathrm{abc}\rightarrow\alpha\beta}\, \boldsymbol{i}_{\mathrm{abcI}} \\ \boldsymbol{i}_{\alpha\beta\mathrm{II}} &= \boldsymbol{T}_{\mathrm{abc}\rightarrow\alpha\beta}\, \boldsymbol{i}_{\mathrm{abcII}}, \end{aligned} \tag{2.2}$$

where $\boldsymbol{i}_{\mathrm{abcI}} = [i_{\mathrm{aI}}\ i_{\mathrm{bI}}\ i_{\mathrm{cI}}]^{\mathrm{T}}$, $\boldsymbol{i}_{\mathrm{abcII}} = [i_{\mathrm{aII}}\ i_{\mathrm{bII}}\ i_{\mathrm{cII}}]^{\mathrm{T}}$, $\boldsymbol{i}_{\alpha\beta\mathrm{I}} = \left[i_{\alpha\mathrm{I}}\ i_{\beta\mathrm{I}}\right]^{\mathrm{T}}$, $\boldsymbol{i}_{\alpha\beta\mathrm{II}} = \left[i_{\alpha\mathrm{II}}\ i_{\beta\mathrm{II}}\right]^{\mathrm{T}}$, and the scaling coefficient $2/3$ gives an amplitude invariant transformation. The stationary reference frame of the first winding set α_{I}–β_{I} and the stationary reference frame of the second winding set α_{II}–β_{II} are symmetrical and equivalent in terms of frequency mapping and energy conversion. All the frequency components in the phase currents are mapped equivalently into both stationary frames, and coupling between the stator and the rotor occurs in both stationary frames.

To obtain a synchronous frame current control, a rotation transformation is applied to the stationary frame signals $\boldsymbol{i}_{\alpha\beta\mathrm{I}}$ and $\boldsymbol{i}_{\alpha\beta\mathrm{II}}$

$$\boldsymbol{T}_{\mathrm{rot}}(\theta_{\mathrm{r}}) = \begin{bmatrix} \cos(\theta_{\mathrm{r}}) & \sin(\theta_{\mathrm{r}}) \\ -\sin(\theta_{\mathrm{r}}) & \cos(\theta_{\mathrm{r}}) \end{bmatrix}, \tag{2.3}$$

$$\begin{bmatrix} i_{\mathrm{dI}} \\ i_{\mathrm{qI}} \end{bmatrix} = \boldsymbol{T}_{\mathrm{rot}}(\theta_{\mathrm{r}}) \begin{bmatrix} i_{\alpha\mathrm{I}} \\ i_{\beta\mathrm{I}} \end{bmatrix},$$
$$\begin{bmatrix} i_{\mathrm{dII}} \\ i_{\mathrm{qII}} \end{bmatrix} = \boldsymbol{T}_{\mathrm{rot}}\left(\theta_{\mathrm{r}} - \frac{\pi}{6}\right) \begin{bmatrix} i_{\alpha\mathrm{II}} \\ i_{\beta\mathrm{II}} \end{bmatrix}, \tag{2.4}$$

where θ_{r} is the electrical angle of the rotor. Assuming that a current control with a zero steady-state error is desired for the fundamental component and for the selected order of harmonics, it should hold for the current controllers $\boldsymbol{C}_{\mathrm{dqI}}(s)$ and $\boldsymbol{C}_{\mathrm{dqII}}(s)$ presented in Fig. 2.2 that

$$\left\|\boldsymbol{C}_{\mathrm{dqI}}(j\omega)\right\|_2 = \infty, \left\|\boldsymbol{C}_{\mathrm{dqII}}(j\omega)\right\|_2 = \infty \ : \ \omega \in \{h\omega_{\mathrm{r}} | h = 1,5,7,17,19 \ldots\}, \tag{2.5}$$

where $\|\cdot\|_2$ denotes the spectral norm (i.e., induced L_2 norm). For the model-based design of the current controllers, the machine model is required. The stator voltage equations of the machine in the synchronous reference frames $\mathrm{d_I}$–$\mathrm{q_I}$ and $\mathrm{d_{II}}$–$\mathrm{q_{II}}$ are

$$\begin{cases} u_{\mathrm{dI}} = R_{\mathrm{s}}\, i_{\mathrm{dI}} + L_{\mathrm{d}} \dfrac{\mathrm{d}\, i_{\mathrm{dI}}}{\mathrm{d}t} + M_{\mathrm{d}} \dfrac{\mathrm{d}\, i_{\mathrm{dII}}}{\mathrm{d}t} - \omega_{\mathrm{r}} L_{\mathrm{q}}\, i_{\mathrm{qI}} - \omega_{\mathrm{r}} M_{\mathrm{q}}\, i_{\mathrm{qII}} \\ u_{\mathrm{qI}} = R_{\mathrm{s}}\, i_{\mathrm{qI}} + L_{\mathrm{q}} \dfrac{\mathrm{d}\, i_{\mathrm{qI}}}{\mathrm{d}t} + M_{\mathrm{q}} \dfrac{\mathrm{d}\, i_{\mathrm{qII}}}{\mathrm{d}t} + \omega_{\mathrm{r}} L_{\mathrm{d}}\, i_{\mathrm{dI}} + \omega_{\mathrm{r}} M_{\mathrm{d}}\, i_{\mathrm{dII}} + \omega_{\mathrm{r}} \psi_{\mathrm{pm}} \\ u_{\mathrm{dII}} = R_{\mathrm{s}}\, i_{\mathrm{dII}} + L_{\mathrm{d}} \dfrac{\mathrm{d}\, i_{\mathrm{dII}}}{\mathrm{d}t} + M_{\mathrm{d}} \dfrac{\mathrm{d}\, i_{\mathrm{dI}}}{\mathrm{d}t} - \omega_{\mathrm{r}} L_{\mathrm{q}}\, i_{\mathrm{qII}} - \omega_{\mathrm{r}} M_{\mathrm{q}}\, i_{\mathrm{qI}} \\ u_{\mathrm{qII}} = R_{\mathrm{s}}\, i_{\mathrm{qII}} + L_{\mathrm{q}} \dfrac{\mathrm{d}\, i_{\mathrm{qII}}}{\mathrm{d}t} + M_{\mathrm{q}} \dfrac{\mathrm{d}\, i_{\mathrm{qI}}}{\mathrm{d}t} + \omega_{\mathrm{r}} L_{\mathrm{d}}\, i_{\mathrm{dII}} + \omega_{\mathrm{r}} M_{\mathrm{d}}\, i_{\mathrm{dI}} + \omega_{\mathrm{r}} \psi_{\mathrm{pm}} \end{cases}, \tag{2.6}$$

where ω_{r} is the electrical angular speed of the rotor, L_{d} and L_{q} are the self-synchronous inductances in the $\mathrm{d_I}$–$\mathrm{q_I}$ and $\mathrm{d_{II}}$–$\mathrm{q_{II}}$ frames, M_{d} and M_{q} are the mutual synchronous inductances between the $\mathrm{d_I}$–$\mathrm{q_I}$ and $\mathrm{d_{II}}$–$\mathrm{q_{II}}$ frames, ψ_{pm} is the permanent magnet flux linkage, and R_{s} is the stator resistance.

As a final step, Fig 2.2 shows that the synchronous frame voltage vectors are transformed back into the stationary reference frames α_{I}–β_{I} and α_{II}–β_{II} with the reverse rotation transformations. From the voltage vectors $\boldsymbol{u}_{\alpha\beta\mathrm{I}}$ and $\boldsymbol{u}_{\alpha\beta\mathrm{II}}$, a standard three-phase space vector modulation can be straightforwardly applied to produce the switching commands for the VSIs.

Note that the current control between the synchronous reference frames $\mathrm{d_I}$–$\mathrm{q_I}$ and $\mathrm{d_{II}}$–$\mathrm{q_{II}}$ is strongly coupled because of the magnetic coupling between the winding sets. In addition, the torque control (i.e., the control of the fundamental component) of the

machine can disturb the current harmonics compensation (and vice versa) because both operations are performed in the same frame. Although there are some problems, it is possible to successfully control the machine and compensate the current harmonics using a double d–q winding representation. The noteworthy benefit of this approach is the possibility to distinctly separate the contributions of each winding set for flux and torque. However, there is a more modern method for modelling and control of dual three-phase machines that can bring important advantages when considering the objectives of this dissertation.

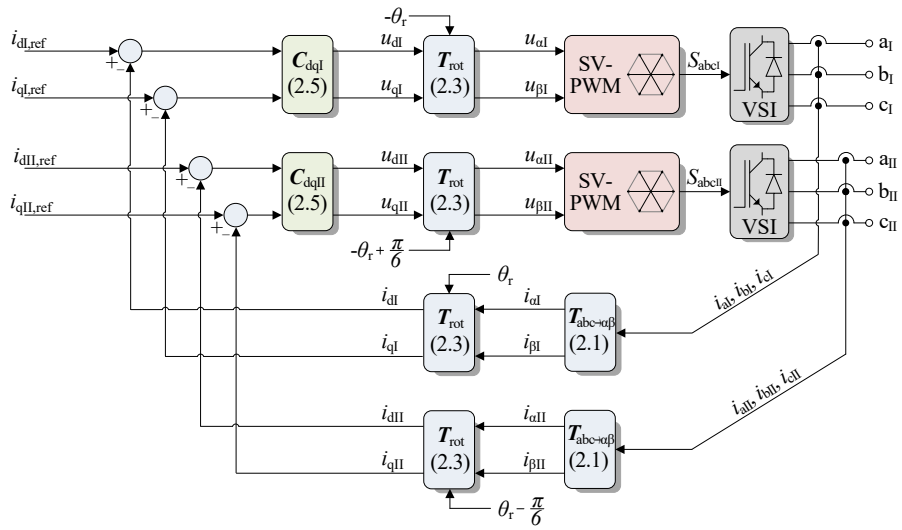

Fig. 2.2. Vector control scheme for dual three-phase PMSMs based on a double d–q winding representation. The control of each winding set is performed separately in a synchronous reference frame of its own.

2.3 Decoupled vector control of both winding sets

An alternative modelling and control approach is to treat both three-phase winding sets as a single entity. This approach is called a VSD method [12]. The VSD transformation has become a standard technique to model and control multiphase machines. The current control scheme presented in Fig. 2.3 is also based on this type of technique. To be specific, the machine model discussed in this section is based on the study of salient pole dual three-phase PMSMs presented in [91]. Methods to determine the parameter values for the machine model have been studied in [92] and [93].

First, using the VSD transformation matrix, the measured phase currents are transformed into two decoupled two-axis stationary reference frames (also frequently referred to as orthogonal subspaces) as follows:

$$\boldsymbol{T}_{\mathrm{abc}\to\mathrm{AB}} = \frac{1}{3}\begin{bmatrix} 1 & -\frac{1}{2} & -\frac{1}{2} & \frac{\sqrt{3}}{2} & -\frac{\sqrt{3}}{2} & 0 \\ 0 & \frac{\sqrt{3}}{2} & -\frac{\sqrt{3}}{2} & \frac{1}{2} & \frac{1}{2} & -1 \\ 0 & \frac{\sqrt{3}}{2} & -\frac{\sqrt{3}}{2} & -\frac{1}{2} & -\frac{1}{2} & 1 \\ -1 & \frac{1}{2} & \frac{1}{2} & \frac{\sqrt{3}}{2} & -\frac{\sqrt{3}}{2} & 0 \end{bmatrix}, \tag{2.7}$$

$$\begin{bmatrix} \boldsymbol{i}_{\mathrm{ABm}} \\ \boldsymbol{i}_{\mathrm{ABs}} \end{bmatrix} = \boldsymbol{T}_{\mathrm{abc}\to\mathrm{AB}}\, \boldsymbol{i}_{\mathrm{abc}}, \tag{2.8}$$

where $\boldsymbol{i}_{\mathrm{abc}} = [i_{\mathrm{aI}}\ i_{\mathrm{bI}}\ i_{\mathrm{cI}}\ i_{\mathrm{aII}}\ i_{\mathrm{bII}}\ i_{\mathrm{cII}}]^{\mathrm{T}}$, $\boldsymbol{i}_{\mathrm{ABm}} = [i_{\mathrm{Am}}\ i_{\mathrm{Bm}}]^{\mathrm{T}}$, and $\boldsymbol{i}_{\mathrm{ABs}} = [i_{\mathrm{As}}\ i_{\mathrm{Bs}}]^{\mathrm{T}}$. In this dissertation, these reference frames are called the main stationary frame $\mathrm{A_m}$–$\mathrm{B_m}$ and the secondary stationary frame $\mathrm{A_s}$–$\mathrm{B_s}$. The characteristic difference between the main frame and the secondary frame is that the transformation (2.7) maps the fundamental component and the harmonics of the order ($12n \pm 1$, $n = 1, 2, 3\ldots$) into the $\mathrm{A_m}$–$\mathrm{B_m}$ frame and the harmonics of the order ($6n \pm 1$, $n = 1, 3, 5\ldots$) into the $\mathrm{A_s}$–$\mathrm{B_s}$frame. Ideally, coupling between the stator and the rotor occurs only in the main $\mathrm{A_m}$–$\mathrm{B_m}$ frame, which thus describes all the electromechanical energy conversion of the machine. The current harmonic components in the secondary $\mathrm{A_s}$–$\mathrm{B_s}$ frame cannot be used to produce torque but they cause additional losses, and consequently, reduce the efficiency of the machine.

To obtain a synchronous frame current control, a rotation transformation (2.3) is applied to the stationary frame signals $\boldsymbol{i}_{\mathrm{ABm}}$ and $\boldsymbol{i}_{\mathrm{ABs}}$

$$\begin{aligned} \begin{bmatrix} i_{\mathrm{Dm}} \\ i_{\mathrm{Qm}} \end{bmatrix} &= \boldsymbol{T}_{\mathrm{rot}}(\theta_{\mathrm{r}}) \begin{bmatrix} i_{\mathrm{Am}} \\ i_{\mathrm{Bm}} \end{bmatrix}, \\ \begin{bmatrix} i_{\mathrm{Ds}} \\ i_{\mathrm{Qs}} \end{bmatrix} &= \boldsymbol{T}_{\mathrm{rot}}(\theta_{\mathrm{r}}) \begin{bmatrix} i_{\mathrm{As}} \\ i_{\mathrm{Bs}} \end{bmatrix}. \end{aligned} \tag{2.9}$$

Considering the frequency mapping between the main $\mathrm{A_m}$–$\mathrm{B_m}$ frame and the secondary $\mathrm{A_s}$–$\mathrm{B_s}$ frame, the DC component of $\boldsymbol{i}_{\mathrm{DQm}}$ gives the synchronous frame current vector of the fundamental component. Because the $\mathrm{D_s}$–$\mathrm{Q_s}$ reference frame is also rotating synchronously at the fundamental frequency, the 5th and 7th harmonics in the phase current appear as positive- and negative-sequence 6th harmonics in the $\mathrm{D_s}$–$\mathrm{Q_s}$ reference frame. Assuming that a current control with a zero steady-state error is desired for the fundamental component and for the selected order of harmonics, it should hold for the current controllers $\boldsymbol{C}_{\mathrm{DQm}}(s)$ and $\boldsymbol{C}_{\mathrm{DQs}}(s)$ presented in Fig. 2.3 that

$$\left\|\boldsymbol{C}_{\mathrm{DQm}}(j\omega)\right\|_2 = \infty \ : \ \omega \in \{h\omega_{\mathrm{r}} | h = 1\}, \tag{2.10}$$

$$\left\|\boldsymbol{C}_{\mathrm{DQs}}(j\omega)\right\|_2 = \infty \ : \ \omega \in \{h\omega_{\mathrm{r}} | h = 5{,}7{,}17{,}19\ldots\}. \tag{2.11}$$

Based on (2.7), the stator voltage equations of the machine in the D_m–Q_m reference frame are

$$\begin{cases} u_{\mathrm{Dm}} = R_{\mathrm{s}}\, i_{\mathrm{Dm}} + L_{\mathrm{Dm}} \dfrac{\mathrm{d}i_{\mathrm{Dm}}}{\mathrm{d}t} - \omega_{\mathrm{r}} L_{\mathrm{Qm}}\, i_{\mathrm{Qm}} \\ u_{\mathrm{Qm}} = R_{\mathrm{s}}\, i_{\mathrm{Qm}} + L_{\mathrm{Qm}} \dfrac{\mathrm{d}i_{\mathrm{Qm}}}{\mathrm{d}t} + \omega_{\mathrm{r}} L_{\mathrm{Dm}}\, i_{\mathrm{Dm}} + \omega_{\mathrm{r}} \psi_{\mathrm{pm}} \end{cases} \tag{2.12}$$

and in the D_s–Q_s reference frame

$$\begin{cases} u_{\mathrm{Ds}} = R_{\mathrm{s}}\, i_{\mathrm{Ds}} + L_{\mathrm{Ds}} \dfrac{\mathrm{d}i_{\mathrm{Ds}}}{\mathrm{d}t} - \omega_{\mathrm{r}} L_{\mathrm{Qs}}\, i_{\mathrm{Qs}} \\ u_{\mathrm{Qs}} = R_{\mathrm{s}}\, i_{\mathrm{Qs}} + L_{\mathrm{Qs}} \dfrac{\mathrm{d}i_{\mathrm{Qs}}}{\mathrm{d}t} + \omega_{\mathrm{r}} L_{\mathrm{Ds}}\, i_{\mathrm{Ds}} \end{cases}, \tag{2.13}$$

where L_{Dm} and L_{Qm} are the D_m–Q_m frame synchronous inductances, L_{Ds} and L_{Qs} are D_s–Q_s frame synchronous inductances, and R_s is the stator resistance.

The current control is performed adopting the VSD approach. However, a standard three-phase space vector modulation is applied to produce the switching commands for the VSIs. Thus, the synchronous frame voltage vectors are first transformed back into the A_m–B_m and A_s–B_s frames with reverse rotation transformations. The resulting signals $\boldsymbol{u}_{\mathrm{ABm}}$ and $\boldsymbol{u}_{\mathrm{ABs}}$ are further transformed into the conventional three-phase stationary frames of the first winding set α_I–β_I and the second winding set α_{II}–β_{II}

$$\boldsymbol{T}_{\mathrm{AB}\to\alpha\beta} = \begin{bmatrix} 1 & 0 & 0 & -1 \\ 0 & 1 & 1 & 0 \\ \dfrac{\sqrt{3}}{2} & \dfrac{1}{2} & -\dfrac{1}{2} & \dfrac{\sqrt{3}}{2} \\ -\dfrac{1}{2} & \dfrac{\sqrt{3}}{2} & -\dfrac{\sqrt{3}}{2} & -\dfrac{1}{2} \end{bmatrix}, \tag{2.14}$$

$$\begin{bmatrix} \boldsymbol{u}_{\alpha\beta\mathrm{I}} \\ \boldsymbol{u}_{\alpha\beta\mathrm{II}} \end{bmatrix} = \boldsymbol{T}_{\mathrm{AB}\to\alpha\beta} \begin{bmatrix} \boldsymbol{u}_{\mathrm{ABm}} \\ \boldsymbol{u}_{\mathrm{ABs}} \end{bmatrix}. \tag{2.15}$$

where $\boldsymbol{u}_{\alpha\beta\mathrm{I}} = \begin{bmatrix} u_{\alpha\mathrm{I}} & u_{\beta\mathrm{I}} \end{bmatrix}^{\mathrm{T}}$, and $\boldsymbol{u}_{\alpha\beta\mathrm{II}} = \begin{bmatrix} u_{\alpha\mathrm{II}} & u_{\beta\mathrm{II}} \end{bmatrix}^{\mathrm{T}}$. The voltage vectors $\boldsymbol{u}_{\alpha\beta\mathrm{I}}$ and $\boldsymbol{u}_{\alpha\beta\mathrm{II}}$ in the conventional three-phase stationary frames α_I–β_I and α_{II}–β_{II} are finally used with a standard three-phase space vector PWM to generate the switching commands for the VSIs.

It is emphasized that the current control between the main D_m–Q_m frame and the secondary D_s–Q_s, frame is fully decoupled. As a result, the torque control (i.e., the control of the fundamental component) of the machine does not regulate the current harmonics in the secondary frame. On the other hand, the control of the current harmonics has no direct effect on the torque control of the machine when the voltage available is not limited.

Considering the current control, D_m–Q_m is the frame where the torque production of the machine is controlled, and D_s–Q_s is the frame where the balance between the winding sets and the current harmonics is controlled. Although torque control is studied in detail in **Publication II**, this introductory part of the dissertation focuses only on the current harmonic control in the D_s–Q_s reference frame.

The frequency mapping properties of the VSD approach make the transformation (2.7) a preferable choice to implement current harmonic compensation methods for dual three-phase PMSMs. The inherent decoupling of the fundamental component from the undesired harmonics facilitates the control design process. Because of the decoupling property, no filters are required to isolate the frequency bands of the controllers for the fundamental component and the harmonics. In addition, it is computationally efficient that a single pair of controllers in the secondary frame can perform the current harmonic compensation of both winding sets.

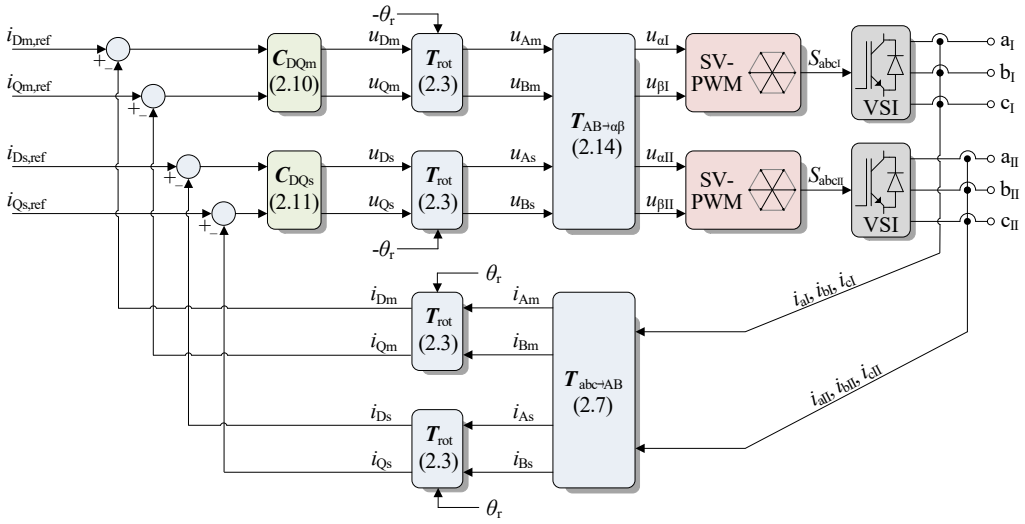

Fig. 2.3. Vector control scheme for dual three-phase PMSMs based on a VSD approach. The current control of both winding sets is performed simultaneously in two decoupled synchronous reference frames.

3 Stability and performance evaluation

Comparing a selection of control methods and stating that one alternative is better than the other always depends on how the methods are evaluated. There are numerous measures that can be applied to evaluate control methods and compare the quality of the controlled responses. The criteria used in this dissertation are explicitly defined in this chapter. The theoretical analysis focuses on the frequency domain measures, and the experimental results consider the time-domain evaluation.

3.1 Time-domain dynamic performance

Time-domain evolution of the transient response of the system is often considered an important source of information when the performance of the system is evaluated. In current harmonic compensation, it is of interest to know how quickly the method in question can remove the harmonics. In addition, it is convenient to design the control parameters based on the desired closed-loop dynamic performance of the harmonic compensation. In this dissertation, the time-domain dynamic performance is measured as a decay rate λ of the exponential envelope of the transient response (see Fig. 3.1). As a very concrete performance indicator, the decay rate λ is easy to comprehend and can be straightforwardly measured from an experimental setup.

In terms of control theory, the pole locations of the closed-loop system determine the dynamic performance. The nominal closed-loop poles can be solved from the transfer function matrix of the system. The real part of a specific pole equals the decay rate λ associated with that pole. Thus, stable poles far from the imaginary axis correspond to a fast dynamic performance, and poles near the imaginary axis correspond to a slow dynamic performance.

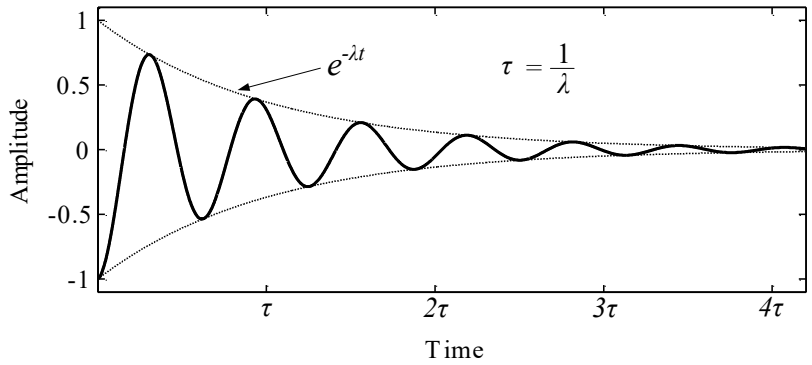

Fig. 3.1. Exponential decay of the transient response. The decay rate λ determines how quickly the system can eliminate the transient. The time constant τ of the exponential envelope curve is the reciprocal of the decay rate.

3.2 Robustness analysis

It can be seen from Fig. 2.3 that the current harmonic compensation scheme can be presented as a simplified one-degree-of-freedom feedback loop shown in Fig. 3.2. Generally speaking, the current harmonic compensation in dual three-phase PMSMs can be viewed as a plant input disturbance rejection problem. Thus, the aim of the harmonic controller $\boldsymbol{C}(s)$ is to minimize the effect of the plant input disturbance $\boldsymbol{d}_{\mathrm{DQ}}$ on the current harmonic $\boldsymbol{i}_{\mathrm{DQ}}$.

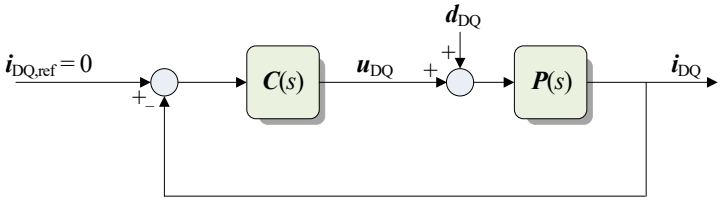

Fig. 3.2. Current harmonic compensation presented as a simplified feedback loop. The disturbance $\boldsymbol{d}_{\mathrm{DQ}}$ consists mainly of back-EMF harmonics and voltage harmonics caused by the VSI. The plant model $\boldsymbol{P}(s)$ is the machine model (3.2).

For the system shown in Fig. 3.2, the nominal closed-loop system is the transfer function matrix from the plant input disturbance $\boldsymbol{d}_{\mathrm{DQ}}$ to the output $\boldsymbol{i}_{\mathrm{DQ}}$

$$\boldsymbol{H}_{\mathrm{di}}(s) = (\boldsymbol{I} + \boldsymbol{PC})^{-1}\boldsymbol{P}, \tag{3.1}$$

where $\boldsymbol{I}$ is the identity matrix and $\boldsymbol{P}(s)$ is the transfer function matrix representation of the nominal machine model

$$\begin{aligned} \boldsymbol{i}_{\mathrm{DQ}} &= \frac{1}{p(s)}\begin{bmatrix} R_{\mathrm{s}} + sL_{\mathrm{Q}} & \omega_{\mathrm{r}}L_{\mathrm{Q}} \\ -\omega_{\mathrm{r}}L_{\mathrm{D}} & R_{\mathrm{s}} + sL_{\mathrm{D}} \end{bmatrix}\boldsymbol{u}_{\mathrm{DQ}} \\ p(s) &= s^2L_{\mathrm{D}}L_{\mathrm{Q}} + s\left(L_{\mathrm{D}}+L_{\mathrm{Q}}\right)R_{\mathrm{s}} + R_{\mathrm{s}}^2 + \omega_{\mathrm{r}}^2L_{\mathrm{D}}L_{\mathrm{Q}} \end{aligned}. \tag{3.2}$$

Note that the presented robustness analysis does not make a difference between the main $\mathrm{D_m}$–$\mathrm{Q_m}$ frame and the secondary $\mathrm{D_s}$–$\mathrm{Q_s}$ frame. Therefore, the subscripts m and s to separate the D–Q frames are omitted in this section.

A control system is said to be robust if it can tolerate variations in the dynamics of the system without significant changes in stability and performance. In the system under study, it is impossible to avoid the fact that the machine model contains some parametric uncertainty. In addition, the exact values of the supply voltages of the machine are not known because of the nonideal behaviour of the VSI. The time delay also greatly affects the stability and performance of the system. In this dissertation, the robustness of the system is analysed with explicit consideration of the time delay, parameter uncertainty, and supply voltage uncertainty. The robustness is studied using the SSV analysis [94]–[96]. This analysis method has been used to investigate the robustness of electric power

systems in [97] and [98]. The SSV analysis is intended for linear systems, and thus, the rotational speed of the machine ω_r is assumed to be a quasi-constant variable compared with the electrical dynamics.

The parametric uncertainty in the machine model (3.2) is specified by assuming that the actual value of each uncertain parameter is bound within some interval but otherwise unknown, thereby giving a parameter set

$$\begin{aligned} R_\mathrm{s} &= R_\mathrm{s0} \pm \Delta R_\mathrm{s} \\ L_\mathrm{Q} &= L_\mathrm{Q0} \pm \Delta L_\mathrm{Q}, \\ L_\mathrm{D} &= L_\mathrm{D0} \pm \Delta L_\mathrm{D} \end{aligned} \tag{3.3}$$

where $R_\mathrm{s}, L_\mathrm{D}$, and L_Q are the actual values of the parameters $R_\mathrm{s0}, L_\mathrm{D0}$, and L_Q0 are the nominal values, and $\Delta R_\mathrm{s}, \Delta L_\mathrm{D}$, and ΔL_Q are the absolute uncertainties in them. In the robustness analysis of this dissertation, it is assumed that there is a ±50% uncertainty in all the parameters.

The supply voltages unavoidably contain delay because of the discrete nature of the control system and the PWM operation of the VSI. It is usually assumed that the length of the time delay T_d caused by the computation and modulation is $T_\mathrm{d} = 1.5T_\mathrm{s}$, where T_s is the sampling time of the control system. In addition, the output voltage vector of the VSI can have some level of error in magnitude and direction. Thus, the supply voltage uncertainty is modelled here using the relation

$$\boldsymbol{u}_\mathrm{DQ}^\mathrm{actual} = e^{-sT_\mathrm{d}}\left(\boldsymbol{u}_\mathrm{DQ}^\mathrm{ideal} + \boldsymbol{E}_\mathrm{U}(s)\boldsymbol{u}_\mathrm{DQ}^\mathrm{ideal}\right), \tag{3.4}$$

where $\boldsymbol{E}_\mathrm{U}(s)$ describes the set of all possible errors in the supply voltage. In this case, $\boldsymbol{E}_\mathrm{U}(s) = \Delta_\mathrm{U}(s)\boldsymbol{W}_\mathrm{U}(s)$, where $\boldsymbol{W}_\mathrm{U}(s)$ is the uncertainty weight, and $\Delta_\mathrm{U}(s)$ is the set of all stable transfer function matrices that satisfy the $\mathcal{H}_\infty$ norm bound $\|\Delta_\mathrm{U}\|_\infty < 1$. The uncertainty weight $\boldsymbol{W}_\mathrm{U}(s)$ specifies the level of tolerance within which the actual voltage is assumed to be found. In the following analysis, a worst-case error of 20% in the voltage and 5 kHz sampling frequency are assumed, thereby yielding $\boldsymbol{W}_\mathrm{U}(s) = 0.2\boldsymbol{I}$ and $T_\mathrm{d} = 0.3$ ms.

The complete uncertainty description of the system is obtained by combining the supply voltage uncertainty (3.4) with the parameter uncertainty (3.3) as presented in Fig. 3.3. Because the uncertainty is described here as it actually physically occurs, the analysis can be expected to give a realistic view of the robustness of the system.

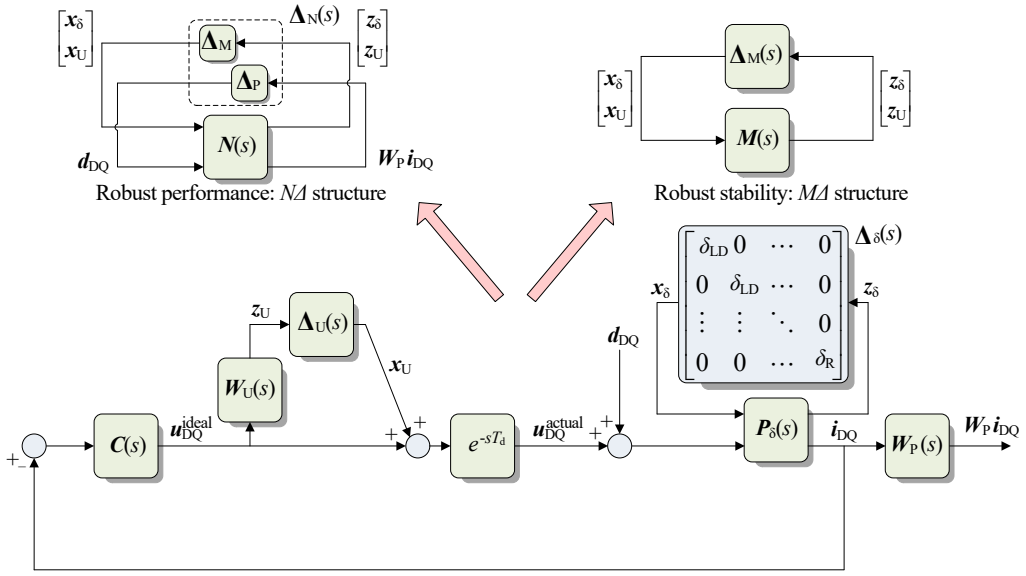

Fig. 3.3. Uncertainty description of the control system. The machine model includes parameter uncertainty, which is combined with the multiplicative supply voltage uncertainty. The system is represented as an *M*Δ structure for the robust stability analysis and as an *N*Δ structure for the robust performance analysis.

3.2.1 Robust stability

In the SSV robust stability analysis, all the separate uncertainty blocks of the system are combined into a single block-diagonal uncertainty matrix $\Delta_{\mathrm{M}}(s)$. For the system in Fig. 3.3, the uncertainty blocks are $\Delta_{\mathrm{U}}(s)$ and $\Delta_{\delta}(s)$. Assuming that the nominal system (i.e., $\Delta_{\mathrm{M}}(s) = 0$) is stable, the feedback loop containing the uncertainty matrix $\Delta_{\mathrm{M}}(s)$ is the only reason for the uncertain system to become unstable. Thus, the stability of the system is determined by the transfer function matrix $\boldsymbol{M}(s)$ that is seen from the input and output of $\Delta_{\mathrm{M}}(s)$.

The loop containing the interconnection matrix $\boldsymbol{M}(s)$ and the block-diagonal uncertainty matrix $\Delta_{\mathrm{M}}(s)$ is known as an *M*Δ structure (see Fig. 3.3). The robust stability of the *M*Δ structure, and consequently, the whole system, is determined by

$$k_{\mathrm{RS}} = \frac{1}{\max\limits_{\omega}\left[\mu_{\Delta_{\mathrm{M}}}\left(\boldsymbol{M}(j\omega)\right)\right]}, \tag{3.5}$$

where k_{RS} is a robust stability margin and μ denotes a structured singular value, which is, in this case, calculated with respect to the structure of $\Delta_{\mathrm{M}}(s)$. The robust stability margin defines how large a percentage of the specified uncertainty level the system can tolerate before becoming unstable.

It can be derived that the transfer function matrix representation $\boldsymbol{P}_\delta(s)$ of the parameter uncertain machine model presented in Fig. 3.3 is

$$\boldsymbol{P}_\delta(s) = \frac{1}{p}\begin{bmatrix} -f_1\Delta L_\mathrm{D} & -g_3\Delta L_\mathrm{D} & -g_3\Delta L_\mathrm{D} & f_1\Delta L_\mathrm{D} & -f_1\Delta L_\mathrm{D} & -g_3\Delta L_\mathrm{D} & f_1\Delta L_\mathrm{D} & g_3\Delta L_\mathrm{D} \\ -f_2\Delta L_\mathrm{D} & -g_4\Delta L_\mathrm{D} & -g_4\Delta L_\mathrm{D} & f_2\Delta L_\mathrm{D} & -f_2\Delta L_\mathrm{D} & -g_4\Delta L_\mathrm{D} & f_2\Delta L_\mathrm{D} & g_4\Delta L_\mathrm{D} \\ f_3\Delta L_\mathrm{Q} & -g_1\Delta L_\mathrm{Q} & -g_1\Delta L_\mathrm{Q} & -f_3\Delta L_\mathrm{Q} & f_3\Delta L_\mathrm{Q} & -g_1\Delta L_\mathrm{Q} & -f_3\Delta L_\mathrm{Q} & g_1\Delta L_\mathrm{Q} \\ f_4\Delta L_\mathrm{Q} & -g_2\Delta L_\mathrm{Q} & -g_2\Delta L_\mathrm{Q} & -f_4\Delta L_\mathrm{Q} & f_4\Delta L_\mathrm{Q} & -g_2\Delta L_\mathrm{Q} & -f_4\Delta L_\mathrm{Q} & g_2\Delta L_\mathrm{Q} \\ -f_5\Delta R_\mathrm{s} & -g_6\Delta R_\mathrm{s} & -g_6\Delta R_\mathrm{s} & f_5\Delta R_\mathrm{s} & -f_5\Delta R_\mathrm{s} & -g_6\Delta R_\mathrm{s} & f_5\Delta R_\mathrm{s} & g_6\Delta R_\mathrm{s} \\ f_6\Delta R_\mathrm{s} & -g_5\Delta R_\mathrm{s} & -g_5\Delta R_\mathrm{s} & -f_6\Delta R_\mathrm{s} & f_6\Delta R_\mathrm{s} & -g_5\Delta R_\mathrm{s} & -f_6\Delta R_\mathrm{s} & g_5\Delta R_\mathrm{s} \\ -f_5 & -g_6 & -g_6 & f_5 & -f_5 & -g_6 & f_5 & g_6 \\ f_6 & -g_5 & -g_5 & -f_6 & f_6 & -g_5 & -f_6 & g_5 \end{bmatrix}, \tag{3.6}$$

$$f_1 = s^2L_\mathrm{Q} + sR_\mathrm{s}, f_2 = sL_\mathrm{Q}\omega_\mathrm{r} + R_\mathrm{s}\omega_\mathrm{r}, f_3 = sL_\mathrm{D}\omega_\mathrm{r}, f_4 = L_\mathrm{D}\omega_\mathrm{r}^2, f_5 = sL_\mathrm{Q} + R_\mathrm{s}, f_6 = L_\mathrm{D}\omega_\mathrm{r}$$

$$g_1 = s^2L_\mathrm{D} + sR_\mathrm{s}, g_2 = sL_\mathrm{D}\omega_\mathrm{r} + R_\mathrm{s}\omega_\mathrm{r}, g_3 = sL_\mathrm{Q}\omega_\mathrm{r}, g_4 = L_\mathrm{Q}\omega_\mathrm{r}^2, g_5 = sL_\mathrm{D} + R_\mathrm{s}, g_6 = L_\mathrm{Q}\omega_\mathrm{r}$$

$$p(s) = s^2L_\mathrm{D}L_\mathrm{Q} + s\big(L_\mathrm{D}{+}L_\mathrm{Q}\big)R_\mathrm{s} + R_\mathrm{s}^2 + \omega_\mathrm{r}^2L_\mathrm{D}L_\mathrm{Q}$$

where the input vector of $\boldsymbol{P}_\delta(s)$ is $\begin{bmatrix} z_1 & z_2 & z_3 & z_4 & z_5 & z_6 & \boldsymbol{i}_\mathrm{DQ} \end{bmatrix}^\mathrm{T}$, and the output vector is $\begin{bmatrix} x_1 & x_2 & x_3 & x_4 & x_5 & x_6 & \boldsymbol{u}_\mathrm{DQ} \end{bmatrix}^\mathrm{T}$. The block diagram in Fig. 3.3 without the uncertain machine model can be represented as a transfer function matrix

$$\boldsymbol{Q}_\mathrm{RS}(s) = \begin{bmatrix} -\boldsymbol{C}e^{-sT_\mathrm{d}} & \boldsymbol{I}e^{-sT_\mathrm{d}} \\ -\boldsymbol{W}_\mathrm{U}\boldsymbol{C} & 0 \end{bmatrix}, \tag{3.7}$$

where the input vector of $\boldsymbol{Q}_\mathrm{RS}(s)$ is $\begin{bmatrix} \boldsymbol{i}_\mathrm{DQ} & \boldsymbol{x}_\mathrm{U} \end{bmatrix}^\mathrm{T}$ and the output vector is $\begin{bmatrix} \boldsymbol{u}_\mathrm{DQ} & \boldsymbol{z}_\mathrm{U} \end{bmatrix}^\mathrm{T}$. The interconnection matrix $\boldsymbol{M}(s)$ of the complete system is obtained from

$$\boldsymbol{M}(s) = \boldsymbol{S}(\boldsymbol{Q}_\mathrm{RS}, \boldsymbol{P}_\delta), \tag{3.8}$$

where operator $\boldsymbol{S}$ denotes the Redheffer star product [95].

3.2.2 Robust performance

The stability of the system is a necessity, but it is also highly desirable that the performance remains satisfactory under modelling errors. The system is said to have a robust performance if it satisfies the performance specifications for all possible plants in the uncertainty set. Note that a robustly stable system does not necessarily have a robust performance. The SSV analysis provides means to study the robust performance in the frequency domain. The performance in the frequency domain is defined here as a magnitude response from the plant input disturbance $\boldsymbol{d}_\mathrm{DQ}$ to the harmonic currents $\boldsymbol{i}_\mathrm{DQ}$.

To include the performance specification in the SSV analysis, a fictitious uncertainty block $\Delta_\mathrm{P}(s)$ is used to produce the block-diagonal uncertainty matrix $\Delta_\mathrm{N}(s)$. The performance weight $\boldsymbol{W}_\mathrm{p}(s) = w_\mathrm{p}(s)\boldsymbol{I}$ determines the desired magnitude response. The stability of the resulting $N\Delta$ structure specifies the robust performance of the system. Robustness of the frequency-domain performance is measured here by determining how large the magnitude response can be for all the plants in the uncertainty set (i.e., the worst-case gain analysis). The worst-case gain curve is obtained by iterating the magnitude of

the performance weight $|w_{\mathrm{p}}(j\omega)|$ for each frequency so that the SSV of the interconnection matrix $\boldsymbol{N}(s)$ becomes unity. When this condition is satisfied, the reciprocal of the performance weight gives the worst-case gain curve

$$\max_{\Delta_{\mathrm{N}}} \|\boldsymbol{H}_{\mathrm{di}}(j\omega)\|_2 = \left|w_{\mathrm{p}}(j\omega)\right|^{-1} \Leftrightarrow \mu_{\Delta_{\mathrm{N}}}\left(\boldsymbol{N}(j\omega)\right) = 1. \tag{3.9}$$

Because $\boldsymbol{N}(s)$ includes the performance specification, representing the block diagram in Fig. 3.3 without the uncertain machine model now yields

$$\boldsymbol{Q}_{\mathrm{RP}}(s) = \begin{bmatrix} -\boldsymbol{C}e^{-sT_{\mathrm{d}}} & \boldsymbol{I}e^{-sT_{\mathrm{d}}} & \boldsymbol{I} \\ -\boldsymbol{W}_{\mathrm{U}}\boldsymbol{C} & 0 & 0 \\ \boldsymbol{W}_{\mathrm{p}} & 0 & 0 \end{bmatrix} \tag{3.10}$$

where the input vector of $\boldsymbol{Q}_{\mathrm{RP}}(s)$ is $\left[\boldsymbol{i}_{\mathrm{DQ}}\, \boldsymbol{x}_{\mathrm{U}}\, \boldsymbol{d}_{\mathrm{DQ}}\right]^{\mathrm{T}}$, and the output vector is $\left[\boldsymbol{u}_{\mathrm{DQ}}\, \boldsymbol{z}_{\mathrm{U}}\, \boldsymbol{W}_{\mathrm{p}}\boldsymbol{i}_{\mathrm{DQ}}\right]^{\mathrm{T}}$. No other changes are required compared with the robust stability analysis. Thus, the interconnection matrix $\boldsymbol{N}(s)$ is

$$\boldsymbol{N}(s) = \boldsymbol{S}(\boldsymbol{Q}_{\mathrm{RP}}, \boldsymbol{P}_{\delta}). \tag{3.11}$$

4 Current harmonic compensation

Stator current harmonics are a well-known disadvantage of dual three-phase machines. The obvious problem is that the current harmonics increase the losses of the machine. The harmonics can also significantly raise the peak of the phase current that may cause a demand for increased device ratings of the power electronics required to supply the machine. Moreover, the increased peak value of the phase current may lead, for example, to overcurrent tripping of the fault protection system. Finally, the performance of some control algorithms may be degraded by the presence of the harmonics.

In the literature, it has been suggested that the stator current harmonics can be reduced by using passive or active methods. Passive methods usually aim to increase the impedance of the harmonic current path. It has been proposed that the impedance seen by the harmonic component can be increased with external filters [54], a special slot shape design of the machine that increases the leakage inductance [48], or adding magnetic rings to the end winding structure of the machine [99]. Current harmonics can also be eliminated by a specific machine design using a dissimilar pole number in each three-phase winding set [100]. Although these approaches work, they also tend to increase the cost and decrease the efficiency of the system, and cannot thus be recommended.

A preferable alternative is to use active methods that aim to counteract and compensate for the excitation of the current harmonics. In this way, current harmonics can be reduced by using the current control and VSI of the electric machine drive. Hence, no external modifications to the system are required. This active approach is often referred to as the current harmonic compensation.

4.1 Stator current harmonics as a control problem

The reason for the major drawback of current harmonics is the winding structure of the dual three-phase machine, which causes the flux components resulting from the stator current harmonics of the order ($6n \pm 1$, $n = 1, 3, 5\ldots$) to cancel each other from the air gap when the supplied currents have a 30-degree phase shift (as it generally always is). Because these current harmonics do not produce the air-gap flux, they are only limited by the stator resistance and the leakage inductance of the machine. Therefore, even a small excitation of these components can lead to significant corresponding current harmonics. The fact that the current harmonics do not affect the air-gap flux also means that they have no impact on torque pulsation. Thus, the feature that is considered an advantage of dual three-phase machines is also causing a notable problem of this machine type.

Dual three-phase PMSM drives have two main sources of stator current harmonics. The first source is the supplying inverters. VSIs can cause stator current harmonics if the supplied voltage contains harmonic components of the order ($6n \pm 1$, $n = 1, 3, 5\ldots$). Thus, the modulated voltage waveform should not contain unwanted low-frequency voltage

harmonics. For example, the inverter dead time can cause voltage harmonics. The modulation method itself also affects the frequency content of the supplied voltages.

The second source of harmonics is the internal structure of the PMSM itself. Permanent magnets may not produce pure sinusoidal flux distribution, and rotor saliency, pole shape, and possible magnetic saturation can cause harmonics in the air gap. These nonidealities can be a major problem in dual three-phase PMSMs because they can easily produce large internally generated current harmonics. The magnitude of the current harmonic component caused by the internal structure of the machine decreases quickly as the order of the harmonic increases because the amount of harmonic excitation decreases and the impedance increases with the frequency. Thus, of all the harmonics of the order ($6n \pm 1$, $n = 1, 3, 5\ldots$), only the 5^{th} and 7^{th} are likely to cause problems in practice. In this dissertation, the current harmonic compensation is aimed to be effective only against the 5^{th}- and 7^{th}-order harmonics in the phase current. The $\mathrm{D_s}$–$\mathrm{Q_s}$ reference frame where the harmonic compensation is analysed and implemented is rotating synchronously at the fundamental frequency. Therefore, it is assumed in the rest of the dissertation that the frequency of the harmonic to be eliminated is $\omega = \pm 6\omega_\mathrm{r}$ in the $\mathrm{D_s}$–$\mathrm{Q_s}$ reference frame.

It can be concluded from the above description that with respect to the control design, the current harmonics are caused by a set of external and internal disturbances. This set can be effectively modelled as a lumped disturbance acting on the input of the machine model as shown in Fig. 3.2.

4.2 Compensation using feedback control

The established solution to eliminate current harmonics is to use some kind of a current harmonic control method. Suitable methods have mostly been studied in relation to active power filters (APFs) and other grid-connected inverter applications. Frequently encountered solutions in this field are a repetitive controller in the fundamental synchronous or stationary reference frame, a proportional-integral (PI) controller in the harmonic synchronous reference frame, a proportional-resonant (PR) controller in the fundamental or stationary reference frame, a vector PI (VPI) controller in the harmonic reference frame, and a vector PR (VPR) controller in the fundamental or stationary reference frame [101]–[104].

The same harmonic control methods can also be used in electric machines. In conventional three-phase machines, the PR and VPR controllers in the fundamental frame have been a common choice for double-fed induction generators and PMSMs [105]–[107]. Similarly, in multiphase machines, the PR and VPR controllers have been suggested for current harmonic compensation in dual three-phase PMSMs, dual three-phase IMs, and symmetrical multiphase machines [56]–[66].

Any controller that can provide an infinite loop gain at the harmonic frequencies and that results in a stable closed-loop system can compensate for the harmonics with a zero

steady-state error. However, in industrial applications, the main interest has been in simple, low-order, linear, one-degree-of-freedom controllers. The repetitive control scheme is difficult to use in variable frequency operation and is not considered further here.

4.2.1 Alternative reference frames

Current harmonic control can be successfully implemented in a reference frame rotating at any angular frequency. However, the fundamental synchronous reference frame and the harmonic synchronous reference frame are the most frequently used ones in the literature. The main argument in favour of the fundamental synchronous reference frame is the reduction of the computational load because the additional rotation transformations are not needed and a single controller can control both the 5th and 7th harmonic components. On the other hand, the current harmonic components appear as DC quantities in harmonic synchronous reference frames thus simplifying the control design process.

Each rotational invariant controller has a mathematically equivalent LTI representation in every reference frame. The common techniques to find the equivalent controllers in different reference frames are based on the frequency shift property of the Laplace transform [108], [109]. If the transfer function matrix of the current controller $\boldsymbol{C}_{\mathrm{DQh}}(s)$ in the harmonic synchronous reference frame rotating at the frequency $(h+1)\omega_{\mathrm{r}}$ is

$$\boldsymbol{C}_{\mathrm{DQh}}(s) = \begin{bmatrix} C_{\mathrm{h,dg}}(s) & C_{\mathrm{h,off}}(s) \\ -C_{\mathrm{h,off}}(s) & C_{\mathrm{h,dg}}(s) \end{bmatrix}, \tag{4.1}$$

then the equivalent current controller $\boldsymbol{C}_{\mathrm{DQs}}(s)$ in the fundament synchronous reference frame is

$$\begin{aligned} \boldsymbol{C}_{\mathrm{DQs}}(s) &= \frac{1}{2}\begin{bmatrix} C_{\mathrm{s,dg}}(s) & C_{\mathrm{s,off}}(s) \\ -C_{\mathrm{s,off}}(s) & C_{\mathrm{s,dg}}(s) \end{bmatrix} \\ C_{\mathrm{s,dg}}(s) &= C_{\mathrm{h,dg}}(s+jh\omega_{\mathrm{r}}) + C_{\mathrm{h,dg}}(s-jh\omega_{\mathrm{r}}) \\ &\quad + j\left(C_{\mathrm{h,off}}(s+jh\omega_{\mathrm{r}}) - C_{\mathrm{h,off}}(s-jh\omega_{\mathrm{r}})\right) \\ C_{\mathrm{s,off}}(s) &= C_{\mathrm{h,off}}(s+jh\omega_{\mathrm{r}}) + C_{\mathrm{h,off}}(s-jh\omega_{\mathrm{r}}) \\ &\quad - j\left(C_{\mathrm{h,dg}}(s+jh\omega_{\mathrm{r}}) + C_{\mathrm{h,dg}}(s-jh\omega_{\mathrm{r}})\right) \end{aligned} \tag{4.2}$$

Using (4.2), it is straightforward to show that the pair of PI controllers in the negative- and positive-sequence harmonic synchronous reference frames is mathematically equivalent to the PR controller in the fundamental synchronous reference frame. For this reason, the methods using PI and PR controllers are basically only alternative ways to implement the same approach. There is a similar equivalency between the VPI and VPR controllers. Because these control methods are mathematically equivalent, their stability and performance properties are, in theory, identical. However, in practice, discretization

and other aspects related to the actual implementation of the methods can cause some difference. The implementation of resonant controllers is covered in detail in [110]–[112] and is not discussed further in this dissertation.

4.2.2 Current harmonic controllers

The type of the current harmonic controller is important, but the parameters of the controller must also be properly selected. A model-based design of controller parameters is used in this dissertation. A common approach in the model-based current control of electric drives and grid-connected inverters has been choosing the controller zero to cancel the plant pole. This principle has also been applied as a design guideline in this dissertation. The machine model (3.2) has an LTI representation only in the fundamental synchronous reference frame. Thus, the fundamental frame is used in the analysis and implementation of the current harmonic compensation here.

In this dissertation, the comparison of simple, low-order, linear, one-degree-of-freedom feedback controllers covers the PR controller, the VPR controller, and the inverse-based (INV) harmonic controller. Comparative studies on harmonic controllers have been published for APFs [113], [114] but not for dual three-phase machines. The harmonic control in multiphase machines is still a relatively recent topic, and thus, there is not yet full agreement on the most suitable methods. The most traditional method to reduce the harmonics is to use the PR controller

$$\boldsymbol{C}_{\mathrm{PR}}(s) = \begin{bmatrix} \alpha L_{\mathrm{Ds}} + \dfrac{\alpha R_{\mathrm{s}} s}{s^2 + (6\omega_{\mathrm{r}})^2} & 0 \\ 0 & \alpha L_{\mathrm{Qs}} + \dfrac{\alpha R_{\mathrm{s}} s}{s^2 + (6\omega_{\mathrm{r}})^2} \end{bmatrix}, \tag{4.3}$$

where the control design parameter α determines the bandwidth of the controller. As a simple rule, increasing the value of α results in a faster dynamic performance. PR controllers have been applied to current control for more than fifteen years [108]. Although some studies with APFs have indicated that PR controllers may suffer from robustness problems [115], they are still widely proposed today for harmonic control in electric machines. To obtain a better performance and robustness than the PR controllers can provide, the VPR controller

$$\boldsymbol{C}_{\mathrm{VPR}}(s) = \begin{bmatrix} \dfrac{\alpha L_{\mathrm{Ds}} s^2 + \alpha R_{\mathrm{s}} s}{s^2 + (6\omega_{\mathrm{r}})^2} & 0 \\ 0 & \dfrac{\alpha L_{\mathrm{Qs}} s^2 + \alpha R_{\mathrm{s}} s}{s^2 + (6\omega_{\mathrm{r}})^2} \end{bmatrix} \tag{4.4}$$

was developed [104]. Comparing (4.3) with (4.4) shows that both controllers have identical poles but the location of the zeros is different. The zeros of the VPR controller are real, and there is always a zero at the origin. The PR controller, instead, can have complex conjugate zeros, and there is no zero at the origin. Although the location of the

zeros does not affect the steady-state performance of the controllers at the harmonic frequency $\omega = \pm 6\omega_\mathrm{r}$ (i.e., both controllers offer a zero steady-state error), it changes the dynamic performance and robustness. Because of the favourable properties, VPR controllers have become an interesting alternative in the current harmonic control.

The PR and VPR controllers, despite their differences, are both diagonal controllers. As such, they cannot directly counteract the cross-coupling of the machine dynamics. The following improved version of the VPR controller

$$\boldsymbol{C}_\mathrm{INV}(s) = \begin{bmatrix} \dfrac{\alpha L_\mathrm{Ds} s^2 + \alpha R_\mathrm{s} s}{s^2 + (6\omega_\mathrm{r})^2} & \dfrac{-\omega_\mathrm{r} \alpha L_\mathrm{Qs} s}{s^2 + (6\omega_\mathrm{r})^2} \\ \dfrac{\omega_\mathrm{r} \alpha L_\mathrm{Ds} s}{s^2 + (6\omega_\mathrm{r})^2} & \dfrac{\alpha L_\mathrm{Qs} s^2 + \alpha R_\mathrm{s} s}{s^2 + (6\omega_\mathrm{r})^2} \end{bmatrix} = \frac{\alpha s}{s^2 + (6\omega_\mathrm{r})^2} \boldsymbol{P}^{-1} \tag{4.5}$$

does not have that deficiency. The difference between (4.4) and (4.5) is the off-diagonal resonant terms. The presence of these terms makes (4.5) a full multivariable controller. Because the structure of (4.5) includes the inverse of the machine model, it is called an INV controller in this dissertation.

4.3 Compensation using disturbance observer

It is clear that conventional current harmonic compensation methods based on one-degree-of-freedom controllers and negative feedback regulation work and can be successfully applied. However, also other alternatives are worth considering. An interesting approach is to recognize that the current harmonics are a result of disturbances and thereby use a disturbance-observer-based control to eliminate the harmonics. The working principle of the disturbance-observer-based control is very simple. The disturbance observer (DOB) produces an estimate of the disturbance and feeds back the estimate as a compensation signal to cancel out the actual disturbance. Thus, the DOB aims to directly counteract the disturbance instead of attenuating the effect of the disturbances through feedback regulation.

The DOB is well known as a simple but effective technique to estimate and suppress disturbances, and it has been widely used in many industrial applications, particularly in motion control systems [116], [117]. The DOB has also been proposed for conventional three-phase PMSMs, IMs, and DC machine drives [118]–[121]. It is here shown that the DOB can also be effectively used to eliminate stator current harmonics in dual three-phase PMSMs.

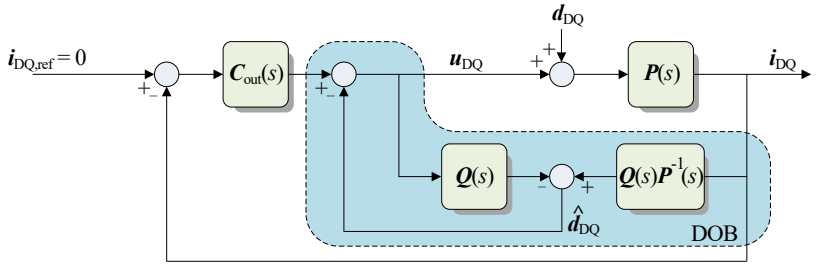

Fig. 4.1. Inverse-model-based DOB loop. The signal $\boldsymbol{d}_{\mathrm{DQ}}$ is a lumped disturbance acting on the input of the plant $\boldsymbol{P}(s)$. $\boldsymbol{Q}(s)$ is the filter specifying the bandwidth where the DOB loop is effective.

Fig. 4.1 shows that the DOB estimates the external disturbance signal $\boldsymbol{d}_{\mathrm{DQ}}$ that is acting on the input of the plant. However, the DOB can also eliminate internal disturbances. Consequently, the disturbance $\boldsymbol{d}_{\mathrm{DQ}}$ should be considered a lumped disturbance that contains model uncertainties and unmodelled dynamics as well as external disturbances. Because the feedback signal of the DOB is nothing more than an estimate of the disturbance, the DOB can only reject disturbances. It does not provide a reference tracking performance. Thus, an additional outer-loop current controller $\boldsymbol{C}_{\mathrm{out}}(s)$ is still needed to achieve such properties. The model of the plant is generally always proper, which causes the inverse of the plant model to be improper. Because an improper transfer function cannot be implemented, the filter $\boldsymbol{Q}(s)$ is needed to make the DOB realizable. The design of the filter $\boldsymbol{Q}(s)$ is critically important as it determines the performance and stability properties of the DOB loop.

The filter $\boldsymbol{Q}(s)$ can be designed to include a specific disturbance model in the DOB. According to the internal model principle, the disturbance $\boldsymbol{d}_{\mathrm{DQ}}$ can be completely eliminated if the transfer function matrix $(\boldsymbol{I} - \boldsymbol{Q}(s))^{-\mathbf{1}}$ in the forward path of the DOB loop includes the model of that disturbance. Because $\boldsymbol{d}_{\mathrm{DQ}}$ is a sinusoidal signal having a frequency of $\pm 6\omega_{\mathrm{r}}$, the filter $\boldsymbol{Q}(s) = \boldsymbol{q}(s)\boldsymbol{I}$ is selected to be a band-pass filter

$$\boldsymbol{q}(s) = \frac{\alpha s}{s^2 + \alpha s + (6\omega_{\mathrm{r}})^2}, \tag{4.6}$$

where the design parameter α determines the bandwidth of the filter. Increasing the value of α increases the bandwidth of the filter. This bandwidth is directly related to the dynamic performance of the nominal control system. The wider is the bandwidth, the faster is the system. It is straightforward to show that the transfer function

$$(\boldsymbol{I} - \boldsymbol{q}(s))^{-\mathbf{1}} = 1 + \frac{\alpha s}{s^2 + (6\omega_{\mathrm{r}})^2} \tag{4.7}$$

clearly includes the model of the sinusoidal disturbance at the desired frequency thereby confirming that perfect current harmonic compensation can theoretically be achieved.

Considering the robustness analysis presented in Section 3.2, the block diagram in Fig. 4.1 can be manipulated (only if $\boldsymbol{i}_{\mathrm{DQ,ref}} = 0$) into an equivalent form of a one-degree-of-freedom controller as presented in Fig. 3.2. The corresponding controller $\boldsymbol{C}_{\mathrm{DOB}}(s)$ that represents equivalently the DOB loop in the robustness analysis can be derived as follows

$$\begin{aligned}\boldsymbol{C}_{\mathrm{DOB}}(s) &= (\boldsymbol{I}-\boldsymbol{Q})^{-1}\left(\boldsymbol{Q}\boldsymbol{P}^{-1}+\boldsymbol{C}_{\mathrm{out}}\right)\\ &= \left(\boldsymbol{P}\boldsymbol{Q}^{-1}(\boldsymbol{I}-\boldsymbol{Q})\right)^{-1}+(\boldsymbol{I}-\boldsymbol{Q})^{-1}\boldsymbol{C}_{\mathrm{out}}\\ &= \left(\boldsymbol{Q}^{-1}-\boldsymbol{I}\right)^{-1}\boldsymbol{P}^{-1}+(\boldsymbol{I}-\boldsymbol{Q})^{-1}\boldsymbol{C}_{\mathrm{out}}\\ &= \frac{\alpha s}{s^2+(6\omega_{\mathrm{r}})^2}\boldsymbol{P}^{-1}+(\boldsymbol{I}-\boldsymbol{Q})^{-1}\boldsymbol{C}_{\mathrm{out}}\\ &= \boldsymbol{C}_{\mathrm{INV}}+\left(1+\frac{\alpha s}{s^2+(6\omega_{\mathrm{r}})^2}\right)\boldsymbol{C}_{\mathrm{out}}\end{aligned} \tag{4.8}$$

Thus, with the selected filter (4.6), the DOB loop is equivalent with the sum of the INV controller and a term resulting from the outer-loop controller. The DOB loop can be straightforwardly analysed using this representation.

4.4 Comparison results

The stability and performance of the following current harmonic compensation methods are compared in this section: the PR controller (4.3), the VPR controller (4.4), the INV controller (4.5), and the DOB (4.8). The comparison of the methods is based on a theoretical analysis and the experimental results. In the theoretical analysis, a simulation study and an SSV robustness analysis are performed. The experimental results focus on the time-domain evaluation.

The experimental setup used in the measurements consists of two three-phase VSIs with a common DC link, a commercial active front end (AFE), a 25 kW salient pole dual three-phase PMSM, and a 180 kW DC machine drive for loading the PMSM. Table I presents the parameters of the laboratory prototype PMSM. The detailed information about the machine used in the experimental measurements can be found from Appendix A. The VSIs operate at a 5 kHz switching frequency with a 2.3 µs dead time. The setup includes an encoder for the rotor angle feedback. The control system is implemented on a dSPACE platform, and it operates at a 5 kHz sampling frequency. Fig. 4.2 presents the schematic of the experimental setup. The machine parameters presented in Table I are also used in all the simulations and other theoretical analyses in this dissertation. Unless otherwise stated, the analysed operating point in all the results has the nominal rotational speed n = 350 r/min, and the $\mathrm{D_m}$–$\mathrm{Q_m}$ reference frame currents are controlled to be i_{Dm} = 0 A and i_{Qm} = -23.1 A (i.e., the machine is operating as a generator). In the analysis of the DOB, the outer-loop controller $\boldsymbol{C}_{\mathrm{out}}(s)$ is a simple diagonal PI controller with a proportional gain $K_{\mathrm{p}} = 2$ and an integral gain $K_{\mathrm{i}} = 100$. The system and measurements are assumed to be unscaled in all the cases.

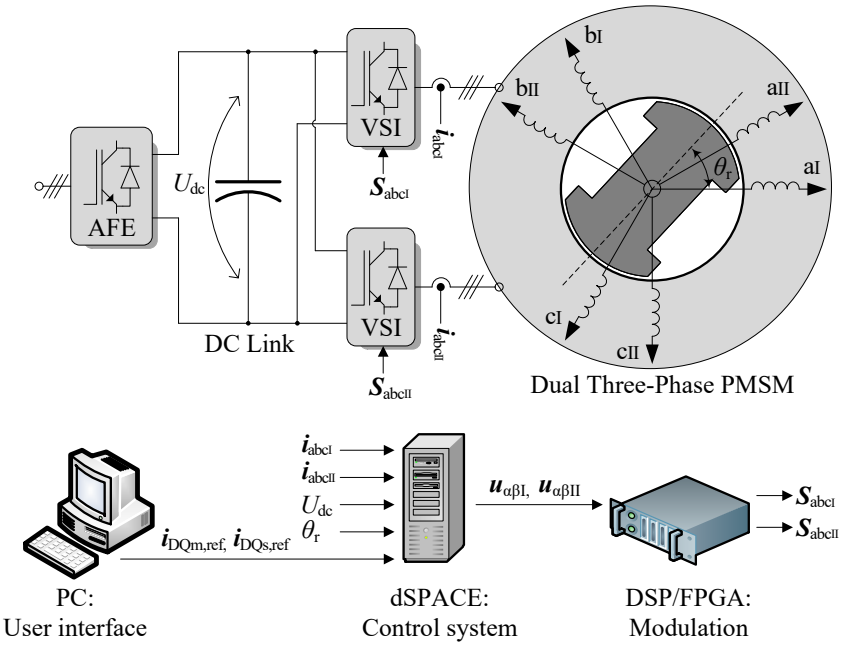

Fig. 4.2. Schematic of the experimental setup. The dual three-phase PMSM is loaded by a DC machine drive not illustrated in the figure. Two three-phase VSIs with a common DC link supply the PMSM. The DC link is connected to the grid through the AFE. The main control system operates on a dSPACE platform. In addition, the setup includes a DSP/FPGA card for signal processing and modulation.

TABLE I
Machine parameters

Nominal power	25 kW
Nominal current	22.5 A
Nominal voltage	380 V
Nominal speed	350 r/min
Number of pole pairs	4
Stator resistance R_s	0.53 Ω
PM flux linkage ψ_{PM}	2.06 Wb
Inductance L_{Dm}, L_{Qm}	31 mH, 42 mH
Inductance L_{Ds}, L_{Qs}	7 mH, 8 mH

4.4.1 Robust stability

The robust stability margins of the methods are compared in Fig. 4.3. The figure shows the margins as a function of the control design parameter α with the low (n = 35 r/min), nominal (n = 350 r/min), and high (n = 595 r/min) rotational speed of the machine. It can be seen that all four methods have excellent robustness in the low-speed region. There is no significant difference in the robust stability margins. However, at the nominal speed, the PR controller is significantly less robust than the other three methods when $\alpha < 600$. Increasing α makes the system with the PR controller more robust up to some point. For

very high values of α, the PR controller, the INV controller, and the DOB become equally robust, and the VPR controller turns into the least robust alternative. Increasing the rotational speed notably above the nominal value severely degrades the robustness of the PR controller. Instead, the excellent robust stability margins of the INV controller and the DOB are not much affected by the high speed. Clearly, the best robustness is achieved with low values of α using the INV controller or the DOB. However, the difference between the VPR and these two methods is not substantial except for very high requirements of dynamic performance.

4.4.2 Robustness of the frequency-domain performance

The robustness of the frequency domain performances of the current harmonic compensation methods is compared in Fig. 4.4. A small proportional gain term ($K_\mathrm{p} = 1.47$) is added to the INV and VPR controllers to improve the magnitude response. Fig. 4.4 shows the worst-case gain curves of the closed-loop harmonic compensation system from the plant input disturbance $\boldsymbol{d}_\mathrm{DQs}$ to the harmonic currents $\boldsymbol{i}_\mathrm{DQs}$. The worst-case gain curves define the maximum possible gain at each frequency for any system in the uncertainty set. Thus, they measure well the robust performance of the system. Low worst-case gains (in particular, close to the harmonic frequency) imply favourable performance properties under modelling errors. To provide better understanding of how the uncertainty level affects the robust performance, the worst-case gain curves are determined for uncertainty levels of 0%, 25%, 50%, 75%, and 100%. The lowest curve (0% uncertainty) is, by definition, the nominal magnitude response of the system.

It can be seen from Fig. 4.4 that the INV controller, the VPR controller, and the DOB produce very desirable nominal magnitude responses. However, uncertainties in the system increase the worst-case gains for low frequencies. All three methods yield similar results. The lack of control effort for low frequencies with these methods is the reason for the increase in the worst-case gain at low frequencies. If required, the low-frequency worst-case gains can be decreased by increasing the value of the added proportional gain term. However, this adjustment may not be necessary because the low frequency range of the magnitude response is not critical for the performance of the harmonic control. The most important observation from Fig. 4.4 for the INV controller, the VPR controller, and the DOB is that the gains near the harmonic frequency are not significantly affected by the uncertainty. Thus, the robust performance of harmonic compensation is guaranteed with these methods.

For the PR controller, Fig. 4.4 shows that the uncertainties in the system increase the gain peak near the harmonic frequency. A large proportional gain term keeps the worst-case gains low for other frequencies. Unfortunately, the performance is notably degraded at frequencies where it matters most. As a result, even a small frequency deviation can almost completely cancel the harmonic compensation performance of the PR controller. The analysis indicates that such a risk is not present with the INV controller, the VPR controller, or the DOB.

4.4.3 Robustness of the time-domain dynamic performance

The robustness of the time-domain dynamic performance is difficult to study analytically. Therefore, an extensive Monte Carlo simulation analysis is performed to study this aspect. Fig. 4.5 shows the result of the analysis. Fig. 4.5 illustrates the nominal transient response and the region filled by the set of responses from uncertain systems. In addition, exponential decay curves calculated from the closed-loop poles are presented. It can be seen that the nominal performances accurately follow the expected decay rates. To obtain a meaningful comparison of the results on a similar time scale, the value of $\alpha = 150$ is used for the INV controller, the VPR controller, and the DOB and $\alpha = 1000$ for the PR controller.

The set of transient responses from uncertain systems deviates only moderately from the nominal response when the INV controller, the VPR controller, and the DOB are used. Thus, the results indicate that the time-domain dynamic performances of these methods are robust. Instead, the PR controller shows a significant degradation of performance. Note that although the PR controller is robustly stable with the value of $\alpha = 1000$ (see Fig. 4.3), it has a very poor robust performance.

When analysing harmonic controllers, the focus has commonly been on the stability properties while ignoring robust performance. However, Fig. 4.5 shows that the robust performance aspects should not be overlooked when deciding upon the most suitable controller.

4.4.4 Experimental results

Uncertainty is inherently included in the experimental results. For this reason, the experimental measurement presented in this dissertation focuses on the time-domain performance. First, the steady-state performances of the current harmonic compensation methods are experimentally compared by analysing the magnitude of the phase current harmonic components at a constant rotational speed and load. The INV controller is tested with the small added proportional gain term and the VPR controller without it to show that the proposed improvement does not have any undesired effects on the time-domain behaviour of the harmonic controllers. Fig. 4.6 shows that all four methods can successfully eliminate the current harmonic components that are seen without the compensation in Fig. 4.7. The discrete Fourier transform (DFT) analysis of the phase currents presented in Fig. 4.8 confirms that the nearly perfect compensation result is achieved considering the 5^{th} and 7^{th} harmonics. It is also clear that the methods have a similar steady-state performance as was theoretically expected.

The dynamic performances of the methods are studied with two different tests. In the first test, the compensation is activated during the steady-state operation. Before the activation, the harmonics are not controlled in any way. The results are presented for two different values of closed-loop bandwidth in Fig. 4.9 and Fig. 4.10. The INV controller, the VPR controller, and the DOB have equivalent dynamic performances in both cases

(α = 100 and α =200). It can be seen that the measured decay rates of the current harmonics have an excellent agreement with the exponential decay curves that are analytically calculated from the closed-loop poles. Although much higher gains (α = 500 and α = 1000) are used with the PR controller, the decay rates are still slower. Especially in Fig. 4.9, the effect of the lower robust stability margin of the PR controller (see Fig. 4.3) can be noticed from the slow and oscillatory response. It was confirmed with the PR controller that decreasing α further caused an unstable operation as the robust stability analysis in Fig. 4.3 alerts. To further verify the robust stability analysis, the INV controller, the VPR controller, and the DOB were tested to be stable at least up to α = 1000. These observations support the expectation that the presented analysis gives a realistic view of the robustness of the system. Considering the results in Fig. 4.9 and Fig. 4.10, the INV controller, the VPR controller, and the DOB appear to have a superior dynamic performance compared with the PR controller. In addition, it can be seen that already a relatively low value of bandwidth obtained with α = 200 can provide a fast 10 ms time constant for the elimination of the harmonics. The obtained dynamic performance can be put into a right perspective by noting that the period of the fundamental component at the nominal rotational speed is approximately 43 ms. Hence, a significant reduction of the current harmonics is possible in less than a fundamental period of the phase current when the most robust range of α is used (see Fig. 4.3).

In the test presented in Fig. 4.11, the methods are operating in the steady state with complete elimination of the current harmonics when a transient is applied to the system. In the cases of the INV controller, the VPR controller, and the PR controller, a speed transient from 350 r/min to 275 r/min and a fundamental component current transient from 6 A to 23 A are simultaneously applied to the machine. In the case of the DOB, the rotational speed of the machine is accelerated from 100 rpm to 350 rpm linearly during a 3 s period. Fig. 4.11 shows that all four methods can satisfactorily compensate for the current harmonics under the transient. However, the INV controller, the VPR controller, and the DOB yield better results than the PR controller again. The results demonstrate a high suitability for variable frequency operation. There is no significant difference between the performances of the VPR controller and the INV controller.

Based on the experimental results, the INV controller, the VPR controller, and the DOB have an equivalent dynamic performance. The results also clearly show that the dynamic performance of the PR controller is not as good as that of the other three current harmonic compensation methods.

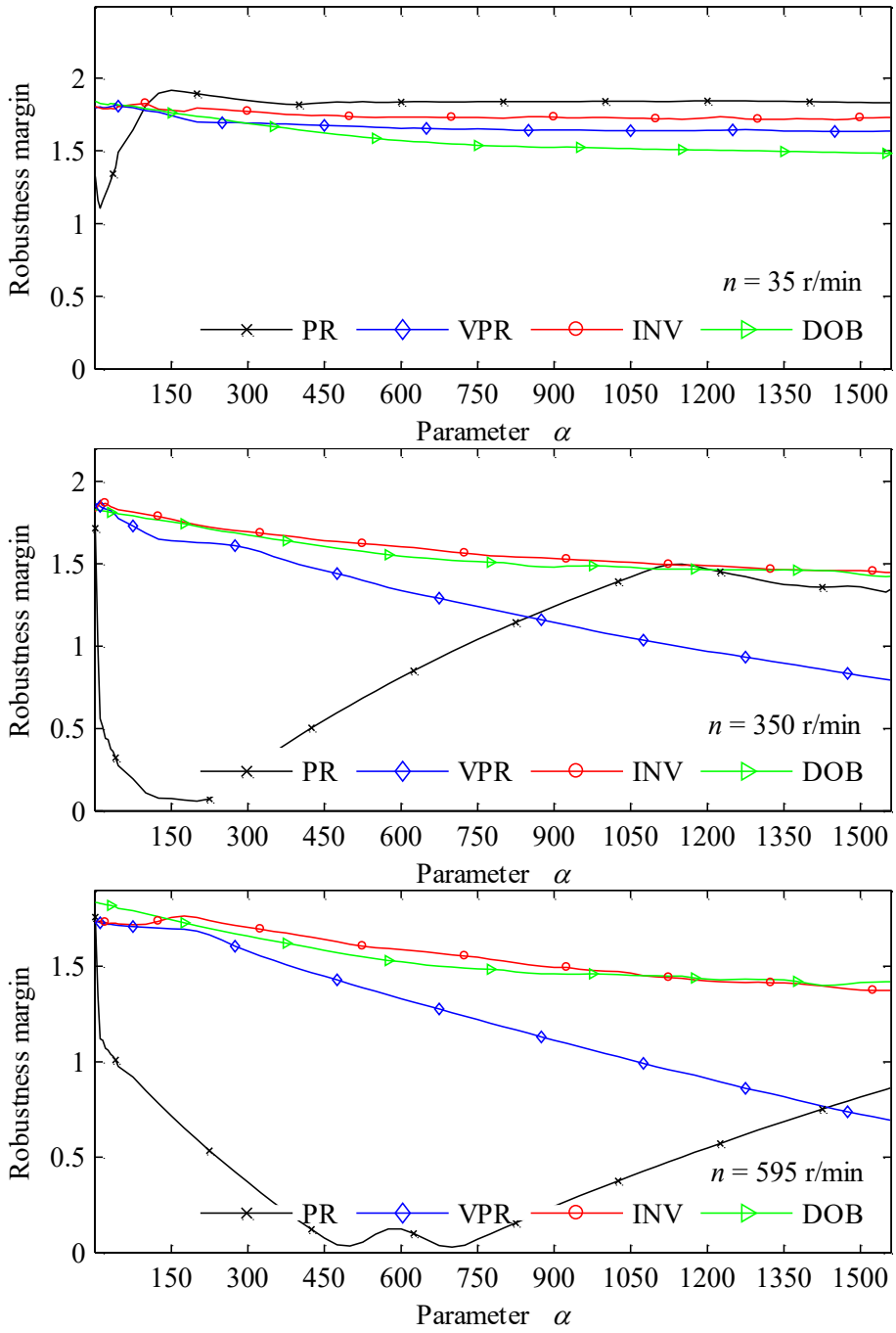

Fig. 4.3. Robust stability margins of the harmonic compensation methods as a function of the control design parameter α. The analysis is shown for the low, nominal, and high rotational speeds of the machine. All the methods are equally robust at the low speed. The INV controller, the VPR controller, and the DOB offer very large robust stability margins. The PR controller with a low value of α provides poor robustness.

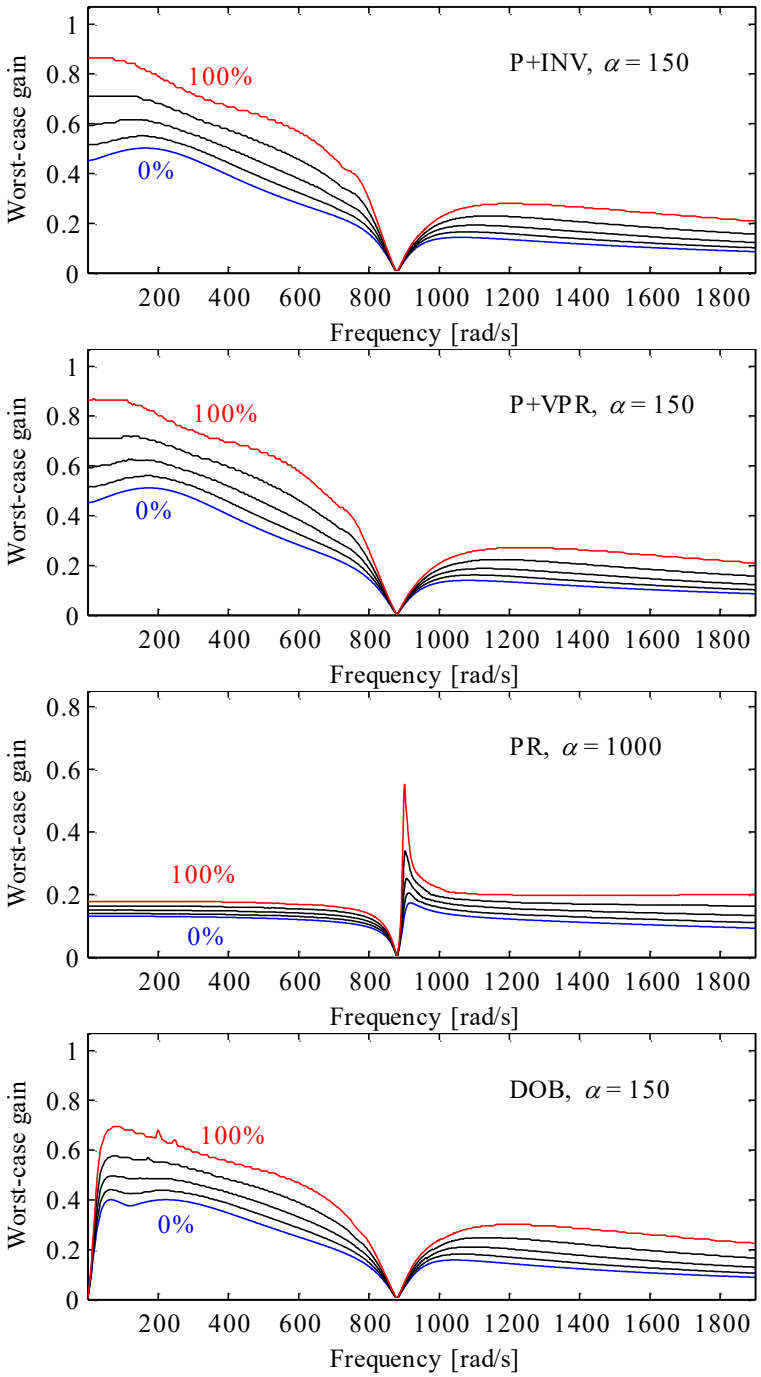

Fig. 4.4. Worst-case gain curves of the closed-loop harmonic compensation systems from the plant input disturbance to the harmonic currents. In the analysis, the uncertainty level is increased from 0% to 100% with increments of 25%. The curves determine the maximum possible gain for any system in the uncertainty set.

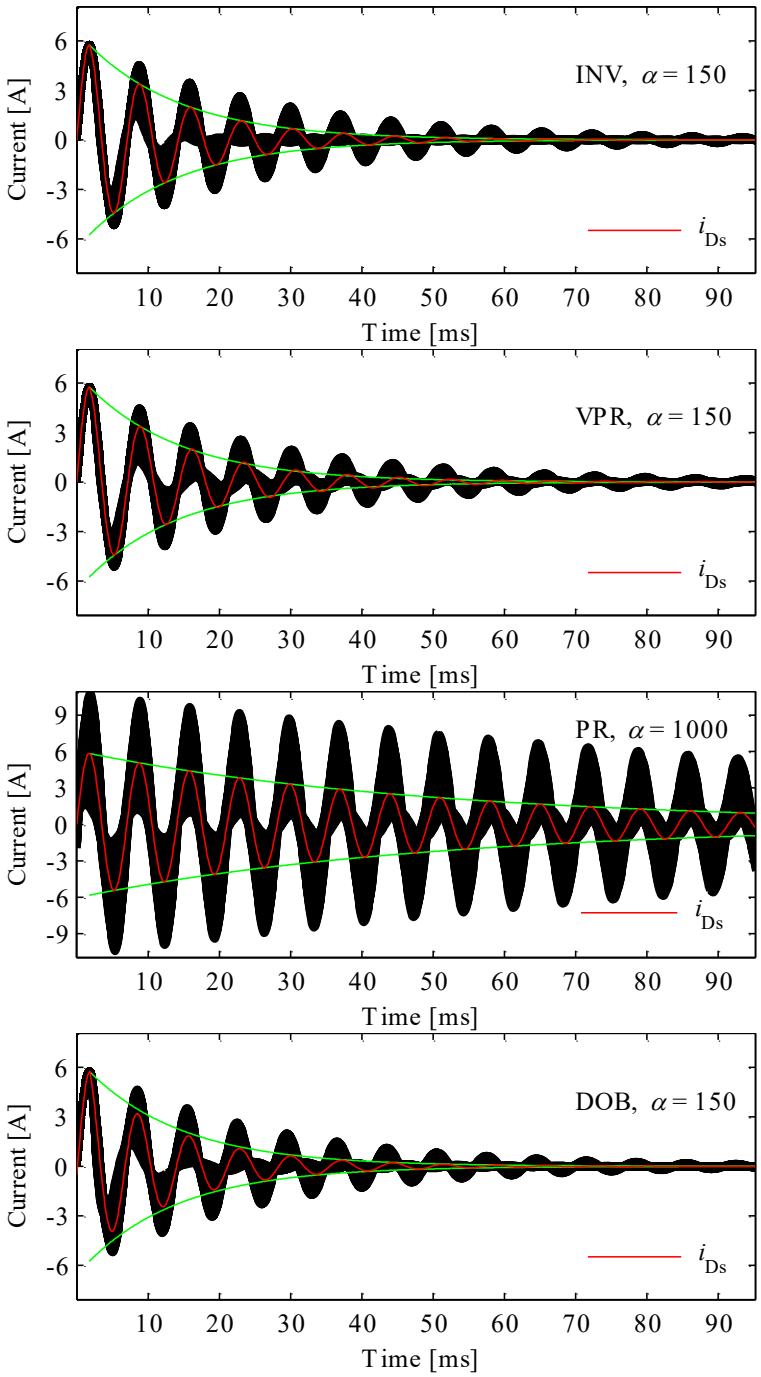

Fig. 4.5. Simulated transient responses of the harmonic compensation methods. The figures present the nominal response and the analytically calculated envelope curve. The filled region is drawn by the set of uncertain systems.

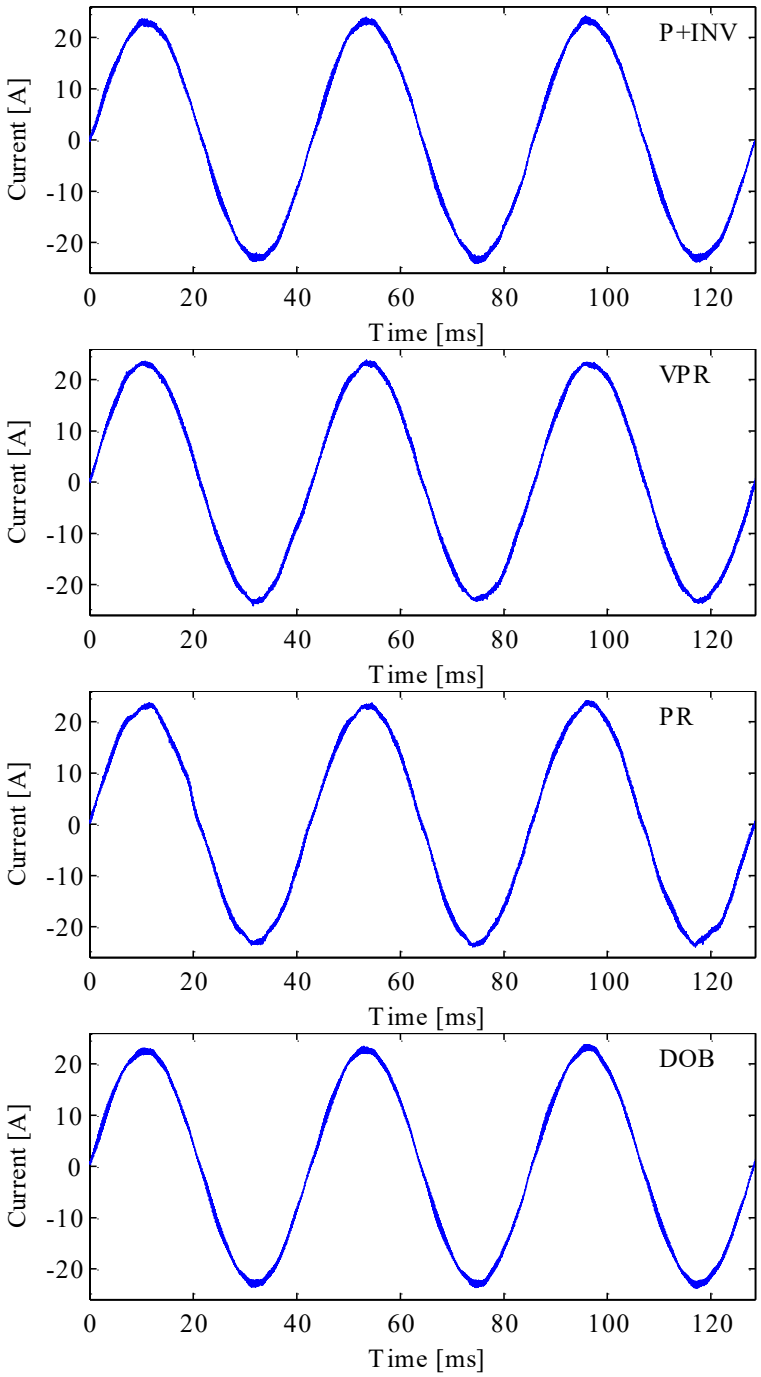

Fig. 4.6. Measured steady-state phase currents with different current harmonic compensation methods. All four methods can successfully produce nearly harmonic free current waveforms.

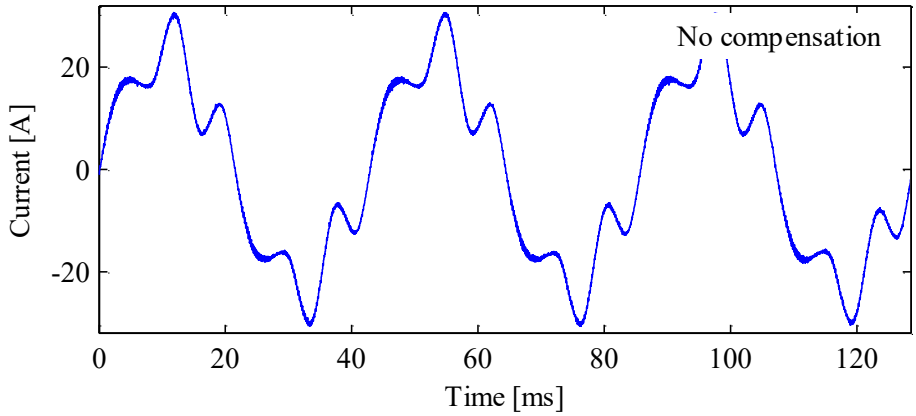

Fig. 4.7. Measured steady-state phase current without any harmonic compensation. The notable harmonic components are clearly visible in the current waveform.

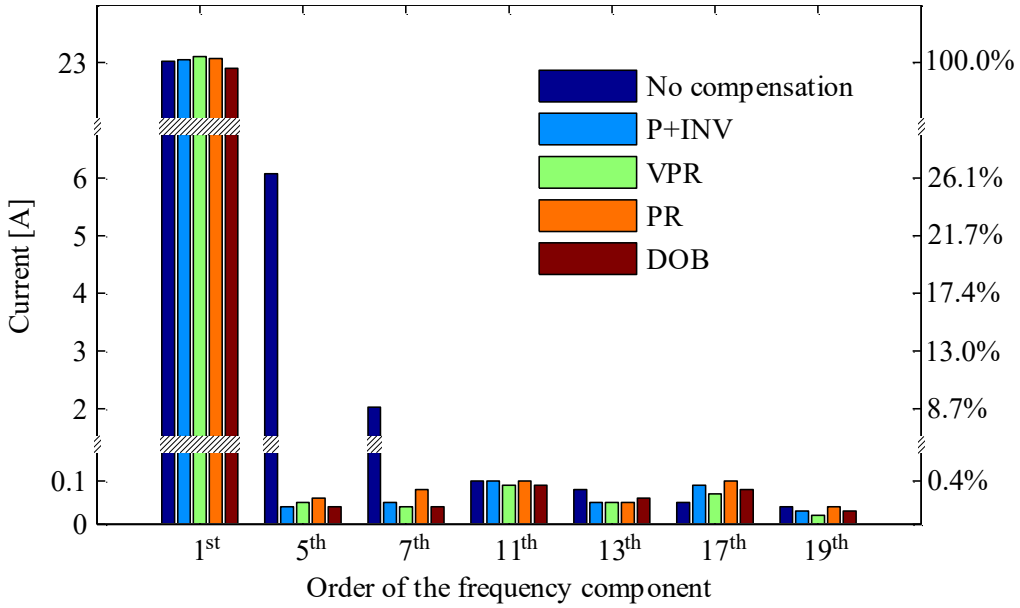

Fig. 4.8. Frequency spectrum analysis of the measured steady-state phase current with different harmonic compensation methods and without any compensation. The result of the DFT analysis shows that all the methods can eliminate the targeted 5th and 7th harmonic components almost completely. The fundamental component of the phase current is approximately 23 A in all the cases. Without compensation, the 5th harmonic is 6 A and the 7th harmonic is 2 A.

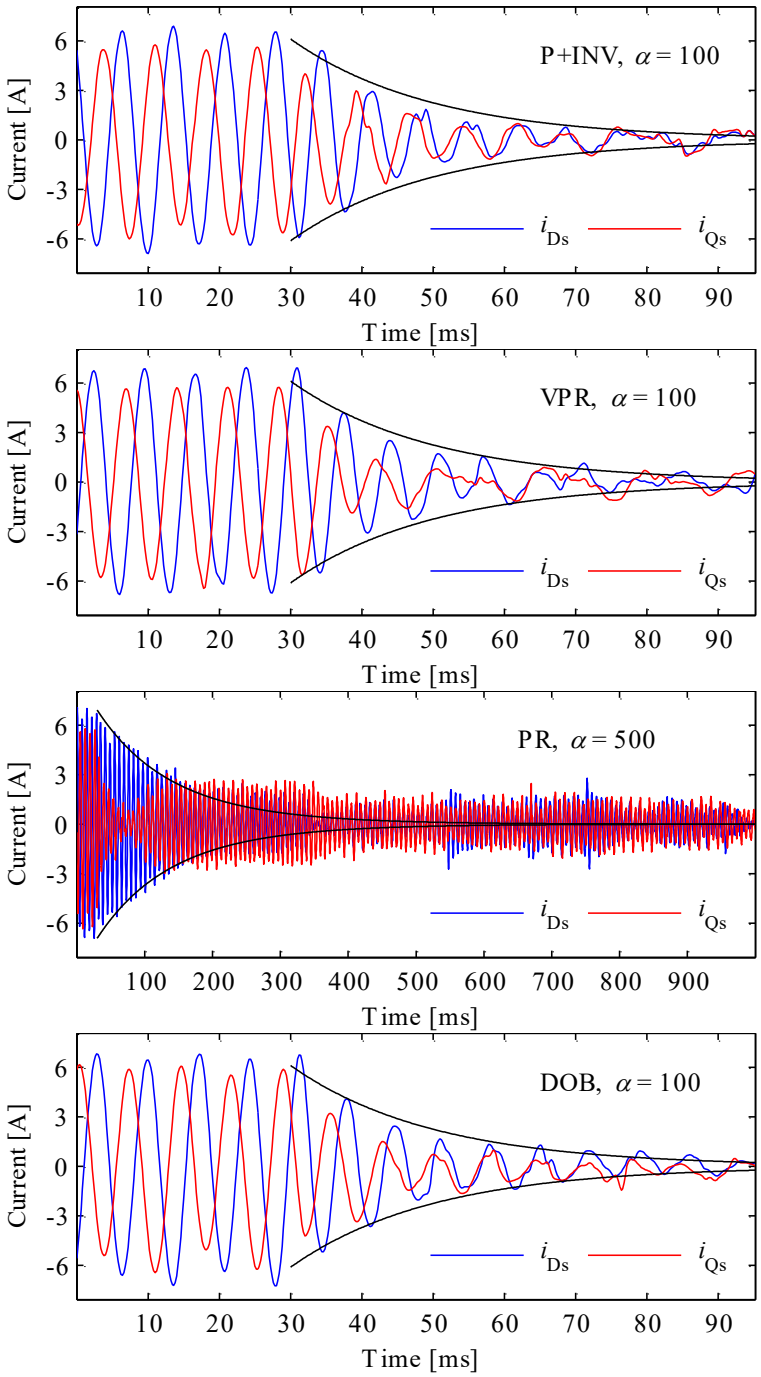

Fig. 4.9. D_s–Q_s frame harmonic currents when the harmonic controllers are activated during the steady-state operation at $t = 30$ ms. The PR controller has the slowest response. The other three responses are close to identical. The figures also present the analytically calculated envelope curve.

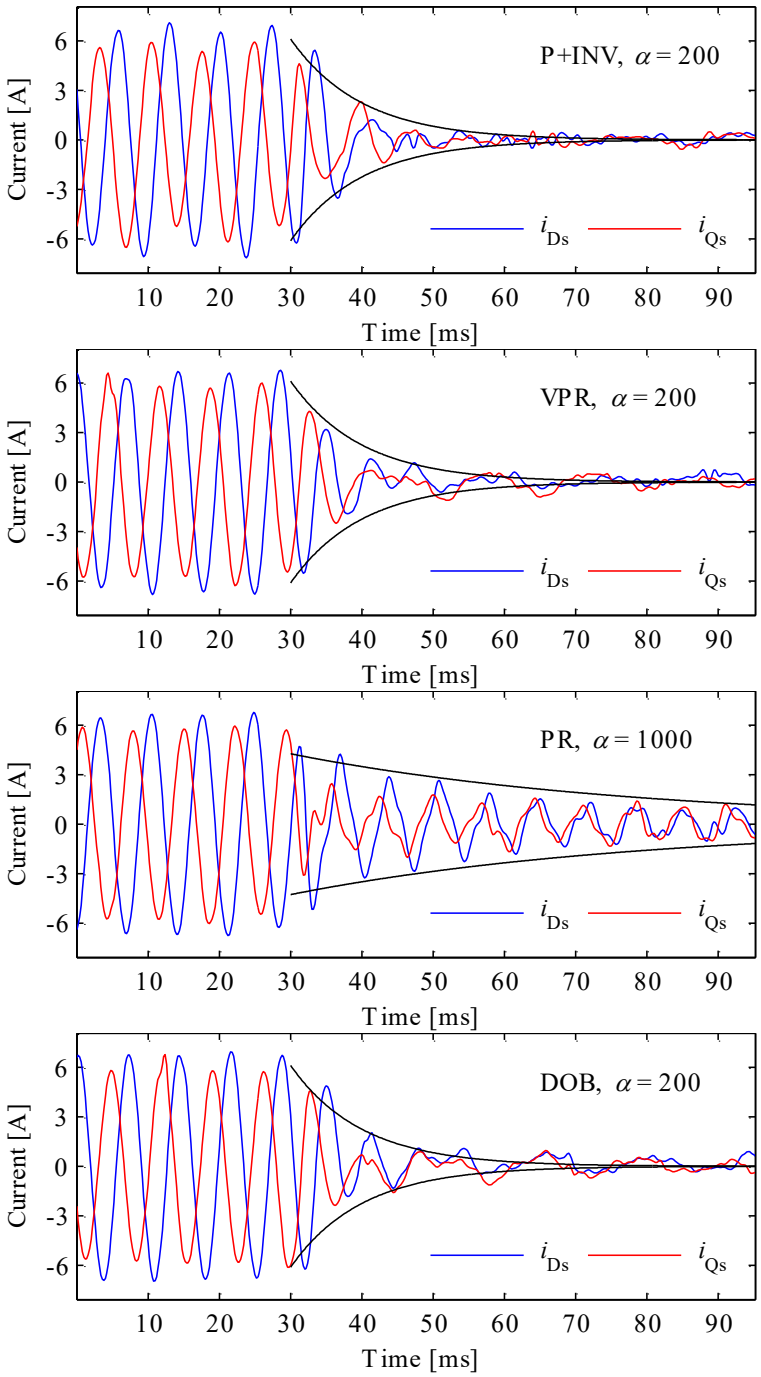

Fig. 4.10. D_s–Q_s frame harmonic currents when the harmonic controllers are activated during the steady-state operation at t = 30 ms. Compared with the previous figure, a higher closed-loop bandwidth has been used. Still, the PR controller has the slowest response and the other three responses are close to identical.

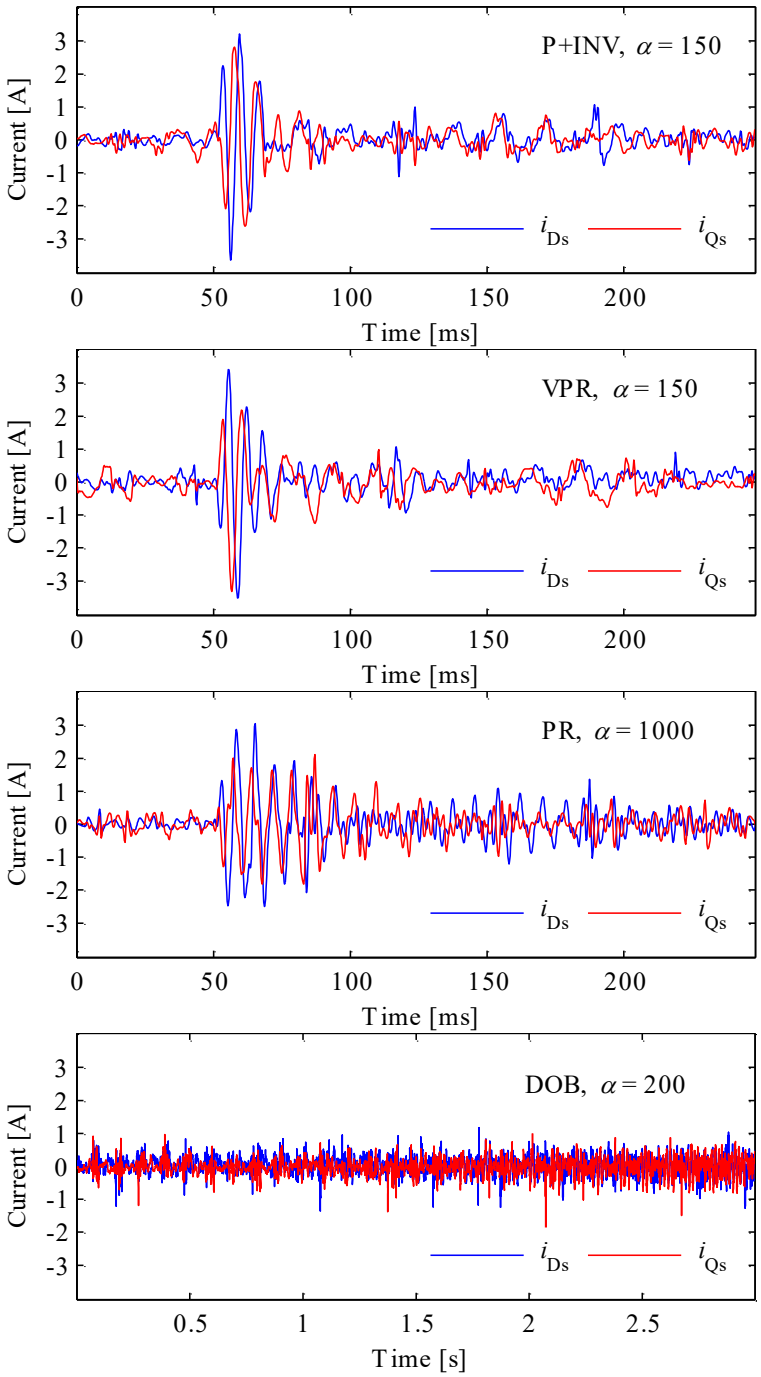

Fig. 4.11. D_s–Q_s frame harmonic currents during a transient. In the cases of the INV, VPR, and PR controllers, a speed transient from 350 r/min to 275 r/min during a 250 ms period and a current transient from 6 A to 23 A during a 10 ms period are applied to the machine at t = 50 ms. In the case of the DOB, the rotational speed of the machine is accelerated linearly from 100 r/min to 350 r/min during a 3 s period.

4.5 Partial compensation because of limited voltage

The results presented in the previous section clearly show that a variety of harmonic compensation methods can successfully provide complete elimination of current harmonics. However, the presented results can be achieved only when there are no constraints on the available voltage. It must be stressed that the limited available voltage can impose significant constraints on the achievable performance.

The working principle of the active harmonic compensation is to cancel current harmonics by adding correct voltage harmonic components to the output voltage of the VSI supplying the machine. As a result, current harmonic compensation can increase the magnitude of the output voltage vector of the VSI. This issue is illustrated for a three-phase VSI in Fig. 4.12. Because the maximum possible voltage vector is limited by the DC link voltage of the VSI, complete elimination of the current harmonics may not be achievable in every operating point. The more voltage is required to produce the fundamental component, the less voltage can be used to harmonic compensation. In variable frequency operation, when the speed of the machine approaches the field weakening point, the voltage available can be very limited.

This problem with harmonic compensation has been recognized in [122] and [123]. If the limited available voltage becomes a problem, obviously, a solution could be to raise the DC link voltage. However, such an action increases the losses. In addition, raising the DC link voltage may not even be possible because of the passive front end or the voltage rating of the VSI. An alternative approach is to optimize the operation inside the existing voltage limits of the VSI. A method, based on the principle of realizable references, can be used to recalculate the current reference of the VSI when the maximum available voltage is reached so that the required voltage vector does not exceed the maximum value. The strategy for recalculation of the current harmonic reference should be aimed at partial compensation of current harmonics caused by external disturbances. Because sources such as back-EMF harmonics and the dead time of the VSI generate current harmonics in dual three-phase PMSMs, the correct strategy must be derived from the objective of the optimal disturbance rejection.

Let the subscript h refer to the order of the harmonic component (here the 5^{th} or 7^{th}). To obtain a maximum reduction in the magnitude of the current harmonic $\boldsymbol{i}_{\mathrm{DQh}}$ when the available voltage harmonic $\boldsymbol{u}_{\mathrm{DQh}}$ is limited, the strategy can be derived from a formal optimization problem

$$\text{minimize } \left|\boldsymbol{i}_{\mathrm{DQh}}\right|, \quad \text{subject to: } \left|\boldsymbol{u}_{\mathrm{DQh}}\right| \leq u_{\mathrm{h,max}}, \tag{4.9}$$

where $u_{\mathrm{h,max}}$ is the magnitude of the maximum available voltage harmonic vector. It can be seen from Fig. 3.2 that the current harmonic $\boldsymbol{i}_{\mathrm{DQh}}$ is determined by the relation

$$\boldsymbol{i}_{\mathrm{DQh}} = \boldsymbol{P}\left(\boldsymbol{u}_{\mathrm{DQh}} + \boldsymbol{d}_{\mathrm{DQh}}\right). \tag{4.10}$$

Thus, if the maximum available voltage is not high enough to provide complete elimination of the current harmonic (i.e., $u_{\mathrm{h,max}} < |\boldsymbol{d}_{\mathrm{DQh}}|$), then $|\boldsymbol{i}_{\mathrm{DQh}}|$ obtains a minimum value in the steady state when the vectors $\boldsymbol{u}_{\mathrm{DQh}}$ and $\boldsymbol{d}_{\mathrm{DQh}}$ are directed in the opposite directions, yielding

$$-\boldsymbol{u}_{\mathrm{DQh}} = (1-\lambda_{\mathrm{h}})\boldsymbol{d}_{\mathrm{DQh}}, \text{ where } \lambda_{\mathrm{h}} = 1 - \frac{u_{\mathrm{h,max}}}{|\boldsymbol{d}_{\mathrm{DQh}}|}. \tag{4.11}$$

Satisfying (4.11) produces the maximum compensation of the disturbance $\boldsymbol{d}_{\mathrm{DQh}}$ that can be achieved with the limited voltage vector $\boldsymbol{u}_{\mathrm{DQh}}$. The optimality condition (4.11) can be satisfied without explicitly determining $\boldsymbol{d}_{\mathrm{DQh}}$. An indirect strategy to meet (4.11) is achieved with

$$\boldsymbol{i}_{\mathrm{DQh}} = \lambda_{\mathrm{h}}\boldsymbol{P}(s)\boldsymbol{d}_{\mathrm{DQh}} = \lambda_{\mathrm{h}}\boldsymbol{i}_{\mathrm{DQh,nat}}, \tag{4.12}$$

where $\boldsymbol{i}_{\mathrm{DQh,nat}}$ is the natural (i.e., uncompensated) current harmonic caused by the disturbance $\boldsymbol{d}_{\mathrm{DQh}}$. In other words, $\boldsymbol{i}_{\mathrm{DQh,nat}}$ is the current harmonic that is seen in the current measurement when no compensation is used (i.e., $\boldsymbol{u}_{\mathrm{DQh}} = 0$). According to (4.12), when the measured current harmonic vector is in the same direction as the natural current harmonic but shorter, the vectors $\boldsymbol{u}_{\mathrm{DQh}}$ and $\boldsymbol{d}_{\mathrm{DQh}}$ are directed in the opposite directions. This principle based on the natural current harmonic can be used to derive a feasible strategy for the maximum partial compensation of the current harmonics.

It is known that $\boldsymbol{i}_{\mathrm{DQh}} = \boldsymbol{i}_{\mathrm{DQh,ref}}$ in the steady state, assuming that a harmonic controller $\boldsymbol{C}_{\mathrm{DQs}}(s)$ providing a zero steady-state error is used. Thus, complete elimination of the current harmonic is achieved by setting $\boldsymbol{i}_{\mathrm{DQh,ref}} = 0$. Instead, to obtain a partial compensation, the control must be given a nonzero reference that is smaller than the current harmonic without compensation (i.e., $0 < |\boldsymbol{i}_{\mathrm{DQh,ref}}| < |\boldsymbol{i}_{\mathrm{DQh,nat}}|$). It can be shown that selecting the reference to be in the same direction as the natural current harmonic

$$\boldsymbol{i}_{\mathrm{DQh,ref}} = \lambda_{\mathrm{h}}\boldsymbol{i}_{\mathrm{DQh,nat}} \implies \arg(\boldsymbol{i}_{\mathrm{DQh,ref}}) = \arg(\boldsymbol{i}_{\mathrm{DQh,nat}}) \tag{4.13}$$

indirectly satisfies (4.11) in the steady state and thereby offers the most favourable selection. Consequently, (4.13) is the optimal strategy for selecting the direction for the current harmonic reference when the available voltage is limited.

The correct direction of the harmonic reference is determined by the natural direction of the current harmonic. The values of the control variables λ_{h} specify the magnitude of the harmonic. Thus, λ_{h} determine the compensation level for the current harmonics. Using $\lambda_{\mathrm{h}} = 0$ produces complete elimination of the harmonic and $\lambda_{\mathrm{h}} = 1$ produces no elimination at all. The values $0 < \lambda_{\mathrm{h}} < 1$ specify the partial compensation level. Partial current harmonic compensation is useful because the required voltage to produce a given harmonic reference $\boldsymbol{i}_{\mathrm{DQh,ref}} = \lambda_h\boldsymbol{i}_{\mathrm{DQh,nat}}$ is directly proportional to the compensation level (assuming that the system is linear). For example, selecting $\lambda_{\mathrm{h}} = 0.5$ requires a 50% lower voltage harmonic component $\boldsymbol{u}_{\mathrm{DQh}}$ than complete elimination. In this way, the limited

available voltage determines the maximum partial compensation that can be achieved. The less the available voltage, the closer to 1 the control variable λ_h must be selected.

It is obviously desirable to reduce the harmonics as much as possible. However, the resulting total voltage vector must stay inside the space vector modulation hexagon. For every feasible value of the fundamental component there is a value for λ_h minimizing the magnitude of the current harmonics so that the voltage limit is not exceeded. Optimal magnitudes for the harmonic references can be obtained by finding this λ_h. Although the optimization problem is simple to state, finding the optimal value for λ_h is somewhat complicated in practice. It can be concluded that when the magnitude of the voltage harmonic component is adjusted with the value of the control variable λ_h, there is no simple general rule for the correct action to avoid voltage vector to exceed the limit. A possible solution is to analyse every control step separately with a trial and error type of iterative algorithm presented in Fig. 4.13.

It must be stressed that when the adjustment of the fundamental component is not allowed and the complete elimination of the current harmonics is not possible, the only options are to disable harmonic compensation completely or to perform a partial compensation of the current harmonics. Although it is desirable to keep the current harmonics as small as possible, a careful consideration is needed to justify the high complexity of the partial current harmonic compensation.

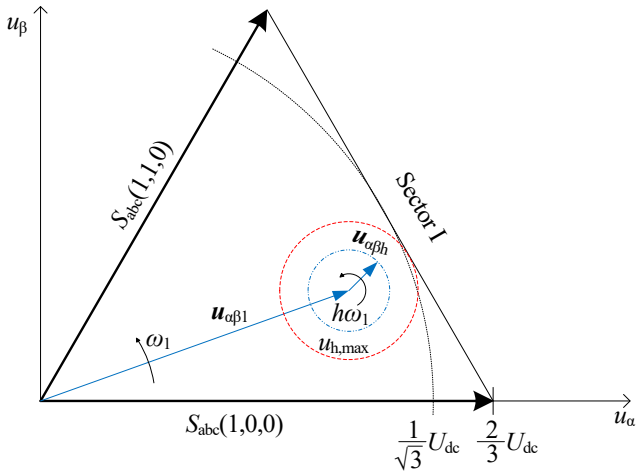

Fig. 4.12. Voltage vector in the space vector modulation hexagon of the two-level three-phase VSI. Harmonic compensation adds the harmonic component $\boldsymbol{u}_{\alpha\beta h}$ to the fundamental component $\boldsymbol{u}_{\alpha\beta 1}$. The vector sum of the components must stay inside the hexagon. This condition strictly limits the magnitude of $\boldsymbol{u}_{\alpha\beta h}$.

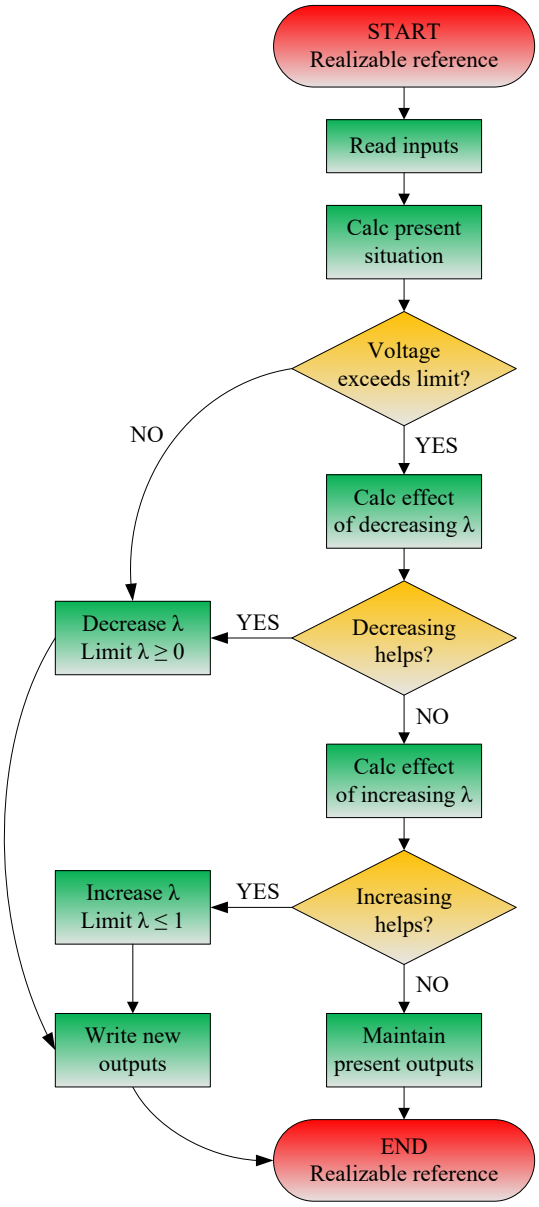

Fig. 4.13. Flow chart of the algorithm for the realizable reference strategy. The magnitudes of the voltage harmonic components are adjusted with the value of the control variable λ_h. Depending on the directions and magnitudes of the voltage vector components, the optimal action is either to increase or decrease λ_h.

5 Conclusion

This doctoral dissertation presented the stability and performance comparison of four distinct fundamental synchronous reference frame current harmonic compensation methods for dual three-phase PMSMs. The comparison covered a theoretical analysis of the robust stability and robust performance against a combination of time delay, parameter uncertainty, and supply voltage uncertainty. In addition, experimental results were used to study the dynamic performance in the time domain.

The results clearly suggest that the PR controller is a disadvantageous alternative for current harmonic compensation. Better stability and performance characteristics are achieved with the other three methods instead. There appears to be no significant difference between the robustness of the INV controller, the VPR controller, and the DOB for low values of α. Comparing the structure of the methods, the INV controller has off-diagonal resonant terms that are not present in traditional diagonal controllers such as the VPR controller. Simple diagonal controllers can be somewhat more computationally efficient. However, the inverse structure was found to be very advantageous in the theoretical analysis. On the other hand, the implementation of the DOB requires an additional inner feedback loop, and thus, it also requires more computation than the VPR controller. Evidently, these differences in the structures have only a minor effect on the robustness properties except for very high requirements of dynamic performance. Because there appears to be no practically relevant performance advantage of one method over another, the obvious choice is to prefer the VPR controller because of its simpler structure. In terms of stability and performance properties, the choice between the INV controller, the VPR controller, and the DOB is not very crucial. However, the results indicate multiple problems in the stability and performance of the PR controller. Because clearly superior alternatives are available, this dissertation strongly recommends to avoid using the traditional PR controller in current harmonic compensation.

An important aspect to consider is that all the active harmonic compensation methods can increase the required output voltage of the inverter supplying the machine. Because the maximum voltage is limited, complete elimination of the current harmonics may not always be possible. For such cases, a strategy for a partial compensation of the current harmonics was discussed. The clear disadvantage of the partial compensation strategy is that it requires information about the natural current harmonics. In addition, the calculation of the realizable references is computationally intensive, and the implementation of the strategy is somewhat complicated. Considering the additional losses and other adverse effects caused by the current harmonics, it is obviously favourable to perform the partial current harmonic compensation. However, the potential benefits in a given application should be carefully judged against the required effort to perform such an operation.

The aim of this doctoral dissertation was to conduct a complete analysis of the current harmonic compensation in dual three-phase PMSMs. The interest in dual three-phase PMSMs has grown significantly in recent years. Because dual three-phase PMSM drives

are susceptible to problems with current harmonics, it was necessary to properly address the issue. The presented discussion covered detailed solutions to the main questions of the topic including the control scheme, transformations between reference frames, compensation methods, control parameter design principles, stability and performance analysis, and the effect of the limited DC link voltage. Thus, it can be stated that a comprehensive analysis of the topic was given.

From the provided set of results, the main contribution of the doctoral dissertation was to establish the most favourable current harmonic compensation method for dual three-phase PMSMs. Considering all the aspects discussed in the previous chapters, it can be recommended to use the VPR controller with the proposed proportional gain improvement to eliminate the current harmonics. This result is in line with the previous studies that have analysed the same problem in active power filters. The current harmonic compensation in multiphase electric machines is a relatively recent topic, and thus, full agreement on the most suitable methods has not been reached yet. With the recommendations made, this work brings important new insight into the current discussion. In a rapidly increasing number of dual three-phase PMSM drives, the potential benefits of the machine can be better achieved when undesirable stator current harmonics are compensated for as suggested here. All in all, the results of the doctoral dissertation can thus help to enhance the performance of dual three-phase PMSMs in many applications.

Based on the presented results, some suggestions for future work can be given. It could be of interest to study how a change from the selected controller design principle to another would impact on the outcome of the comparison. With the given presentation, the analysis is simple to repeat using any desired controller tuning method. However, it should be taken into account that any acceptable combination of controller gains must offer sufficient robust stability, robust performance, and measurement noise attenuation. Although the properties of the harmonic controllers are more a result of the structure than parameters of the controller, the controller tuning that could yield optimal stability and performance should be investigated. Moreover, other types of harmonic controllers could be considered. The main interest here was in simple, low-order, linear, one-degree-of-freedom controllers. Study of more complex controller structures could produce some useful information. Finally, it would be advisable to further develop the proposed strategy for partial current harmonic compensation under voltage constraints. Operation with the limited available voltage clearly constitutes a major challenge, and additional research on the subject would be most welcome.

References

[1] P. Waide and C. Brunner, “Energy-efficiency policy opportunities for electric motor-driven systems,” *International Energy Agency Working Paper*, Energy Efficiency Series, pp. 1–128, 2011.

[2] P. Alger, E. Freiburghouse, and D. Chase, “Double windings for turbine alternators,” *Trans. Am. Inst. Elect. Eng.*, vol. 49, no. 1, pp. 226–244, Jan. 1930.

[3] R. Robert, J. Dispaux, and J. Dacier, “Improvement of turbo alternators efficiency”, in *Cigre Meeting, International Conference on Large Electric. Systems (CIGRE)*. June 8–18, Paris, France, 1966.

[4] E. Fuchs and L. Rosenberg, “Analysis of an alternator with two displaced stator windings,” *IEEE Trans. Power App. Syst.*, vol. 93, no. 6, pp. 1776-1786, Nov. 1974.

[5] R. Nelson and P. Krause, “Induction machine analysis for arbitrary displacement between multiple winding sets,” *IEEE Trans. Power App. Syst.*, vol. 93, no. 3, pp. 841–848, May 1974.

[6] P. Franklin, “A theoretical study of the three phase salient pole type generator with simultaneous ac and bridge rectified dc output-part I,” *IEEE Trans. Power App. Syst.*, vol. 92, no. 2, pp. 543–551, Mar. 1973.

[7] T. Kataoka and E. Watanabe, "Steady-state characteristics of a current-source inverter/double-wound synchronous machine system for ac power supply," *IEEE Trans. Ind. Appl.*, vol. 16, no. 2, pp. 262–270, Mar. 1980.

[8] P. Schiferl and C. Ong, “Six phase synchronous machine with ac and dc stator connections, part I: equivalent circuit representation and steady-state analysis,” *IEEE Trans. Power App. Syst.*, vol. 102, no. 8, pp. 2685–2693, Aug. 1983.

[9] T. A. Lipo, “A d-q model for six phase induction machines,” in *Proc. Int. Conf. Electrical Machines (ICEM)*, Athens, Greece, pp. 860–867, 1980.

[10] M. Abbas, R. Christen and T. Jahns, “Six-phase voltage source inverter driven induction motor,” *IEEE Trans. Ind. Appl.*, vol. 20, no. 5, pp. 1251–1259, Sep. 1984.

[11] C. Fortescue, “Method of symmetrical co-ordinates applied to the solution of polyphase networks,” *Trans. Am. Inst. Elect. Eng.*, vol. XXXVII, no. 2, pp. 1027–1140, Jul. 1918.

[12] Y. Zhao and T. Lipo, “Space vector pwm control of dual three-phase induction machine using vector space decomposition,” *IEEE Trans. Ind. Appl.*, vol. 31, no. 5, pp. 1100–1109, Sep./Oct. 1995.

[13] K. Gopakumar, V. Ranganthan and S. Bhat, “Split-phase induction motor operation from pwm voltage source inverter,” *IEEE Trans. Ind. Appl.*, vol. 29, no. 5, pp. 927–932, Sep./Oct. 1993.

[14] H. Knudsen, “Extended park's transformation for 2×3-phase synchronous machine and converter phasor model with representation of ac harmonics,” *IEEE Trans. Energy Conv.*, vol. 10, no. 1, pp. 126–132, Mar. 1995.

[15] E. Levi, “Multiphase electrical machines for variable-speed applications,” *IEEE Trans. Ind. Electron.*, vol. 55, no. 5, pp. 1893–1909, May 2008.

[16] E. Levi, R. Bojoi, F. Profumo, H.A. Toliyat, and S. Williamson, “Multiphase induction motor drives – a technology status review,” *IET Electr. Power Appl.*, vol. 4, no. 1, pp. 489–516, Jul. 2007.

[17] R. Bojoi, F. Farina, F. Profumo, and A. Tenconi, “Dual three-phase induction machine drives control – a survey,” *IEEJ Trans Ind. Appl.*, vol. 126, no. 4, pp. 420–429, Jul. 2006.

[18] E. Levi, “Advances in converter control and innovative exploitation of additional degrees of freedom for multiphase machines,” *IEEE Trans. Ind. Electron*., vol. 63, no. 1, pp. 433–448, Jan. 2016.

[19] F. Barrero and M. Duran, “Recent advances in the design, modeling and control of multiphase machines-part 1,” *IEEE Trans. Ind. Electron*., vol. 63, no. 1, pp. 449–458, Jan. 2016.

[20] M. Duran and F. Barrero, “Recent advances in the design, modeling and control of multiphase machines-part 2,” *IEEE Trans. Ind. Electron*., vol. 63, no. 1, pp. 459–468, Jan. 2016.

[21] R. Bojoi, S. Rubino, A. Tenconi, and S. Vaschetto, "Multiphase electrical machines and drives: a viable solution for energy generation and transportation electrification," in *2016 International Conference and Exposition on Electrical and Power Engineering (EPE)*, Iasi, 2016, pp. 632–639.

[22] R. Bojoi, A. Cavagnino, A. Tenconi, A. Tessarolo, and S. Vaschetto, "Multiphase electrical machines and drives in the transportation electrification," in *2015 IEEE 1st International Forum on Research and Technologies for Society and Industry Leveraging a better tomorrow (RTSI)*, Turin, 2015, pp. 205–212.

[23] R. Bojoi, A. Cavagnino, A. Tenconi, and S. Vaschetto, "Control of shaft-line-embedded multiphase starter/generator for aero-engine," *IEEE Trans. Ind. Electron*., vol. 63, no. 1, pp. 641–652, Jan. 2016.

[24] R. Bojoi, A. Cavagnino, M. Cossale, and A. Tenconi, "Multiphase starter generator for a 48-V mini-hybrid powertrain: design and testing," *IEEE Trans. Ind. Appl*., vol. 52, no. 2, pp. 1750–1758, Mar./Apr. 2016.

[25] H. Burzanowska, P. Schroderus, C. Stulz, M. Lehti, and J. Kaukonen, “Novel concept for full redundant drive with direct torque control (DTC) and dual-star synchronous machine,” *Electr. Eng. Res. Rep.*, no. 20, pp. 24–32, Dec. 2005.

[26] A. Tessarolo, G. Zocco, and C. Tonello, “Design and testing of a 45-MW 100-Hz quadruple-star synchronous motor for a liquefied natural gas turbo-compressor drive,” *IEEE Trans. Ind. Appl.*, vol. 47, no. 3, pp. 1210–1219, May/Jun. 2011.

[27] M. Duran, S. Kouro, B. Wu, E. Levi, F. Barrero, and S. Alepuz, “Six-phase pmsg wind energy conversion system based on medium-voltage multilevel converter,” in *Proc. 2011 14th European Conf. Power Electronics and Applications (EPE), Birmingham*, 2011, pp. 1–10.

[28] D. Vizireanu, S. Brisset, X. Kestelyn, P. Brochet, Y. Milet, and D. Laloy, "Investigation on multi-star structures for large power direct-drive wind generator," *Electric Power Components and Systems*, vol. 35, no. 2, pp. 135–152. 2007.

[29] W. Cao, B. Mecrow, G. Atkinson, J. Bennett, and D. Atkinson, “Overview of electric motor technologies used for more electric aircraft (mea),” *IEEE Trans. Ind. Electron.*, vol. 59, no. 9, pp. 3523–3531, Sept. 2012.

[30] L. Parsa and H. Toliyat, “Fault-tolerant interior-permanent magnet machines for hybrid electric vehicle applications,” *IEEE Trans. Veh. Technol*., vol. 56, no. 4, pp. 1546–1552, Jul. 2007.

[31] S. Williamson and S. Smith, “Pulsating torque and losses in multiphase induction machines,” *IEEE Trans. Ind. Appl.*, vol. 39, no. 4, pp. 986–993, Jul./Aug. 2003.

[32] A. Boglietti, R. Bojoi, A. Cavagnino, and A. Tenconi, “Efficiency analysis of pwm inverter fed three-phase and dual three-phase high frequency induction machines for low/medium power applications,” *IEEE Trans. Ind. Electron.*, vol. 55, no. 5, pp. 2015–2023, May 2008.

[33] H. Che, E. Levi, M. Jones, M. Duran, W. Hew, and N. Rahim, "Operation of a six-phase induction machine using series-connected machine-side converters," *IEEE Trans. Ind. Electron.*, vol. 61, no. 1, pp. 164–176, Jan. 2014.

[34] I. Subotic, N. Bodo, E. Levi, M. Jones and V. Levi, "Isolated chargers for evs incorporating six-phase machines," *IEEE Trans. Ind. Electron.*, vol. 63, no. 1, pp. 653–664, Jan. 2016.

[35] M. Correa, C. da Silva, H. Razik, C. Jacobina, and E. da Silva, "Independent voltage control for series-connected six- and three-phase induction machines," *IEEE Trans. Ind. Appl.*, vol. 45, no. 4, pp. 1286–1293, Jul./Aug. 2009.

[36] E. Levi, M. Jones, S. Vukosavic, and H. Toliyat, "Steady-state modeling of series-connected five-phase and six-phase two-motor drives," *IEEE Trans. Ind. Appl.*, vol. 44, no. 5, pp. 1559–1568, Sep./Oct. 2008.

[37] M. Duran, I. Gonzalez-Prieto, F. Barrero, and M. Mengoni, "A simple braking method for six-phase induction motor drives with unidirectional power flow in the base-speed region," *IEEE Trans. Ind. Electron.*, accepted for publication in a future issue.

[38] I. Gonzalez-Prieto, M. Duran, and F. Barrero, "Fault-tolerant control of six-phase induction motor drives with variable current injection," *IEEE Trans. Power Electron.*, accepted for publication in a future issue.

[39] M. Duran, I. Gonzalez-Prieto, N. Garcia, and F. Barrero, "A simple, fast and robust open-phase fault detection technique for six-phase induction motor drives" *IEEE Trans. Power Electron.*, accepted for publication in a future issue.

[40] I. Gonzalez-Prieto, M. Duran, F. Barrero, M. Bermudez, and H. Guzmán, "Impact of postfault flux adaptation on six-phase induction motor drives with parallel converters," *IEEE Trans. Power Electron.*, vol. 32, no. 1, pp. 515–528, Jan. 2017.

[41] M. Duran, I. Gonzalez Prieto, M. Bermudez, F. Barrero, H. Guzman, and M. Arahal, "Optimal fault-tolerant control of six-phase induction motor drives with parallel converters," *IEEE Trans. Ind. Electron.*, vol. 63, no. 1, pp. 629–640, Jan. 2016.

[42] W. Munim, M. Duran, H. Che, M. Bermudez, I. Gonzalez-Prieto, and N. Rahim, "A unified analysis of the fault tolerance capability in six-phase induction motor drive," *IEEE Trans. Power Electron.*, accepted for publication in a future issue.

[43] I. Gonzalez-Prieto, M. Duran, H. Che, E. Levi, M. Bermúdez, and F. Barrero, "Fault-tolerant operation of six-phase energy conversion systems with parallel machine-side converters," *IEEE Trans. Power Electron.*, vol. 31, no. 4, pp. 3068–3079, Apr. 2016.

[44] H. Che, M. Duran, E. Levi, M. Jones, W. Hew, and N. Rahim, "Postfault operation of an asymmetrical six-phase induction machine with single and two isolated neutral points," *IEEE Trans. Power Electron.*, vol. 29, no. 10, pp. 5406–5416, Oct. 2014.

[45] F. Baneira, J. Doval-Gandoy, A. Yepes, O. Lopez, and D. Perez-Estevez, "Control strategy for multiphase drives with minimum losses in the full torque operation range under single open-phase fault," *IEEE Trans. Power Electron.*, accepted for publication in a future issue.

[46] W. Wang, J. Zhang, M. Cheng, and S. Li, "Fault-tolerant control of dual three-phase permanent-magnet synchronous machine drives under open-phase faults," *IEEE Trans. Power Electron.*, vol. 32, no. 3, pp. 2052–2063, Mar. 2017.

[47] R. Bojoi, M. Lazzari, F. Profumo, and A. Tenconi, “Digital field-oriented control for dual three-phase induction motor drives,” *IEEE Trans. Ind. Appl.*, vol. 39, no. 3, pp. 752–760, May/Jun. 2003.

[48] D. Hadiouche, H. Razik, and A. Rezzoug, “On the modeling and design of dual-stator windings to minimize circulating harmonic currents for vsi fed ac machines,” *IEEE Trans. Ind. Appl.*, vol. 40, no. 2, pp. 506–515, Mar./Apr. 2004.

[49] R. Bojoi, A. Tenconi, G. Griva, and F. Profumo, “Vector control of dual-three phase induction-motor drives using two current sensors,” *IEEE Trans. Ind. Appl.*, vol. 42, no. 5, pp. 1284–1292, Sept./Oct. 2006.

[50] R. Bojoi, E. Levi, F. Farina, A. Tenconi, and F. Profumo, “Dual three-phase induction motor drive with digital current control in stationary reference frame,” *IEE Proc.-Electr. Power Appl.*, vol. 153, no. 1, pp. 129–139, Jan. 2006.

[51] D. Hadiouche, L. Baghli, and A. Rezzoug, “Space-vector pwm techniques for dual three-phase ac machine: analysis, performance evaluation, and dsp implementation,” *IEEE Trans. Ind. Appl.*, vol. 42, no. 4, pp. 1112–1122, Jul./Aug. 2006.

[52] K. Marouani, L. Baghli, D. Hadiouche, A. Kheloui, and A. Razzoug, “A new pwm strategy based on a 24-sector vector space decomposition for a six-phase vsi-fed dual stator induction motor,” *IEEE Trans. Ind. Electron.*, vol. 55, no. 5, pp. 1910–1920, May 2008.

[53] A. Tessarolo and C. Bassi, “Stator harmonic currents in vsi-fed synchronous motors with multiple three-phase armature windings,” *IEEE Trans. Energy Convers.*, vol. 25, no. 4, pp. 974–982, Dec. 2010.

[54] T. Wang, F. Fang, X. Wu, and X. Jiang, “Novel filter for stator harmonic currents reduction in six-step converter fed multiphase induction motor drives,” *IEEE Trans. Power Electron.*, vol. 28, no. 1, pp. 498–506, Jan. 2013.

[55] J. Malvar, O. Lopez, A. Yepes, A. Vidal, F. Freijedo, P. Fernanze-Comesana, and J. Doval-Gandoy, “Graphical diagram for subspace and sequence indentification of time harmonics in symmetrical multiphase machines,” *IEEE Trans. Ind. Electron.*, vol. 61, no. 1, pp. 29–42, Jan. 2014.

[56] A. Yepes, J. Malvar, A. Vidal, O. López and J. Doval-Gandoy, "Optimized harmonic current control strategy for nonlinearities compensation in multiphase ac drives," in *2013 IEEE Energy Conversion Congress and Exposition*, Denver, CO, pp. 1458–1464, 2013.

[57] A. Yepes, J. Malvar, A. Vidal, O. López and J. Doval-Gandoy, "Current harmonic compensation in symmetrical multiphase machines by resonant controllers in synchronous reference frames–part 2: computational load," in *39th Annual Conference of the IEEE Industrial Electronics Society (IECON)*, Vienna, pp. 5161–5166, 2013.

[58] A. Yepes, J. Malvar, A. Vidal, O. López and J. Doval-Gandoy, "Current harmonic compensation in symmetrical multiphase machines by resonant controllers in synchronous reference frames–part 1: extension to any phase number," in *39th Annual Conference of the IEEE Industrial Electronics Society (IECON)*, Vienna, pp. 5155–5160, 2013.

[59] H. Che, E. Levi, M. Jones, M. Duran, W. Hew, and N. Rahim, “Current control methods for an asymmetrical six-phase induction motor drive,” *IEEE Trans. Power Electron.*, vol. 29, no. 1, pp. 407–417, Jan. 2014.

[60] F. Yuan and S. Huang, “A hybrid current controller for dual-three-phase permanent magnet synchronous motors,” *IEEJ Trans. Electr. Electron. Eng.*, vol. 9, no. 2, pp. 214–218, Mar. 2014.

[61] Y. Hu, Z. Zhu, and K. Liu, “Current control for dual 3-phase pm synchronous motors accounting for current unbalance and harmonics,” *IEEE Trans. Emerg. Sel. Topics Power Electron*., vol. 2, no. 2, pp. 272–284, Jun. 2014.

[62] A. Yepes, J. Malvar, A. Vidal, O. Lopez, and J. Doval-Gandoy, “Current harmonic compensation based on multi-resonant control in synchronous frames for symmetrical n-phase machines,” *IEEE Trans. Ind. Electron*., vol. 62, no. 5, pp. 2708–2720, May 2015.

[63] L. Yuan, M. Chen, J. Shen, F. Xiao, "Current harmonics elimination control method for six-phase pm synchronous motor drives," *ISA Transactions*, vol. 59, no. 11, pp. 443–449, Nov. 2015.

[64] L. Yuan, K. Wei, B. Hu, and S. Chen, "Current control method with enhanced pi controller for six-phase pm synchronous motor drive," in *19th International Conference on Electrical Machines and Systems (ICEMS)*, Chiba, Japan, pp. 1–6, 2016.

[65] L. Yuan, B. Hu, K. Wei, and Y. Lin, "A novel current vector decomposition controller design for six-phase permanent magnet synchronous motor," *J. Cent. South Univ*., vol. 23, no. 4, pp. 841–849, Apr. 2016.

[66] A. Yepes, J. Doval-Gandoy, F. Baneira, D. Pérez-Estévez, and O. López, "Current harmonic compensation for n-phase machines with asymmetrical winding arrangement," in *IEEE Energy Conversion Congress and Exposition (ECCE)*, Milwaukee, WI, pp. 1–8, 2016.

[67] Z. Zhu, A. Almarhoon, and P. Xu, "Improved rotor position estimation accuracy by rotating carrier signal injection utilizing zero-sequence carrier voltage for dual three-phase pmsm," *IEEE Trans. Ind. Electron*., accepted for publication in a future issue.

[68] A. Almarhoon, Z. Zhu, and P. Xu, "Improved pulsating signal injection using zero-sequence carrier voltage for sensorless control of dual three-phase pmsm," *IEEE Trans. Energy Conv.*, accepted for publication in a future issue.

[69] K. Wang, Z. Zhu, Y. Ren, and G. Ombach, “Torque improvements of dual-three-phase permanent magnet machine with 3rd harmonic current injection,” *IEEE Trans. Ind. Electron.*, vol. 62, no. 11, pp. 6833–6844, Nov. 2015.

[70] Y. Ren and Z. Zhu, “Reduction of both harmonic current and torque ripple for dual-three-phase permanent magnet synchronous machine using modified switching-table-based direct torque control,” *IEEE Trans. Ind. Electron.*, vol. 62, no. 11, pp. 6671–6683, Nov. 2015.

[71] C. Zhou, G. Yang, and J. Su, “PWM strategy with minimum harmonic distortion for dual-three-phase permanent magnet synchronous motor drives operating in the overmodulation region,” *IEEE Trans. Power Electron.*, vol. 31, no. 2, pp. 1367–1380, Feb. 2016.

[72] F. Baneira, A. Yepes, O. Lopez, and J. Doval-Gandoy, “Estimation method of stator winding temperature for dual-three-phase machines based on dc-signal injection,” *IEEE Trans. Power Electron.*, vol. 31, no. 7, pp. 5141–5148, Jul. 2016.

[73] A. Abdel-Khalik, S. Ahmed, and A. Massoud, "Effect of multilayer windings with different stator winding connections on interior pm machines for ev applications," *IEEE Trans. Magn.*, vol. 52, no. 2, pp. 1–7, Feb. 2016.

[74] Y. Demir and M. Aydin, "A novel dual three-phase permanent magnet synchronous motor with asymmetric stator winding," *IEEE Trans. Magn.*, vol. 52, no. 7, pp. 1–5, Jul. 2016.

[75] R. Bojoi, F. Farina, G. Griva, and F. Profumo, "Direct torque control for dual three-phase induction motor drives," *IEEE Trans. Ind. Appl.*, vol. 41, no. 6, pp. 1627–1636, Nov./Dec. 2005.

[76] K. Hatua and V. Ranganathan, "Direct torque control schemes for split-phase induction machine," *IEEE Trans. Ind. Appl.*, vol. 41, no. 5, pp. 1243–1254, Sept./Oct. 2005.

[77] H. Burzanowska, P. Schroderus, C. Stulz, M. Lehti, and J. Kaukonen, "Novel concept for full redundant drive with direct torque control (dtc) and dual-star synchronous machine," *Electr. Eng. Res. Rep.*, no. 20, pp. 24–32, Dec. 2005.

[78] J. Pandit, M. Aware, R. Nemade, and E. Levi, "Direct torque control scheme for a six-phase induction motor with reduced torque ripple," *IEEE Trans. Power Electron.*, accepted for publication in a future issue.

[79] K. Hoang, Y. Ren, Z. Zhu, and M. Foster, "Modified switching-table strategy for reduction of current harmonics in direct torque controlled dual-three-phase permanent magnet synchronous machine drives," *IET Elect. Power Appl.*, vol. 9, no. 1, pp. 10–19, Jan. 2015.

[80] Y. Ren and Z. Zhu, "Enhancement of steady-state performance in direct-torque-controlled dual three-phase permanent-magnet synchronous machine drives with modified switching table," *IEEE Trans. Ind. Electron.*, vol. 62, no. 6, pp. 3338–3350, Jun. 2015.

[81] A. Taheri, "Harmonic reduction of direct torque control of six-phase induction motor," *ISA Transactions*, vol. 63, no. 1, pp. 299–314, Jul. 2016.

[82] F. Barrero, M. Arahal, R. Gregor, S. Toral, and M. Duran, "A proof of concept study of predictive current control for vsi-driven asymmetrical dual three-Phase ac machines," *IEEE Trans. Ind. Electron.*, vol. 56, no. 6, pp. 1937–1954, Jun. 2009.

[83] F. Barrero, M. Arahal, R. Gregor, S. Toral, and M. Duran, "One-step modulation predictive current control method for the asymmetrical dual three-phase induction machine," *IEEE Trans. Ind. Electron.*, vol. 56, no. 6, pp. 1974–1983, Jun. 2009.

[84] M. Duran, J. Prieto, F. Barrero, and S. Toral, "Predictive current control of dual three-phase drives using restrained search techniques," *IEEE Trans. Ind. Electron.*, vol. 58, no. 8, pp. 3253–3263, Aug. 2011.

[85] F. Barrero, J. Prieto, E. Levi, R. Gregor, S. Toral, M. Duran, and M. Jones, "An enhanced predictive current control method for asymmetrical six-phase motor drive," *IEEE Trans. Ind. Electron.*, vol. 58, no. 8, pp. 3242–3252, Aug. 2011.

[86] R. Gregor, F. Barrero, S. Toral, M. Duran, M. Arahal, J. Prieto, and J. Mora, "Predictive-space vector pwm current control method for asymmetrical dual three-phase induction motor drives," *IET Elect. Power Appl.*, vol. 4, no. 1, pp. 26–34, Jan. 2010.

[87] C. Lim, E. Levi, M. Jones, N. Rahim, and W. Hew, "FCS-mpc-based current control of a five-phase induction motor and its comparison with pi-pwm control," *IEEE Trans. Ind. Electron.*, vol. 61, no. 1, pp. 149–163, Jan. 2014.

[88] B. Bogado, F. Barrero, M. Arahal, S. Toral, and E. Levi, "Sensitivity to electrical parameter variations of predictive current control in multiphase drives," in *39th Annual Conference of the IEEE Industrial Electronics Society (IECON)*, Vienna, pp. 5215–5220, 2013.

[89] G. Singh, K. Nam, and S. Lim, "A simple indirect field-oriented control scheme for multiphase induction machine," *IEEE Trans. Ind. Electron*., vol. 52, no. 4, pp. 1177–1184, Aug. 2005.

[90] L. Nezli and M. Mahmoudi, "Vector control with optimal torque of a salient-pole double star synchronous machine supplied by three-level inverters," *J. Electr. Eng.*, vol. 61, no. 5, pp. 257–263, Sep. 2010.

[91] S. Kallio, M. Andriollo, A. Tortella, and J. Karttunen, "Decoupled d-q model of double-star interior permanent magnet synchronous machines," *IEEE Trans. Ind. Electron.*, vol. 60, no. 6, pp. 2486–2494, Jun. 2013.

[92] S. Kallio, J. Karttunen, P. Peltoniemi, P. Silventoinen, and O. Pyrhönen, "Online estimation of double-star ipm machine parameters using rls algorithm," *IEEE Trans. Ind. Electron.*, vol. 61, no. 9, pp. 4519–4530, Sept. 2014.

[93] S. Kallio, J. Karttunen, P. Peltoniemi, P. Silventoinen, and O. Pyrhönen, "Determination of the inductance parameters for the decoupled d–q model of double-star permanent-magnet synchronous machines," *IET Electr. Power Appl.*, vol. 8, no. 2, pp. 39–49, Feb. 2014.

[94] I. Petersen and R. Tempo, "Robust control of uncertain systems: classical results and recent developments," *Automatica*, vol. 50, no. 5, pp. 1315–1335, May. 2014.

[95] A. Packard and J. Doyle, "The complex structured singular value," *Automatica*, vol. 29, no. 1, pp. 71–109. Jan. 1993.

[96] D. Piga, "Computation of the structured singular value via moment lmi relaxations," *IEEE Trans. Autom. Control*, vol. 61, no. 2, pp. 520–525, Feb. 2016.

[97] M. Marvali, M. Dai, and A. Keyhani, "Robust stability analysis of voltage and current control for distributed generation systems," *IEEE Trans. Energy Convers.*, vol. 21, no. 2, pp. 516–526, Jun. 2006.

[98] S. Sumsurooah, M. Odavic, and S. Bozhko, "A modeling methodology for robust stability analysis of nonlinear electrical power systems under parameter uncertainties," *IEEE Trans. Ind. Appl.*, vol. 52, no. 5, pp. 4416–4425, Sept./Oct. 2016.

[99] L. Ye and L. Xu, "Analysis of a novel stator winding structure minimizing harmonic current and torque ripple for dual six-step converter-fed high power ac machines," in *Conference Record of the 1993 IEEE Industry Applications Conference Twenty-Eighth IAS Annual Meeting*, Toronto, Ont., vol. 1, pp. 197–202, 1993.

[100] A. Munoz and T. Lipo, "Dual stator winding induction machine drive," *IEEE Trans. Ind. Appl.*, vol. 36, no. 5, pp. 1369–1379, Sep./Oct. 2000.

[101] Y. Yang, K. Zhou, H. Wang, F. Blaabjerg, D. Wang, and B. Zhang, "Frequency adaptive selective harmonic control for grid-connected inverters," *IEEE Trans. Power Electron.*, vol. 30, no. 7, pp. 3912–3924, Jul. 2015.

[102] A. Yepes, F. Freijedo, O. Lopez, and J. Doval-Gandoy, "Analysis and design of resonant current controllers for voltage-source converters by means of nyquist diagrams and sensitivity function," *IEEE Trans. Ind. Electron.*, vol. 58, no. 11, pp. 5231–5250, Nov. 2011.

[103] H. Yi, F. Zhuo, Y. Zhang, Y. Li, W. Zhan, W. Chen, and J. Liu, "A source-current-detected shunt active power filter control scheme based on vector resonant controller," *IEEE Trans. Ind. Appl.*, vol. 50, no. 3, pp. 1953–1965, May/Jun. 2014.

[104] C. Lascu, L. Asiminoaei, I. Boldea, and F. Blaabjerg, "High performance current controller for selective harmonic compensation in active power filters," *IEEE Trans. Power Electron.*, vol. 22, no. 5, pp. 1826–1835, Sep. 2007.

[105] H. Nian and Y. Song, "Optimized parameter design of proportional integral and resonant current regulator for doubly fed induction generator during grid voltage distortion," *IET Renew. Power Gener.*, vol. 8, no. 3, pp. 299–313, Apr. 2014.

[106] H. Nian and Y. Song, "Direct power control of doubly fed induction generator under distorted grid voltage," *IEEE Trans. Power Electron.*, vol. 29, no. 2, pp. 894–905, Feb. 2014.

[107] C. Xia, B. Ji, and Y. Yan, "Smooth speed control for low speed high torque permanent magnet synchronous motor using proportional integral resonant controller," *IEEE Trans. Ind. Electron.*, vol. 62, no. 4, pp. 2123–2134, Apr. 2015.

[108] D. Zmood, D. Holmes, and G. Bode, "Frequency domain analysis of three-phase linear current regulators," *IEEE Trans. Ind. Appl.*, vol. 37, no. 2, pp. 601–610, Mar./Apr. 2001.

[109] L. Harnefors, "Modeling of three-phase dynamic systems using complex transfer functions and transfer matrices," *IEEE Trans. Ind. Electron.*, vol. 54, no. 4, pp. 2239–2248, Aug. 2007.

[110] A. Yepes, F. Freijedo, J. Doval-Gandoy, O. Lopez, J. Malvar, and P. Fernandez-Comesana, "Effects of discretization methods on the performance of resonant controllers," *IEEE Trans. Power Electron.*, vol. 25, no. 7, pp. 1692–1712, Jul. 2010.

[111] L. Harnefors, "Implementation of resonant controllers and filters in fixed-point arithmetic," *IEEE Trans. Ind. Electron.*, vol. 56, no. 4, pp. 1273–1281, Apr. 2009.

[112] A. Yepes, F. Freijedo, O. Lopez, and J. Doval-Gandoy, “High-performance digital resonant controllers implemented with two integrators,” *IEEE Trans. Power Electron.*, vol. 26, no. 2, pp. 563–576, Feb. 2011.

[113] C. Lascu, L. Asiminoaei, I. Boldea, and F. Blaabjerg, “Frequency response analysis of current controllers for selective harmonic compensation in active power filters,” *IEEE Trans. Ind. Electron*., vol. 56, no. 2, pp. 337–347, Feb. 2009.

[114] R. Bojoi, L. Limongi, F. Profumo, D. Roiu and A. Tenconi, “Analysis of current controllers for active power filters using selective harmonic compensation schemes,” *IEEJ Trans. Electr. Electron. Eng.*, vol. 4, no. 2, pp. 139–157, Mar. 2009.

[115] H. Yi, F. Zhuo, and F. Wang, “Analysis about overshoot peaks appearing in the current loop with resonant controller,” *IEEE Trans. Emerg. Sel. Topics Power Electron.* vol. 4, no. 1, pp. 26–36, Mar. 2016.

[116] L. Wang, J. Su, and G. Xiang, "Robust motion control system design with scheduled disturbance observer," *IEEE Trans. Ind. Electron.*, vol. 63, no. 10, pp. 6519–6529, Oct. 2016.

[117] E. Sariyildiz and K. Ohnishi, “Stability and robustness of disturbance observer based motion control systems,” *IEEE Trans. Ind. Electron.*, vol. 62, no. 1, pp. 414–422, Jan. 2015.

[118] B. Lee, J. Kim, and K. Nam, “Simple on-line dead-time compensation scheme based on disturbance voltage observer,” in *IEEE Energy Conversion Congress and Exposition (ECCE)*, Raleigh, pp. 1857–1863, 2012.

[119] Y. Mohamed, “Design and implementation of a robust current-control scheme for a pmsm vector drive with a simple adaptive disturbance observer,” *IEEE Trans. Ind. Electron.*, vol. 54, no. 4, pp. 1981–1988, Aug. 2007.

[120] M. Dal, R. Teodorescu, and F. Blaabjerg, “Complex state variable- and disturbance observer based current controllers for ac drives: an experimental comparison,” *IET Power Electron*., vol. 6, no. 9, pp. 1792–1802, Nov. 2013.

[121] N. H. Jo, C. Jeon, and H. Shim, "Noise reduction disturbance observer for disturbance attenuation and noise suppression," *IEEE Trans. Ind. Electron*, vol. 64, no. 2, pp. 1381–1391, Feb. 2017.

[122] C. Liu, F. Blaabjerg, W. Chen, and D. Xu, “Stator current harmonic control with resonant controller for doubly fed induction generator,” *IEEE Trans. Power Electron.*, vol. 27, no. 7, pp. 3207–3220, Jul. 2012.

[123] L. Harnefors, A. Yepes, A. Vidal, J. Doval-Gandoy, “Multifrequency current control with distortion free saturation,” *IEEE J. Emerg. Sel. Topics Power Electron*., vol. 4, no. 1, pp. 37–43, Mar. 2016.

Appendix A: Detailed machine parameters

This appendix gives the detailed information about the dual three-phase PMSM used in the experimental measurements in this doctoral dissertation. The machine has v-shaped interior permanent magnets in the rotor. The stator was rewound from a standard three-phase machine.

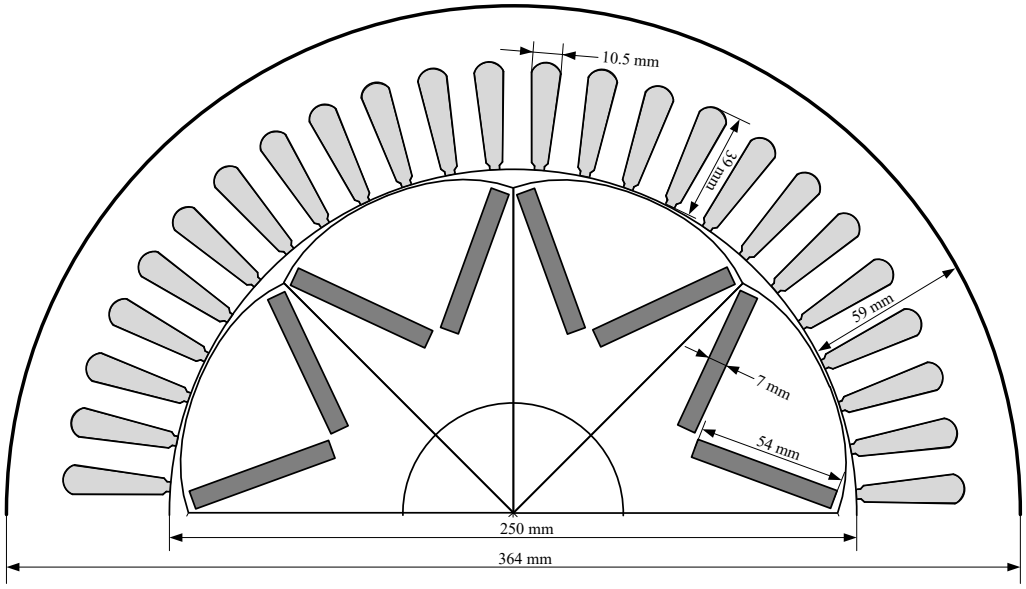

Fig. A.1. Geometrical dimensions of the dual three-phase PMSM.

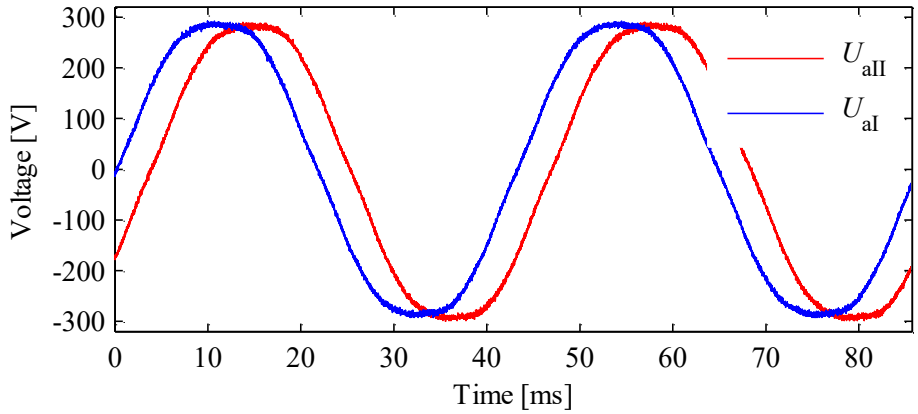

Fig. A.2. Measured back-EMF voltage between the phase terminal (a_I and a_{II}) and the neutral point at the nominal speed of the machine.

TABLE A.I
Magnitude of the frequency components of the measured back-EMF

1st	3rd	5th	7th	9th	11th	13th
303.30 V	11.13 V	6.04 V	0.98 V	0.96 V	0.69 V	<0.10 V

TABLE A.II
Detailed machine parameters

Plate values	
Nominal power	25 kW
Nominal current	22.5 A
Nominal voltage	380 V
Nominal torque	682.1 Nm
Nominal speed	350 r/min
Nominal frequency	23.3 Hz
Electrical parameters	
Stator resistance R_s	0.53 Ω
PM flux linkage ψ_{PM}	2.06 Wb
Inductance L_{Dm}, L_{Qm}	31 mH, 42 mH
Inductance L_{Ds}, L_{Qs}	7 mH, 8 mH
Structure data	
Number of pole pairs	4
Phases	6
Stator slots	48
Slots per pole per phase	1
Stator skewing	1 slot
Dimensions	
Frame size	225
Outer diameter	364 mm
Air-gap diameter	250mm
Stack length	270 mm
Air-gap minimum length	1.2 mm
Slot cross-sectional are	240 mm^2
Insulated slot area	215 mm^2
Winding data	
Winding type	full-pitch
Winding step	1-7
Winding factor 1st	0.989
Winding factor 5th	0.738
Winding factor 7th	0.527
Winding factor 11th	0.090
Winding factor 13th	0.073
Diameters of wires	1.12 mm × 3
	0.9 mm × 2
Turns in series per phase	120
Conductors per slot	30
Copper fill factor	0.6
Parallel paths	1
Nominal current density	5.3 A/ mm^2

Publication I

J. Karttunen, S. Kallio, P. Peltoniemi, P. Silventoinen, and O. Pyrhönen.
Dual Three-Phase Permanent Magnet Synchronous Machine Supplied by Two Independent Voltage Source Inverters

21st edition of the IEEE International Symposium on Power Electronics, Electrical Drives, Automation and Motion (SPEEDAM), Sorrento
pp. 741–747, 2012.

Publication II

J. Karttunen, S. Kallio, P. Peltoniemi, P. Silventoinen, and O. Pyrhönen.
Decoupled Vector Control Scheme for Dual Three-Phase Permanent Magnet Synchronous Machines

IEEE Transactions on Industrial Electronics
vol. 61, no. 5, pp. 2486–2494, May 2014.

Publication III

J. Karttunen, S. Kallio, P. Peltoniemi, and P. Silventoinen.
Transforming Dynamic System Models Between Two-Axis Reference Frames Rotating at Different Angular Frequencies

16th European Conference on Power Electronics and Applications (EPE'14 ECCE Europe), Lappeenranta
pp. 1–10, 2014.

Publication IV

J. Karttunen, S. Kallio, P. Peltoniemi, and P. Silventoinen.
Current Harmonic Compensation in Dual Three-Phase PMSMs Using a Disturbance Observer

IEEE Transactions on Industrial Electronics
vol. 63, no. 1, pp. 583–594, Jan. 2016.

Publication V

J. Karttunen, S. Kallio, P. Peltoniemi, J. Honkanen, and P. Silventoinen.
Inverse-Based Current Harmonic Controller for Multiphase PMSMs

International Review of Electrical Engineering (I.R.E.E.)
vol. 11, no. 4, pp. 359–396, Aug. 2016.

Publication VI

J. Karttunen, S. Kallio, P. Peltoniemi, J. Honkanen, and P. Silventoinen.
Stability and Performance of Current Harmonic Controllers for Multiphase PMSMs

Control Engineering Practice
vol. 65, pp. 59–69, Aug. 2017.

Publication VII

J. Karttunen, S. Kallio, P. Peltoniemi, J. Honkanen, and P. Silventoinen.
Partial Current Harmonic Compensation in Dual Three-Phase PMSMs Considering the Limited Available Voltage

IEEE Transactions on Industrial Electronics
vol. 64, no. 2, pp. 1038–1048, Feb. 2017.

ACTA UNIVERSITATIS LAPPEENRANTAENSIS

713. NEVARANTA, NIKO. Online time and frequency domain identification of a resonating mechanical system in electric drives. 2016. Diss.

714. FANG, CHAO. Study on system design and key technologies of case closure welding for ITER correction coil. 2016. Diss.

715. GARCÍA PÉREZ, MANUEL. Modeling the effects of unsteady flow patterns on the fireside ash fouling in tube arrays of kraft and coal-fired boilers.

716. KATTAINEN, JARI. Heterarkkisen verkostoyhteistyön johtamistarpeet verkoston muotoutumisvaiheessa. 2016. Diss.

717. HASAN, MEHDI. Purification of aqueous electrolyte solutions by air-cooled natural freezing. 2016. Diss.

718. KNUTAS, ANTTI. Increasing beneficial interactions in a computer-supported collaborative environment. 2016. Diss.

719. OVASKA, SAMI-SEPPO. Oil and grease barrier properties of converted dispersion-coated paperboards. 2016. Diss.

720. MAROCHKIN, VLADISLAV. Novel solutions for improving solid-state photon detector performance and manufacturing. 2016. Diss.

721. SERMYAGINA, EKATERINA. Modelling of torrefaction and hydrothermal carbonization and heat integration of torrefaction with a CHP plant. 2016. Diss.

722. KOTISALO, KAISA. Assessment of process safety performance in Seveso establishments. 2016. Diss.

723. LAINE, IGOR. Institution-based view of entrepreneurial internationalization. 2016. Diss.

724. MONTECINOS, WERNER EDUARDO JARA. Axial flux permanent magnet machines – development of optimal design strategies. 2016. Diss.

725. MULTAHARJU, SIRPA. Managing sustainability-related risks in supply chains. 2016. Diss.

726. HANNONEN, JANNE. Application of an embedded control system for aging detection of power converter components. 2016. Diss.

727. PARKKILA, JANNE. Connecting video games as a solution for the growing video game markets. 2016. Diss.

728. RINKINEN, SATU. Clusters, innovation systems and ecosystems: Studies on innovation policy's concept evolution and approaches for regional renewal. 2016. Diss.

729. VANADZINA, EVGENIA. Capacity market in Russia: addressing the energy trilemma. 2016. Diss.

730. KUOKKANEN, ANNA. Understanding complex system change for a sustainable food system. 2016. Diss.

731. SAVOLAINEN, JYRKI. Analyzing the profitability of metal mining investments with system dynamic modeling and real option analysis. 2016. Diss.

732. LAMPINEN, MATTI. Development of hydrometallurgical reactor leaching for recovery of zinc and gold. 2016. Diss.

733. SUHOLA, TIMO. Asiakaslähtöisyys ja monialainen yhteistyö oppilashuollossa: oppilashuoltoprosessi systeemisenä palvelukokonaisuutena. 2017. Diss.

734. SPODNIAK, PETR. Long-term transmission rights in the Nordic electricity markets: An empirical appraisal of transmission risk management and hedging. 2017. Diss.

735. MONTONEN, JUHO. Integrated hub gear motor for heavy-duty off-road working machines – Interdisciplinary design. 2017. Diss.

736. ALMANASRAH, MOHAMMAD. Hot water extraction and membrane filtration processes in fractionation and recovery of value-added compounds from wood and plant residues. 2017. Diss.

737. TOIVANEN, JENNI. Systematic complaint data analysis in a supply chain network context to recognise the quality targets of welding production. 2017. Diss.

738. PATEL, GITESHKUMAR. Computational fluid dynamics analysis of steam condensation in nuclear power plant applications. 2017. Diss.

739. MATTHEWS, SAMI. Novel process development in post-forming of an extruded wood plastic composite sheet. 2017. Diss.

740. KÄHKÖNEN, TOMMI. Understanding and managing enterprise systems integration. 2017. Diss.

741. YLI-HUUMO, JESSE. The role of technical dept in software development. 2017. Diss.

742. LAYUS, PAVEL. Usability of the submerged arc welding (SAW) process for thick high strength steel plates for Arctic shipbuilding applications. 2017. Diss.

743. KHAN, RAKHSHANDA. The contribution of socially driven businesses and innovations to social sustainability. 2017. Diss.

744. BIBOV, ALEKSANDER. Low-memory filtering for large-scale data assimilation. 2017. Diss.

745. ROTICH, NICOLUS KIBET. Development and application of coupled discrete and continuum models in solid particles classification. 2017. Diss.

746. GAST, JOHANNA. The coopetition-innovation nexus: Investigating the role of coopetition for innovation in SMEs. 2017. Diss.

747. KAPOOR, RAHUL. Competition and disputes in the patent life cycle. 2017. Diss.

748. ALI-MARTTILA, MAAREN. Towards successful maintenance service networks – capturing different value creation strategies. 2017. Diss.

749. KASHANI, HAMED TASALLOTI. On dissimilar welding: a new approach for enhanced decision-making. 2017. Diss.

750. MVOLA BELINGA, ERIC MARTIAL. Effects of adaptive GMAW processes: performance and dissimilar weld quality. 2017. Diss.